MTORC2 PROMOTES LIPID STORAGE AND SUPPRESSES THERMOGENESIS IN BROWN ADIPOSE TISSUE IN PART THROUGH AKT-INDEPENDENT REGULATION OF FOXO1

A Dissertation Presented

By

Chien-Min Hung

Submitted to the Faculty of the

University of Massachusetts Graduate School of Biomedical Sciences, Worcester

in partial fulfillment of the requirements for the degree of

DOCTOR OF PHILOSOPHY

Oct. 23th, 2016

Interdisciplinary Graduate Program

MTORC2 PROMOTES LIPID STORAGE AND SUPPRESSES THERMOGENESIS IN BROWN ADIPOSE TISSUE IN PART THROUGH AKT-INDEPENDENT REGULATION OF FOXO1

A Dissertation Presented
By
Chien-Min Hung

This work was undertaken in the Graduate School of Biomedical Sciences
Interdisciplinary Graduate Program

The signature of the Thesis Advisor signifies
validation of Dissertation content

David A. Guertin, Ph.D., Thesis Advisor

The signatures of the Dissertation Defense Committee signify
completion and approval as to style and content of the Dissertation

Dohoon Kim, Ph.D., Member of Committee

Amy Walker, Ph.D., Member of Committee

Heidi Tissenbaum, Ph.D., Member of Committee

Brendan D. Manning, Ph.D., External Member of Committee

The signature of the Chair of the Committee signifies that the written dissertation meets
the requirements of the Dissertation Committee

Eric Baehrecke, Ph.D., Chair of Committee

The signature of the Dean of the Graduate School of Biomedical Sciences signifies
that the student has met all graduation requirements of the School.

Anthony Carruthers, Ph.D.,
Dean of the Graduate School of Biomedical Sciences

Oct. 23th, 2016

Acknowledgements

First of all, I wish to express my deep appreciation and gratitude to my advisor, Dr. David Guertin, for the patient guidance and mentor ship he provided to me, all the way from the first day of my rotation in his laboratory through to completion of this degree. Dr. Guertin's intellectual heft and encouragement have guided me through numerous obstacles and challenges. I am truly fortunate to have had the opportunity to work with him.

I would also like to pay my thankfulness to my committee members, Dr. Eric Baehrecke, Dr. Amy Walker, Dr. Dohoon Kim, Dr. Heidi Tissenbaum, and Dr. Brendan Mannning. I want to specially thank the chair, Dr. Baehrecke, for the friendly guidance and supports over the years. I also want to thank Dr. Walker for her patient and thought-provoking suggestions she have provided to me. Last, I would like to recognize all committee members for the contributions that each of them made to this thesis work during my years of study at the University of Massachusetts Medical School.

I would also like to express my warm and whole-hearted gratitude to my colleagues in the Guertin lab. Words cannot express how fortunate I am to be your co-walker and friend.

Finally, I would be remiss if I didn't acknowledge the innumerable sacrifices made by my wife, Mei-Yu, in carrying far more than her fair share of the household burdens and the parenting while I pursued my degree. Also, I would like to thank my parents for their continuous supports and cares.

Abstract

Recent studies suggest adipose tissue plays a critical role in regulating whole body energy homeostasis in both animals and humans. In particular, activating brown adipose tissue (BAT) activity is now appreciated as a potential therapeutic strategy against obesity and metabolic disease. However, the signaling circuits that coordinate nutrient uptake and BAT function are poorly understood. Here, I investigated the role of the nutrient-sensing mTOR signaling pathway in BAT by conditionally deleting *Rictor*, which encodes an essential component of mTOR Complex 2 (mTORC2) either in brown adipocyte precursors or mature brown adipocytes. In general, inhibiting BAT mTORC2 reduces glucose uptake and de novo lipogenesis pathways while increases lipid uptake and oxidation pathways indicating a switch in fuel utilization. Moreover, several key thermogenic factors (*Ucp1*, *Pgc1α,* and *Irf4*) are elevated in Rictor-deficient BAT, resulting in enhanced thermogenesis. Accordingly, mice with mTORC2 loss in BAT are protected from HFD-induced obesity and metabolic disease at thermoneutrality. In vitro culture experiments further suggest that mTORC2 cell-autonomously regulates the BAT thermogenic program, especially *Ucp1* expression, which depends on FoxO1 activity. Mechanistically, mTORC2 appears to inhibit FoxO1 by facilitating its lysine-acetylation but not through the canonical AKT-mediated phosphorylation pathway. Finally, I also provide evidence that β-adrenergic signaling which normally triggers thermogenesis also induces FoxO1 deacetylation in BAT. Based on these data, I propose a model in which mTORC2 functions in BAT as a critical signaling hub for coordinating nutrient uptake, fuel utilization, and thermogenic gene expression. These data provide a foundation for

future studies into the mTORC2-FoxO1 signaling axis in different metabolic tissues and physiological conditions.

Table of Contents

List of Tables

List of Figures

CHAPTER V

List of copyrighted Materials Produced by the Author

- CM Hung, C Martinez-Calejman, J Sanchez-Gurmaches, H Li, CB Clish, S Hettmer, AJ Wagers, DA Guertin. (2014) Rictor/mTORC2 loss in the Myf5 lineage reprograms brown fat metabolism and protects mice against obesity and metabolic disease *Cell Reports* 8 (1), 256-271

- CM Hung, L Garcia-Haro, CA Sparks, DA Guertin. mTOR-dependent cell survival mechanisms. (2012) Cold Spring Harbor perspectives in biology 4 (12), a008771 (Charpter)

List of Abbreviations

Adipocyte differentiation marker

C/ebpα ─ CCAAT-enhancer-binding proteins α

C/ebpβ ─ CCAAT-enhancer-binding proteins β

Pparγ1 ─ Peroxisome proliferator-activated receptor γ isoform 1

Pparγ2 ─ Peroxisome proliferator-activated receptor γ isoform 2

Fabp4 ─ Fatty Acid Binding Protein 4

Adipoq ─ Adiponectin

De novo lipogenesis

Srebf1 ─ Sterol Regulatory Element Binding Transcription Factor 1

Chrebpα ─ Carbohydrate-responsive element-binding protein α

Chrebpβ ─ Carbohydrate-responsive element-binding protein β

Acly ─ ATP-citrate lyase

Acc ─ Acetyl CoA carboxylase

Fasn ─ Fatty acid synthase

Elovl6 ─ Elongation of very long-chain fatty acid 6

Scd1 ─ Stearoyl-CoA desaturase 1

Brown enriched and/or thermogenic genes

Ucp1 ─ Uncoupler protein 1

Elovl3 ─ Elongation of very long-chain fatty acid 3

Dio2 ─ Deiodonase-2

Prdm16 ─ PR domain containing 16

Pgc1α ─ Peroxisome proliferator-activated receptor gamma coactivator 1-α

Irf4 ─ Interferon regulatory factor 4

Cidea ─ Cell death-inducing DFFA-like effector A

Lipolysis and lipid oxidation

Lpl ─ lipoprotein lipase

Hsl ─ Hormone-sensitive lipase

Atgl ─ Adipose Triglyceride Lipase

Pparα ─ Peroxisome proliferator-activated receptor α

Ehhadh ─ Enoyl-CoA hydratase and 3-hydroxyacyl CoA dehydrogenase

Cpt1a ─ Carnitine palmitoyltransferase 1A

Cpt1b ─ Carnitine palmitoyltransferase 1B

Triacylglyceride biosynthesis

Gyk ─ Glycerol kinase

Gpat ─ Glycerol-3-phosphate acyltransferase

Dgat1 ─ Diacylglycerol O-acyltransferase 1

Dgat2 ─ Diacylglycerol O-acyltransferase 2

Agpat1 ─ 1-acylglycerol-3-phosphate O-acyltransferase 1

Agpat2 ─ 1-acylglycerol-3-phosphate O-acyltransferase 2

CHAPTER I:

Introduction

This chapter contains materials that are reprinted with permission from the *Cold Spring Harbor perspectives in biology* article:

mTOR-dependent cell survival mechanisms. (2012) *Cold Spring Harbor perspectives in biology* 4 (12), a008771 (Charpter).

The Obesity Pandemic Is a Global Health Issue

Treating obesity and obesity-related disease are among the greatest health challenges around the world. It is not only a huge threat to human health and but also a burden for society and health care. Obesity is now viewed as a chronic disease and its comorbidities often includes coronary heart disease, high blood pressure, type II diabetes and certain types of cancer (Bornfeldt and Tabas, 2011). Excessive weight gain is mainly caused by long-term intake of excess energy and to a lesser extent by reduced physical activity. However, treatment or interventions that can reverse the obese state are limited and often lack long-term efficacy. One possible therapeutic strategy is to induce "negative energy balance", which can be achieved by decreasing energy intake and/or increasing energy expenditure. Accordingly, efforts focused on understanding molecular, biochemical and physiological mechanisms of whole body energy homeostasis have been made, which could ultimately lead to novel and effective therapies.

A Trio of Fat: White, Brown and Beige/Brite Adipocytes

Adipose tissue plays essential roles in maintaining whole body metabolic homeostasis, and its dysfunction contributes to the development and the progression of metabolic disease. There are two major classes of adipose tissue: white adipose tissue (WAT) and brown adipose tissue (BAT) (Figure 1.1). Most body fat mass is composed of white adipose tissue, which serves as the primary energy storage site in the body to accommodate excess nutrients and energy. WAT was long considered as metabolically inert, and its function was merely to release the stored energy during food deprivation.

On the contrary, it is now widely recognized that WAT has important endocrine functions linked to glucose and lipid homeostasis through release of adipokines (e.g., leptin and adiponectin) or non-peptide metabolites to communicate locally or with distant organs. For example, glucose intake in WAT drives activation of the *de novo* lipogenesis (DNL) pathway to produce palmitate, which is further modified by elongases and desaturases to generate diverse lipids. Some of lipid species, like C16:1n7-palmitoleate (Cao et al., 2008), when released to the circulation via lipolysis can stimulate insulin action on other tissues, such as liver and muscle. Moreover, carbohydrate-responsive element-binding protein β isoform (ChREBPβ) drives DNL gene expression in response to glucose flux (Herman et al., 2012). The abundance of *Chrebpβ* in human adipose tissue positively correlates with whole body insulin sensitivity (Eissing et al., 2013; Kursawe et al., 2013), supporting a role of adipose tissue in regulating systemic glucose homeostasis. In addition, WAT has a tremendous capacity to expand its mass by either increasing cell size (i.e., hypertrophy) or recruiting new adipocytes (i.e., hyperplasia) in overfeeding or sedentary lifestyles. This plasticity provides protection for other tissues from ectopic lipid accumulation and lipotoxicity. However, in obese or diabetic conditions, white adipocyte hypertrophy could lead to a vicious cycle with metabolic dysregulation, altered adipokine profiles, and chronic inflammation, which conversely drives the pathogenesis of metabolic disease.

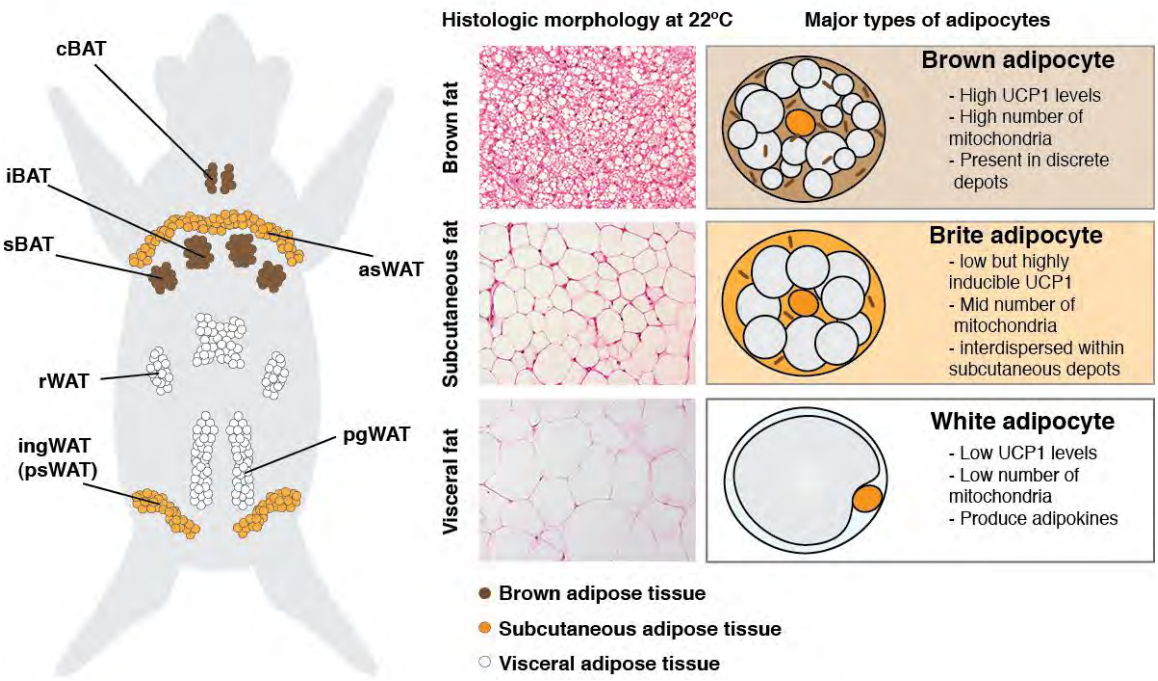

Figure 1.1 Major adipose tissue depots in mice

There are several discrete depots of Brown adipose tissue (BAT) which consists of brown adipocytes, including interscapular BAT (iBAT), subscapular BAT (sBAT), and cervical BAT (cBAT). According to their anatomical locations, white adipose tissue (WAT) can classified as subcutaneous fat or visceral fat. Anterior subcutaneous WAT (asWAT) and posterior subcutaneous WAT (psWAT or ingWAT) contain both white and brite adipocytes. Peri-gonadal WAT (pgWAT) is a major depot of visceral fat and it mostly consists of white adipocytes.

In contrast, BAT is able to dissipate energy into the form of heat through the process called non-shivering thermogenesis (Cannon and Nedergaard, 2011), which contributes to thermoregulation. Brown adipocytes contain many features that distinguish them from white adipose adipocytes, including multilocular lipid droplets, more abundant mitochondria with a high amount of uncoupler protein 1 (UCP1). UCP1,which belongs to the family of mitochondrial anion carrier protiens, embeds in the inner membrane of mitochondria. Biophysical studies showed UCP1 is normally kept inactive owing to the presence of purine nucleotides (ATP or GDP) (Nicholls, 2006). In general, cold exposure potently stimulates BAT thermogenesis through the sympathetic nerve system (SNS) (Figure 1.2). Catecholamines, particularly norepinephrine, released from sympathetic neurons activate the β_3-adrenergic receptor (β-AR) signaling cascades of brown adipocytes, including cyclic AMP production and protein kinase A (PKA) activation. The β-AR-induced PKA signaling subsequently activates p38-MAPK (mitogen-activated protein kinases) and transcription factors that are required for the induction of thermogenic gene program, including *Ucp1* and *Peroxisome proliferator-activated receptor gamma coactivator 1-alpha* (*Pgc1α*). Simultaneously, the PKA signaling also triggers lipolysis that breaks down intracellular triglycerides to liberate free fatty acids (FAs), which serve not only as the fuel for thermogenesis but also as allosteric activators for UCP1 activity (Fedorenko et al., 2012). The activated UCP1 facilitates proton movement across the mitochondrial inner membrane, thereby dissipating chemical energy generated by mitochondrial respiration in the form of heat. In rodents, it is estimated that fully-activated BAT could increase whole body energy expenditure by up

to ~60% over basal metabolic rate (Foster and Frydman, 1978). Thus, harnessing the potential of UCP1-mediated thermogenesis has become an attractive strategy that could enhance energy expenditure in humans to fight against obesity and its comorbidities.

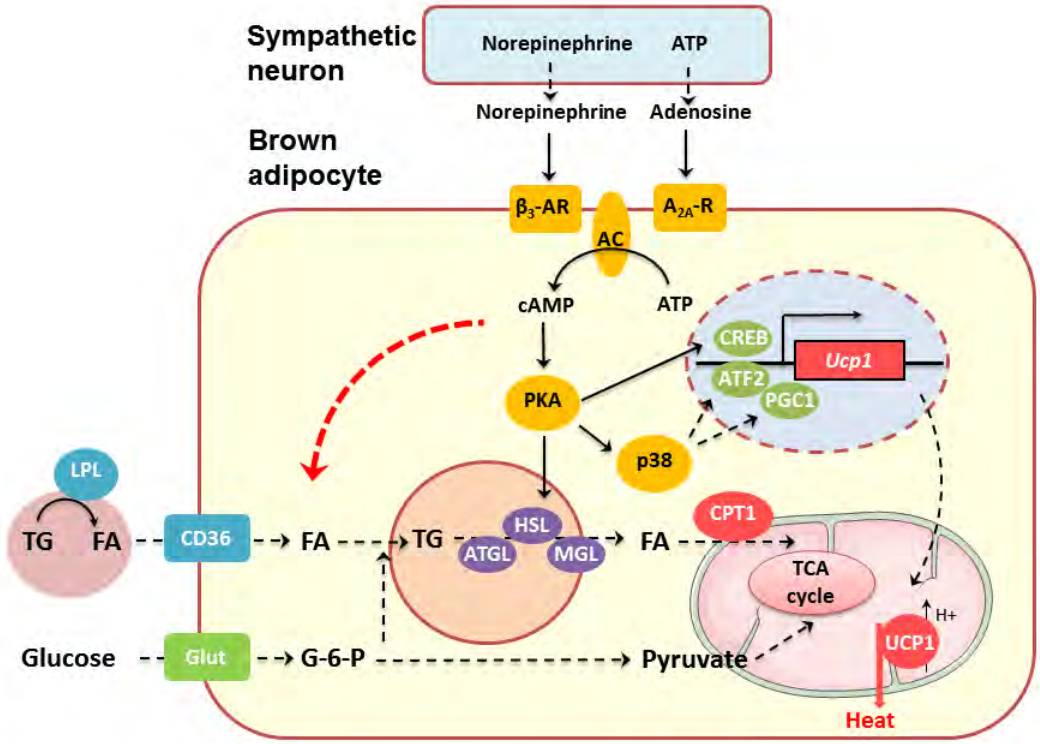

Figure 1.2 A schematic representation of BAT activation
BAT is highly innervated by the sympathetic neuron system (SNS). Upon cold exposure, the hypothalamus intergates sensory signals and activates SNS. Norepinepherin and ATP, which is then converted into adenosine, released from sympathetic neuron terminals stimulates the β_3-adrenergic receptor and the adenosine receptor 2A. Both receptors subsequently activates adenylyl cyclase (AC), which produces cAMP. PKA is then activated by increased levels of cAMP and plays dual roles in BAT thermogenesis: (1) promotes lipolysis through activating hormone-sensitive lipase (HSL); (2) activates the p38-MAPK signaling and transcription factors involved in *Ucp1* expression. In chronic BAT activation, the intracellular triglyceride (TG) is restored via fatty acids uptake which depends on

lipoprotein lipase (LPL) activtiy and CD36 (FA transporter) and via glucose uptake through the *de novo* lipogenesis pathway.

More recent studies have discovered a different class of thermogenic adipocytes called beige adipocytes or brite (brown-in-white) adipocytes (Cousin et al., 1992; Young et al., 1984). Unlike brown adipocytes, beige/brite adipocytes develop postnatally and express low basal levels of UCP1. These cells are normally interspersed within white adipose tissue and are characteristically indistinguishable from white adipocytes. Their development and activity are induced in response to various physiological conditions and environmental cues, including chronic cold stress, exercise, cytokines (e.g., FGF-21) and several insulin-sensitizing reagents (Inagaki et al., 2016). This recruitment process is usually termed "browning" of white adipose tissue, which mainly happens in subcutaneous WAT (sWAT) in rodents. Interestingly, trauma and some disease states, such as severe burns and cancer cachexia, also induce browning of WAT by increasing serum levels of cytokines and catecholamines (Petruzzelli et al., 2014; Sidossis et al., 2015; Tsoli et al., 2012). However, the functional significance and physiological relevance of beige/brite adipocytes in different physiologic states are still under investigation.

Human BAT and Its Physiological Relevance

Evolutionarily, brown fat thermogenesis is conserved in small mammals and hibernating animals to fight hypothermia. In humans, brown fat exists in the interscapular region of infants and shares molecular features and characteristics with brown adipocytes in rodents (Lidell et al., 2013). Until recently it was widely assumed that adult humans lack significant brown fat deposits. This view changed in early 2000 when radiologists reported the existence of brown fat in human adults by using the ^{18}F-fluoro-2-deoxy-D-glucose (^{18}F-FDG) positron emission tomography (Hany et al., 2002). Several landmark papers later confirmed some adult human fat exhibits BAT characteristics (Cypess et al., 2009; Lichtenbelt et al., 2009; Saito et al., 2009; Virtanen et al., 2009), thereby inspiring the idea that activating thermogenic fat in humans could be a strategy to fight obesity. The fact that brown fat activity is negatively associated with BMI (Cypess et al., 2009; Lichtenbelt et al., 2009) further supports the notion. Moreover, administration of a β_3-adrenergic agonist to humans significantly increases resting metabolic rate by 13% (Cypess et al., 2015). Recently, several studies reported that adult human BAT depots are mainly composed of beige/brite adipocytes (Sharp et al., 2012; Shinoda et al., 2015; Wu et al., 2012). However, other groups also found classical brown adipocytes in the deep cervical region (Cypess et al., 2013; Jespersen et al., 2013; Xue et al., 2015). Thus the prevalence of classic brown or brite/beige fat in human is currently under debate. Importantly, because people typically live in thermoneutral conditions, the distinction between ‘brown’ and ‘brite’ may be difficult to make. Thus, understanding both brown

and beige/brite adipocyte biology in mice is of equal interest at present.

Brown Fat Fuel Utilization and Thermogenesis

Active brown fat imports glucose and fatty acids (FAs) from circulation to sustain the metabolic demand of thermogenesis. This high metabolic rate provides the basis for using BAT as a therapeutic target to treat diabetes, hyperdyslipidemia, cardiovascular disease and other metabolic syndromes. During cold exposure, genes involved in glucose metabolism, *de novo* lipogenesis, lipid uptake and FA oxidation are accordantly upregulated in BAT as part of cold adaption (Yu et al., 2002). However, exactly how anabolic and catabolic pathways, especially lipogenesis and lipid oxidation, are tightly regulated by different physiological states remains to be elucidated. As mentioned above, fatty acids are the primary fuel source for BAT thermogenesis. When BAT is activated, intracellular triglycerides (TGs) are preferentially utilized via lipolysis. Concurrently, cold exposure drastically increases clearance of plasma triglyceride-rich lipoproteins, which is dependent on LPL activity and CD36 (FA transporter) (Bartelt et al., 2011). After being internalized, FAs are further re-esterified for oxidation or for the synthesis of TGs. Numerous studies employing genome-wide gene expression profiles have revealed that genes involved in handling glucose metabolism are extensively upregulated in cold-activated BAT (Hao et al., 2015). First, glucose transporters, Glut1 and Glut4, are highly induced after cold exposure (Bartelt et al., 2011), while β_3-adrenergic signaling also stimulates their translocation to the plasma membrane (Shimizu et al., 1998). Second, although glycolysis is highly upregulated, glucose oxidation by mitochondria is restricted

because of increased levels of Pdk2 and Pdk4. Third, glucose flux is directed to the pentose phosphate pathway, which provides reducing equivalents (NAPDH) for de novo fatty acid synthesis. Fourth, glycerol synthesis from glucose is also elevated to facilitate de novo lipid synthesis and FA re-esterification. Thus, it is clear that glucose is not primarily used as fuel source in thermogenesis but rather replenishes ATP demand and supports lipogenesis. In fact, it is estimated in one study that intracellular TG pools could contribute up to 80% of respiration in acute or chronic cold conditions (Labbe et al., 2015). Nonetheless, the signaling circuits and molecular mechanisms that orchestrate these metabolic pathways during BAT activation are not entirely understood.

mTOR Signaling: a Master Regulator of Cell Metabolism

The mechanistic target of rapamycin (mTOR) kinase is a master regulator of growth that functions in two distinct complexes called mTORC1 (defined by the Raptor subunit) and mTORC2 (defined by the Rictor subunit) (Figure 1.3). Given the importance of the mTOR signaling pathway in cellular metabolism and growth, it was not clear whether the two mTOR complexes have distinct roles in controlling tissue development *in vivo*. mTORC1 integrates systemic growth factor signaling and local nutrient availability to coordinate activity of a multitude of anabolic processes, including proteins, nucleotides and lipid biosynthesis (Figure 1.3). In general, growth factors activate mTORC1 through a well-characterized signaling cascade, including PI3K and AKT, to inhibits the TSC1/TSC2 complex (Manning et al., 2002). TSC complex negatively regulates mTORC1 via inhibiting its activator, Rheb-GTPase (Castro et al., 2003; Inoki et al.,

2003a; Tee et al., 2003; Zhang et al., 2003). Also, inhibitory signals such as energy deprivation can activate TSC complex through the AMP-activated protein kinase (AMPK) to suppress mTORC1 activity (Inoki et al., 2003b; Shaw et al., 2004). On the other hand, mTORC1 is also sensitive to certain amino acids through TSC complex-independent pathways [reviewed in (Efeyan et al., 2015)]. The best-known function of mTORC1 in controlling growth is to directly phosphorylate two regulators of protein translation, p70-S6 kinase1 (S6K1) and 4E binding protein 1 (4E-BP1). mTORC1-dependent phosphorylation of S6K at T389 activates its kinase activity toward several substrates involved in mRNA maturation and protein translation. Recently, several new substrates of mTORC1 have been identified and characterized. For example, mTORC1 also negatively regulates autophagy through the direct phosphorylation of Unc-51-like kinase (ULK1) (Ganley et al., 2009; Hosokawa et al., 2009; Jung et al., 2009). Lipin1, which regulates lipid metabolism through SREBP1, is also directly phosphorylated by mTORC1 (Peterson et al., 2011). In addition, mTORC1 also controls the growth factor receptor-bound protein 10 (Grb10) as a part of a negative feedback loop towards insulin receptor signaling (Hsu et al., 2011; Yu et al., 2011).

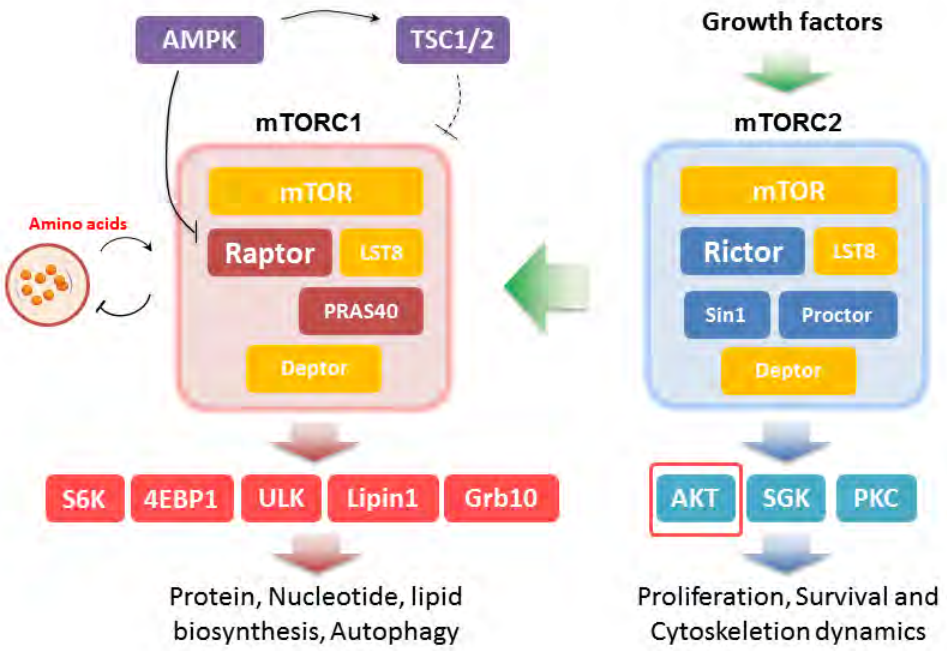

Figure 1.3 The mTOR Signaling Pathway
mTOR kinase exists in two distinct complexes: mTORC1 and mTORC2. Each of these complexes shares some common components but also contains unique proteins. Growth factor signaling activates mTORC2 which then phosphorylates it substrates, including AKT, SGK, and PKC. AKT promotes mTORC1 activation via inhibiting the TSC1/2 complex, which is a negative regulator of mTORC1. In addition, energy-sensing AMPK signaling also negatively regulates mTORC1. There are also other signals that can affect mTORC1 signaling, such intracellular amino acid levels. Several mTORC1 substrates have been discovered, including S6K, 4EBP-1, ULK, Lipin1, and Grb10.

Although much is known about the inputs, outputs, and regulatory features of mTORC1, mTORC2 regulation and function remains more enigmatic (Figure 1.4). The best-described biochemical function of mTORC2 is to phosphorylate the hydrophobic motif (HM) of AKT (S473 in AKT1) and the related SGK (S422 in SGK1) kinases (Garcia-Martinez and Alessi, 2008; Sarbassov et al., 2005). AKT has many effectors including GSK3β, FoxO1/3, and mTORC1 (through TSC2 and PRAS40), and most models indicate mTORC2 is an essential upstream regulator of pan-AKT activity (Laplante and Sabatini, 2012). However, Rictor-deficient mouse embryo fibroblasts (MEF), which lack mTORC2, have seemingly normal GSK3β phosphorylation, mTORC1 activity, and only partially decreased FoxO1/3 phosphorylation (Guertin et al., 2006; Jacinto et al., 2006; Shiota et al., 2006). It was later elegantly shown *in vitro* that AKT-S473 phosphorylation (i.e. the mTORC2 site) is only partially required for the PDK1-regulated AKT-T308 phosphorylation site (Najafov et al., 2012), which is thought to be essential for AKT activation (Figure 1.4). Therefore, the requirement of mTORC2 activity for AKT functions *in vivo* remains elusive.

Mice lacking Rictor die around embryonic day 10.5 (E10.5) (Guertin et al., 2006; Jacinto et al., 2006; Shiota et al., 2006); therefore, mTORC2 function *in vivo* is mostly investigated by using conditional knockout models (Cre-LoxP recombination). In adipose tissue, two studies using *aP2* (*adipocyte protein 2* or called *Fabp4*) *-cre* to delete Rictor reported no effect on individual adipocyte size or overall adipose tissue mass (Cybulski et al., 2009; Kumar et al., 2010). One of the studies finds *aP2-cre;Rictor* mice eventually develop mild glucose intolerance and ectopic lipid deposition, although a

mechanism was not elucidated (Kumar et al., 2010). However, the specificity of *aP2-cre* to target adipocytes has recently been questioned (Lee et al., 2013; Mullican et al., 2013; Wang et al., 2013); therefore, the exact function of mTORC2 in adipose tissue remains unclear. Deleting *Rictor* in skeletal muscle with *Hsa* (*human α-skeletal actin*)-*cre* or *Mck* (*muscle creatine kinase*)-*cre* also has no effect on muscle fiber size or overall muscle mass and only minor effects on insulin-mediated glucose metabolism (Bentzinger et al., 2008; Kumar et al., 2008). These relatively mild phenotypes are somewhat surprising considering the importance of AKT signaling in metabolism; however, in both cases (adipose tissue and muscle), the Cre drivers are only active in mature tissues. On the contrary, the *in vivo* role of mTORC2 in regulating tissue-specific precursor cells is almost unknown.

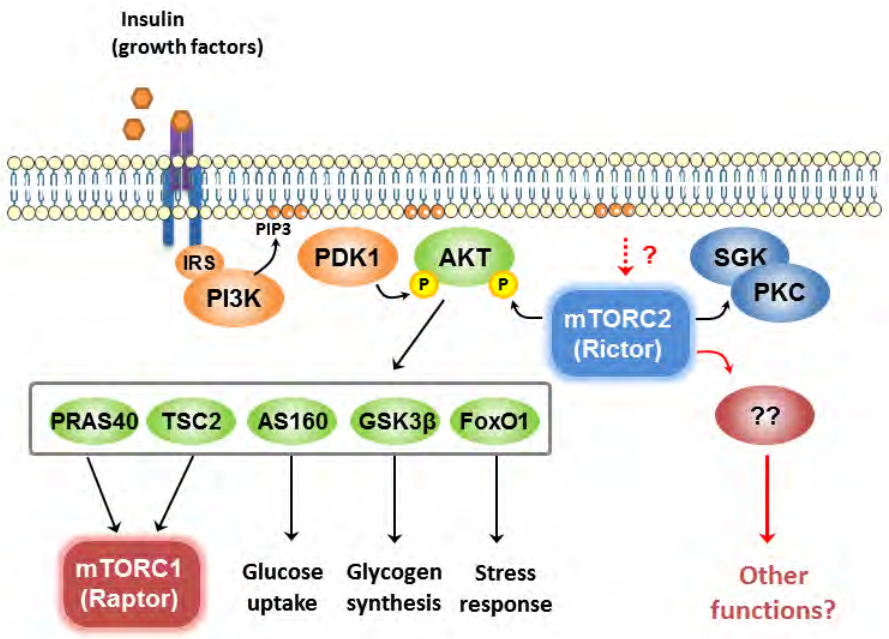

Figure 1.4 Overview of the mTOR2 Signaling Pathway
Schematic showing the key signaling molecules in the mTOR signaling pathway. In this work, the in vivo role of mTORC2 will be extensively examined by multiple approaches. The mechanisms underlying mTORC2-mediated metabolism changes will also be discussed.

Downstream of the phosphoinositide 3-kinase (PI3K)-AKT signaling pathway (Figure 1.4), Forkhead box O (FoxO) family transcription factors (FoxO1, FoxO3, and FoxO4) regulate multiple target genes involved in various cellular processes, including apoptosis, stress resistance, proliferation and metabolism. Growth factors and other hormones negatively regulate FoxO activity through inhibitory phosphorylation mediated by AKT. This phosphorylation recruits 14-3-3 protein binding and prevents its nuclear localization, thus inhibiting FoxO transcriptional activity. While it is generally accepted that FoxO activity is predominantly controlled by the PI3K-AKT signaling, FoxO is also modulated by other kinases, including p38-MAPK, extracellular signal–regulated kinases (ERKs) and c-Jun N-terminal kinases (JNKs), and by various post-translational modifications, such as acetylation and methylation. In skeletal muscle, FoxO proteins are characterized to drive muscle atrophy through upregulating genes involved in proteolysis and lysosomal autophagy pathways (Mammucari et al., 2007; Zhao et al., 2007). On the other hand, FoxO1 was shown to negatively regulate adipocyte differentiation (i.e. precursor cells develop into lipid-enriched mature adipocytes) by interfering with peroxisome proliferator-activated receptor gamma (PPARγ). Accumulating evidence has suggested that FoxO proteins are an important downstream mediator of mTORC2 function (Guertin et al., 2006; Hagiwara et al., 2012; Masui et al., 2013). However, the mechanisms by which mTORC2 controls FoxOs *in vivo* remain largely elusive.

In this dissertation, one major goal is to elucidate the role of mTORC2 in metabolic tissues, especially adipose tissue and skeletal muscle. I first hypothesized that mTORC2 could have a role in tissue stem/precursor cells to control development and

growth. In Chapter II, the study (Hung et al., 2014) was designed to test this hypothesis by using a model with mTORC2 specifically eliminated in mesenchymal *Myf5 (myogenic factor 5)*+ precursors, which give rise to muscle, brown adipose and some white adipocytes. To our surprise, mTORC2 activity seems to be dispensable for muscle development and regeneration. However, I discovered that mTORC2 promotes adipocyte differentiation *in vitro* and adipose tissue growth *in vivo*. Regardless of some caveats, there is evidence showing that mTORC2 plays a critical role in regulating lipid metabolism and mitochondria activity in brown adipose tissue (BAT). In particular, mTORC2-deficient BAT displays an enhancement in thermogenic function.

The insulin/growth factor signaling pathway activates the mTOR complexes which promote anabolic pathways, including lipid biosynthesis, in adipocytes. In contrast, epinephrine or norepinephrine normally stimulates catabolic processes, such as lipid breakdown and oxidation. While the insulin and catecholamine-induced signaling pathways seem to regulate opposing functions, crosstalk and feedback regulation between these two pathways have been discovered (Figure 1.5). Based on the findings in Chapter II, I further hypothesized that mTORC2 could be a key regulator in controlling BAT metabolism and thermogenesis downstream of insulin and catecholamine-induced signaling. This was further tested in a second study presented in Chapter III by using brown fat-specific Cre drivers (Cre recombinase regulated by the promoter of *Ucp1* gene) to activate gene deletion in mature brown adipocytes. To summarize, I find that the mTORC2 signaling is critical in modulating BAT thermogenic program by regulating FoxO1. Interestingly, this branch of mTORC2 signaling works through AKT-

independent mechanisms that involve the regulation of FoxO1 acetylation levels. Importantly, mice with BAT-specific mTORC2 inhibition are more resistant to diet-induced obesity at thermoneutral conditions, presumably due to increased brown fat activity. Collectively, the specific role of mTORC2 in BAT have been thoroughly examined by a series of *in vivo* and *in vitro* models in this work, which could provide some advances in understanding brown fat biology for future studies.

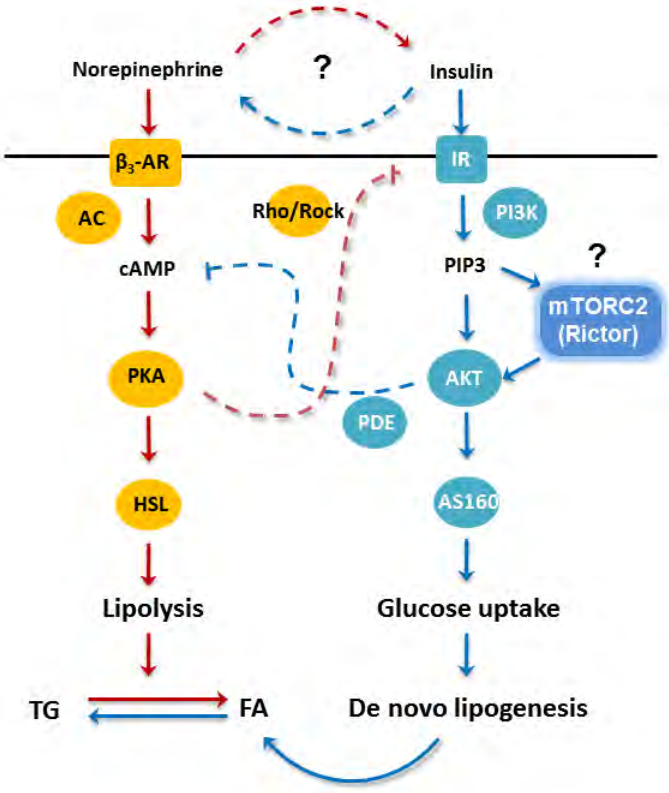

Figure 1.5 Crosstalk between the Insulin Signaling Pathway and the β-Adrenergic Signaling Pathway
In brown adipocytes, insulin signaling and norepinephrine-stimulated β-adrenergic signaling have opposing or synergic effects on each other. Insulin signaling promotes glucose uptake and *de novo* lipogenesis through AKT activity, which also negatively regulates intracellular cAMP levels through PDE3b (Phosphodiesterase 3b) activity. On the other hand, β-adrenergic signaling stimulates lipolysis via

cAMP-dependent PKA pathway. PKA can inhibit insulin receptor activation through Rho/ROCK.

CHAPTER II:

Rictor/mTORC2 Loss in the Myf5 Lineage Reprograms Brown Fat Metabolism and Protects Mice against Obesity and Metabolic Disease

This chapter contains materials that are reprinted with permission from the *Cell Reports* article:

Chien-Min Hung, Camila Martinez Calejman, Joan Sanchez-Gurmaches, Huawei Li, Clary B. Clish, Simone Hettmer, Amy J. Wagers, David A. Guertin.

Rictor/mTORC2 loss in the Myf5 lineage reprograms brown fat metabolism and protects mice against obesity and metabolic disease. *Cell Reports* 8 (1), 256-271

Author contributions:
C.-M.H. and D.A.G. designed the project and wrote and edited the manuscript.
C.-M.H. performed most experiments, and D.A.G. assisted in analysis and interpretation.
C.M.C., J.S.-G., and H.L. assisted with rescue, lineage tracing, and mouse experiments.
C.B.C. performed metabolite profiling. S.H. and A.J.W. assisted with muscle experiments

Summary

The in vivo functions of mechanistic target of rapamycin complex 2 (mTORC2) and the signaling mechanisms that control brown adipose tissue (BAT) fuel utilization and activity are not well understood. Here, by conditionally deleting Rictor in the Myf5 lineage, we provide in vivo evidence that mTORC2 is dispensable for skeletal muscle development and regeneration but essential for BAT growth. Furthermore, deleting Rictor in Myf5 precursors shifts BAT metabolism to a more oxidative and less lipogenic state and protects mice from obesity and metabolic disease at thermoneutrality. We additionally find that Rictor is required for brown adipocyte differentiation in vitro and that the mechanism specifically requires AKT1 hydrophobic motif phosphorylation but is independent of pan-AKT signaling and is rescued with BMP7. Our findings provide insights into the signaling circuitry that regulates brown adipocytes and could have important implications for developing therapies aimed at increasing energy expenditure as a means to combat human obesity.

Introduction

Adipose tissue is essential for many biological processes, and its dysfunction, for example in obesity, is associated with a growing spectrum of human diseases. Thus, understanding the developmental and metabolic regulation of adipose tissue has broad clinical implications. There are two main classifications of adipose tissue: white adipose tissue (WAT) and brown adipose tissue (BAT). WAT is the major energy storage site in

the body and has critical endocrine functions (Gesta et al., 2007), whereas BAT dissipates energy as heat in a process called nonshivering thermogenesis (Cannon and Nedergaard, 2004). BAT is particularly important in small rodents and newborn humans to defend against cold exposure, and its functional relevance in adult humans was only recently appreciated (Cannon and Nedergaard, 2010; Tseng et al., 2010). Brown adipocytes are thermogenic because they express uncoupling protein 1 (UCP1), which embeds in the inner mitochondrial membrane and produces heat by uncoupling oxidative metabolism from ATP production. The energy expending properties of brown adipocytes coupled with the observation that human BAT amount inversely correlates with body fat mass is garnering interest in developing strategies to increase brown adipocyte number and/or activity to treat obesity. However, the mechanisms, and in particular the signaling circuitry, by which BAT regulates its energy supply are poorly understood (Townsend and Tseng, 2014). With the obesity pandemic seemingly out of control, and with a desperate need for novel therapeutics, the importance of elucidating mechanisms controlling adipocyte growth and function cannot be overstated.

Studying the in vivo mechanisms of adipose tissue growth has been challenging because adipocyte origins are poorly understood, and consequently few tools are available for genetically targeting adipocyte precursors in vivo (e.g., by Cre-Lox). Lineage tracing studies indicate early mesenchymal precursor cells expressing Myf5 give rise to myocytes, brown adipocytes, and a subset of white adipocytes (Sanchez-Gurmaches and Guertin, 2014b; Sanchez-Gurmaches et al., 2012; Seale et al., 2008), and several recent studies have used the *Myf5-Cre* knockin allele (Tallquist et al., 2000) to

study BAT development (Harms et al., 2014; Ohno et al., 2013; Sanchez-Gurmaches et al., 2012; Schulz et al., 2013). Thus, the multi-fate potential of Myf5 precursors provides an opportunity to use genetics to distinguish between signaling mechanisms that are required in vivo for the growth of myocytes versus adipocytes.

Here, we take advantage of the fact that *Myf5-Cre* expresses in precursors of muscle and brown adipocytes to investigate the role of Rictor (i.e., mTORC2) and for comparison Raptor (i.e., mTORC1) in muscle and BAT growth. We report that Raptor is essential in the *Myf5* lineage for myogenesis, establishing BAT precursors, and viability. In contrast, Rictor is dispensable for myogenesis and viability but essential for normal BAT growth. Moreover, Rictor-deficient BAT is more metabolically active, having elevated mitochondrial activity and decreased lipogenesis. Importantly, deleting Rictor in the *Myf5* lineage also augments diet-induced thermogenesis, which protects mice from an obesogenic diet at thermoneutrality. We additionally find that *Myf5*-lineage white adipocytes require Rictor for normal growth in vivo, suggesting a broader role for mTORC2 in adipose tissue development. Finally, we show that Rictor is also required in vitro for brown adipocyte differentiation, but not for pan-AKT activity, and that this differentiation defect is rescued with BMP7. Collectively, our results provide insight into the regulation of brown adipocytes and implicate Rictor/mTORC2 as a critical signaling node that balances oxidative and lipogenic metabolic states.

Results

Rictor Is Dispensable in the *Myf5* Lineage during Embryogenesis

We investigated the role of mTORC1 versus mTORC2 in vivo in fat versus muscle development by generating *Myf5-Cre;Raptorfl/fl* (*Raptor*^{Myf5cKO}) and *Myf5-Cre;Rictorfl/fl* (*Rictor*^{Myf5cKO}) conditional knockout (KO) mice. The *Rictor*^{Myf5cKO} mice are born at the expected Mendelian ratio and show no obvious motor or behavioral defects (data not shown). In contrast, *Raptor*^{Myf5cKO} mice die perinatally. E16.5 *Raptor*^{Myf5cKO} embryos are smaller due to a muscle development defect that is not apparent in control or *Rictor*^{Myf5cKO} embryos (Figure 2.1A-D). Transverse sections through the head and neck of *Rictor*^{Myf5cKO} embryos reveal an underdeveloped tongue and the absence of the masseter, sternohyoid, hyglossus, supraspinatus, prevertebral, and trapezius muscles, the later deficiency resulting in hindneck body-wall fragility during specimen preparation (Figure 2.1A-D). Thus, *Raptor* is essential in the *Myf5* lineage for viability and muscle development, whereas *Rictor* is dispensable for both.

To confirm that *Rictor* is dispensable for myogenesis, we purified satellite cells (which express *Myf5*) from *Rictor*^{Myf5cKO} skeletal muscles, confirmed they are deleted for *Rictor* (Figure 2.1E), and show they differentiate ex vivo into myosin heavy chain-positive multinucleate myofibers (Figure 2.1F and 2.1G). Moreover, deleting *Raptor* in satellite cells in vivo with *Pax7-CreER* blocks skeletal muscle repair, whereas deleting *Rictor* by the same approach does not prevent muscle regeneration following acute injury

(Figure 2.1H and 2.1I). Thus, Rictor is also dispensable for satellite cell differentiation ex vivo and for adult myogenesis induced by injury.

WATs develop postpartum in mice, but early brown adipocyte precursor cells (bAPCs) are detectable in E16.5 embryos by hematoxylin and eosin (H&E) staining. Qualitatively similar pools of cervical, interscapular, and subscapular bAPCs are detectable in control and *Rictor*^{Myf5cKO} E16.5 embryos (Figure 2.1A-D). In contrast, interscapular and subscapular bAPCs are absent in E16.5 *Raptor*^{Myf5cKO} embryos (Figures 2.1A-D). Notably, a diminished pool of cervical bAPCs is detectable in the *Raptor*^{Myf5cKO} embryos consistent with our lineage tracing data showing that only about half of the cervical brown adipocytes arise from *Myf5*-*Cre*-expressing precursors (Figure 2.1D) (Sanchez-Gurmaches and Guertin, 2014). Thus, Raptor, but not Rictor, is also essential in the Myf5 lineage for establishing bAPCs during embryogenesis.

Brown and White Adipose Tissue Growth Requires *Rictor*

Although *Rictor*^{Myf5cKO} mice show no obvious embryonic phenotypes, they tend to weigh less (not significantly) than controls at postnatal day 1 (P1) (Figure 2.1J), which reaches significance from 6 to 15 weeks of life (Figure 2.2A). Individual tissue analysis indicates that the weight difference results from decreased adipose tissue mass. For example, the interscapular BAT (iBAT) in P1 *Rictor*^{Myf5cKO} neonates weighs about 30% less than normal (Figure 2.1K), and during the first weeks of life, the mutant BAT grows but to a much smaller size, resulting in mutant iBAT and subscapular BAT (sBAT) depots at 6

weeks that weigh about 50% less than controls and are darker (Figure 2.2B). Adipocytes in the retroperitoneal and anterior subcutaneous WAT depots (rWAT and asWAT, respectively) are also derived largely from *Myf5*-*Cre*-expressing precursors (Sanchez-Gurmaches and Guertin, 2014 and Sanchez-Gurmaches et al., 2012), and both of these depots also decrease in mass by approximately 50% in the $Rictor^{Myf5cKO}$ mice (Figure 2.2C). In contrast, the posterior subcutaneous and perigonadal WAT depots (psWAT and pgWAT, respectively), which are composed of *Myf5*-negative lineage adipocytes, do not differ in weight (Figure 2.2C). Skeletal muscles (e.g., triceps, quadriceps, and gastrocnemius) and all other lean tissues examined except the kidneys (which are slightly larger) are of normal size in the KO (Figure 2.2D). Western analysis for Rictor protein confirms Rictor deletion and reduced AKT-S473 phosphorylation in iBAT and muscle and, to a lesser extent, in rWAT and asWAT, but not in psWAT, pgWAT, or liver (Figure 2.2E).

From 6 weeks to 6 months, the mutant iBAT and sBAT show no additional growth increase, whereas asWAT and rWAT grow to about half (asWAT) or one-third (rWAT) the size of their anatomically matched control tissues (Figure 2.2F). In contrast, $Rictor^{Myf5cKO}$ psWAT, pgWAT, muscles, and liver grow to their normal size in the same time frame (Figure 2.2F). Thus, $Rictor^{Myf5cKO}$ mice can grow small BAT tissues in the first weeks of life; however, as $Rictor^{Myf5cKO}$ mice age, the iBAT and sBAT maintain their weight, whereas asWAT and rWAT grow at a reduced rate. Collectively, these results indicate Rictor is essential in the Myf5 lineage for adipose tissue growth, but not for skeletal muscle growth.

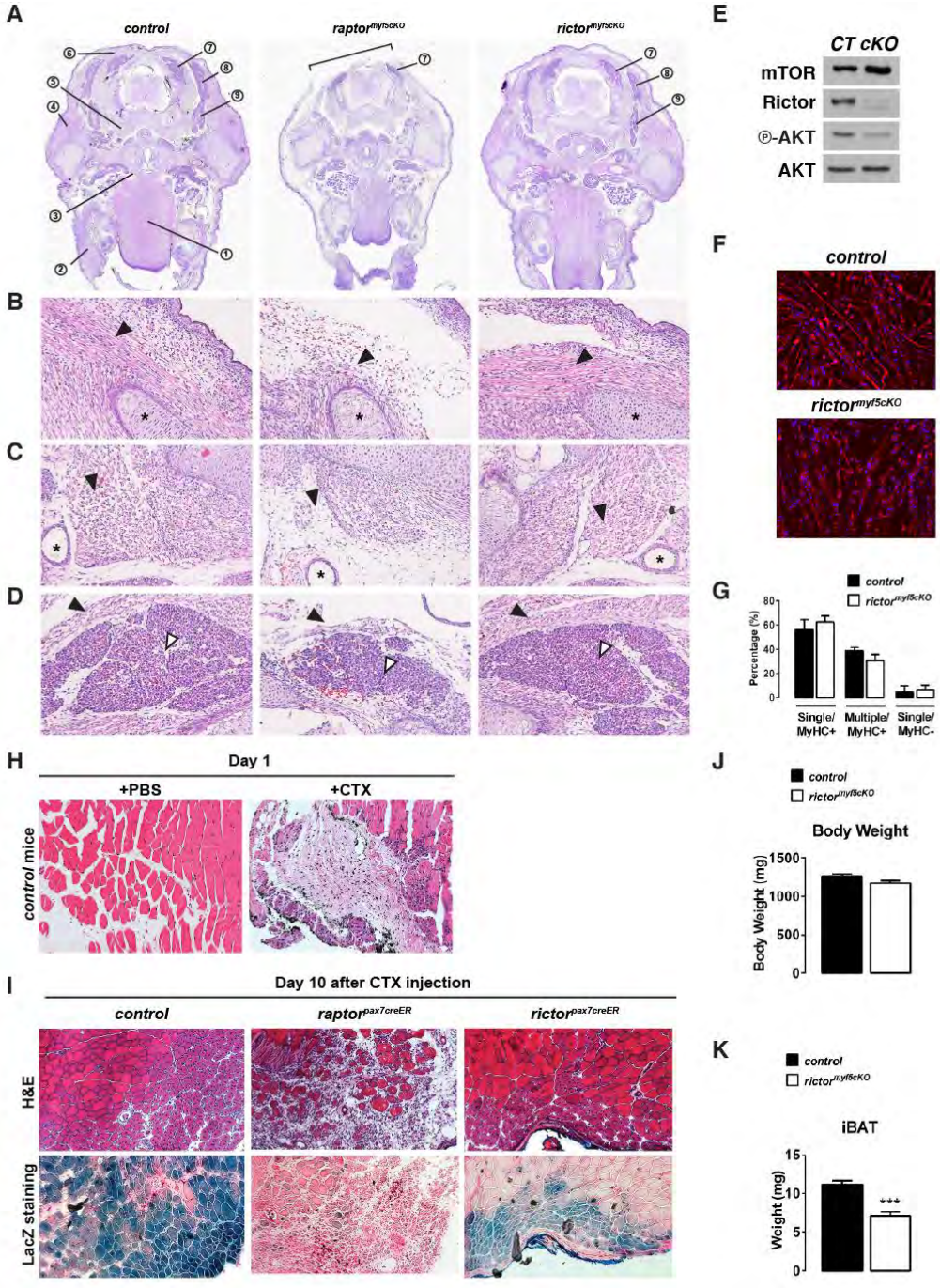
A
control
raptor myf5cKO
rictor myf5cKO
B
C
D
E
CT cKO
mTOR
Rictor
Ⓟ-AKT
AKT
F
control
rictor myf5cKO
G
control
rictor myf5cKO
Percentage (%)
Single/ MyHC+
Multiple/ MyHC+
Single/ MyHC-
H
Day 1
+PBS
+CTX
control mice
I
Day 10 after CTX injection
control
raptor pax7creER
rictor pax7creER
H&E
LacZ staining
J
control
rictor myf5cKO
Body Weight
Body Weight (mg)
K
control
rictor myf5cKO
iBAT
Weight (mg)
***

Figure 2.1 *Rictor* Is Dispensable in the Myf5 Lineage during Embryogenesis

(A) Transverse sections of E16.5 embryos. Tongue (1), masseter (2), sternohyoid and hyoglossus (3), supraspinatus (4), prevertebral (5), and trapezius muscles (7), and cervical BAT (7), interscapular BAT (8), and subscapular BAT precursors (9) are indicated. Bracket marks region of hind neck fragility. **(B)** Enlarged image of supraspinatus muscle (arrowhead). Ossifying cartilage of the scapula marked with (*). **(C)** Enlarged image of prevertebral muscles of the neck (arrowhead). Carotid artery marked with (*). **(D)** Enlarged image of trapezius muscle (closed arrowhead) and cervical BAT precursors (open arrowhead). **(E)** Western blots of satellite cell lysates from control (*CT*) and *Rictor*^{Myf5cKO} conditional knockout (*cKO*) mice. Phospho-S473 AKT antibody was used here. **(F)** Differentiated satellite cells stained with myosin heavy chain antibody. **(G)** Quantification of nuclei number in individual differentiated satellite cells. **(H)** H&E images of tibialis anterior (TA) muscle 1 day after PBS or cardiotoxin injection in control mice (see also supplementary methods). **(I)** Mice deleted for *Raptor* or *Rictor* specifically in satellite cells with *Pax7*-CreER were subjected to an acute cardiotoxin injury assay. Mice also carried the *Rosa26-LacZ* reporter to follow the deleted cells. H&E images and corresponding images for LacZ staining of TA muscle 10 days after cardiotoxin injection. Regenerated muscle cells in the control and *Rictor* KO are indicated by the centrally localized nuclei in H&E stained sections. No regenerated cells are detectable in the *Raptor* KO. **(J-K)** Total body weight (J) and average iBAT weight (K) at postnatal day 1 (n=6; bars represent mean ± SEM; t-test; ***p<0.001).

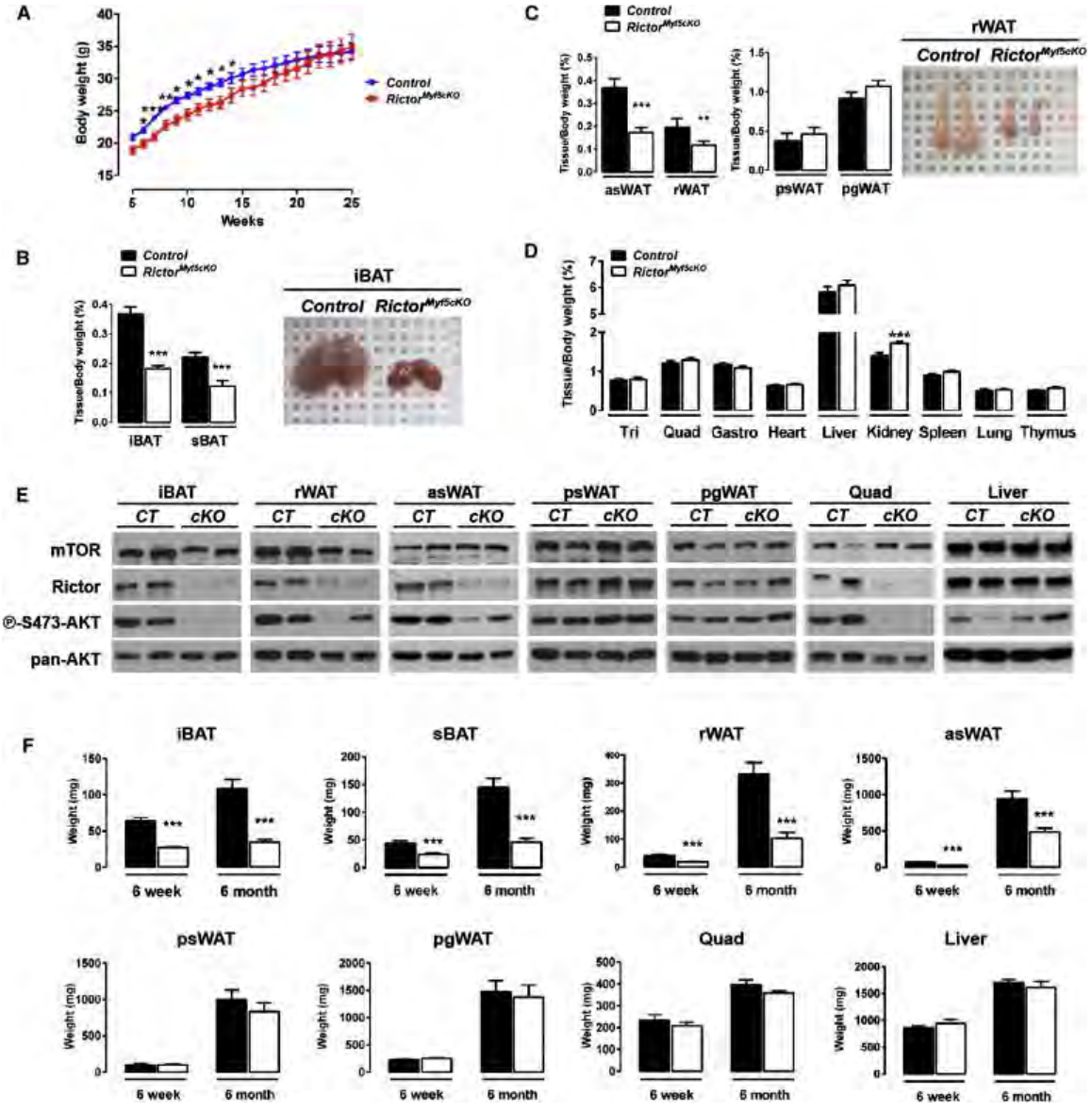
A
Body weight (g)
Weeks
Control
Rictor^Myf5cKO
B
Tissue/Body weight (%)
iBAT
sBAT
C
asWAT
rWAT
psWAT
pgWAT
D
Tri
Quad
Gastro
Heart
Liver
Kidney
Spleen
Lung
Thymus
E
iBAT
rWAT
asWAT
psWAT
pgWAT
Quad
Liver
CT
cKO
mTOR
Rictor
Ⓟ-S473-AKT
pan-AKT
F
sBAT
Weight (mg)
6 week
6 month

Figure 2.2 Postnatal Brown and White Adipose Tissue Growth Requires Rictor

(A) Growth curves (n = 13; bars represent mean ± SEM; t test; ∗p < 0.05, ∗∗p < 0.01, ∗∗∗p < 0.001). (B) BAT mass at 6 weeks (left) (n = 19–21; mean ± SEM; t test; ∗∗∗p < 0.001) and representative image (right). (C) Mass of WATs at 6 weeks (n = 14–16; mean ± SEM; t test; ∗∗p < 0.01, ∗∗∗p < 0.001) (left) and representative image of control and mutant rWAT (6 weeks) (right). (D) Lean tissue mass at 6 weeks (n = 15–19; mean ± SEM; t test; ∗∗∗p < 0.001). (E) Westerns of tissue lysates (6 weeks). (F) Average tissue mass (mg) at 6 weeks and 6 months (n = 14–21 for 6 weeks; n = 7 for 6 months; mean ± SEM; t test; ∗∗∗p < 0.001).

Brown Adipocytes Lacking Rictor Are Smaller

To better define the BAT growth defect, we histologically examined iBAT in control and *Rictor*^{Myf5cKO} mice. At E18.5, there is no qualitative difference between control and *Rictor*^{Myf5cKO} bAPCs pools (Figure 2.3A). In P1 neonates, however, lipids begin accumulating in control BAT, but not in the *Rictor*^{Myf5cKO} BAT (Figure 2.3A). From P1 to 6 months, lipid droplets grow in size in control BAT but remain small in the *Rictor*^{Myf5cKO} BAT (Figure 2.3A), resulting in smaller cells measured by the increase in nuclei per mm^2 (Figure 2.4A). Total genomic DNA content is also lower in the *Rictor*^{Myf5cKO} BAT, indicating additional hypoplasia (Figure 2.4B). In contrast, *Rictor*^{Myf5cKO} skeletal muscle fibers appear histologically identical to control fibers

(Figure 2.4C).

Myf5-Lineage White Adipocytes Lacking Rictor Are Also Small and Multilocular

Compared to controls, many adipocytes in the *Rictor*^{Myf5cKO} rWAT and asWAT are also smaller and multilocular (Figure 2.3B), but the pattern is heterogeneous in that several large unilocular white adipocytes are also detectable. The psWAT and pgWAT adipocytes appear unchanged in the KO (Figure 2.4C). The adipocyte precursor pools in rWAT and asWAT are a mix of *Myf5*-*Cre*-lineage-positive and negative precursors (Sanchez-Gurmaches et al., 2012). Therefore, we reasoned that the size heterogeneity in *Rictor*^{Myf5cKO} rWAT and asWAT could reflect a mosaic of *Myf5*-lineage-negative (i.e., undeleted) and *Myf5*-lineage-positive (i.e., Rictor KO) cells. To test this, we incorporated the Rosa26-mTmG reporter (Muzumdar et al., 2007) into control and *Rictor*^{Myf5cKO} mice to irreversibly label Cre-expressing cells and their lineages with membrane-targeted enhanced GFP (mGFP); all other (Cre^{neg}) cells and their descendants are labeled with membrane-targeted tdTomato fluorescent protein (mTFP). The result is unequivocal; only the small adipocytes are mGFP+ in *Rictor*^{Myf5cKO} rWAT and asWAT, whereas all the large unilocular adipocytes are mTFP+ (Figure 2.3C). As expected, in both the control and *Rictor*^{Myf5cKO} mice, the iBAT adipocytes are mGFP+ and the psWAT and pgWAT adipocytes are mTFP+ (Figure 2.4D). We also detect a slight increase in UCP1 staining in the *Rictor*^{Myf5cKO} adipocytes, suggesting the cells might have brown-adipocyte-like characteristics (Figure 2.4E) (not shown). These data confirm that the heterogeneous

small-cell phenotype results from cell-autonomous Rictor deletion in the *Myf5*-lineage white adipocytes.

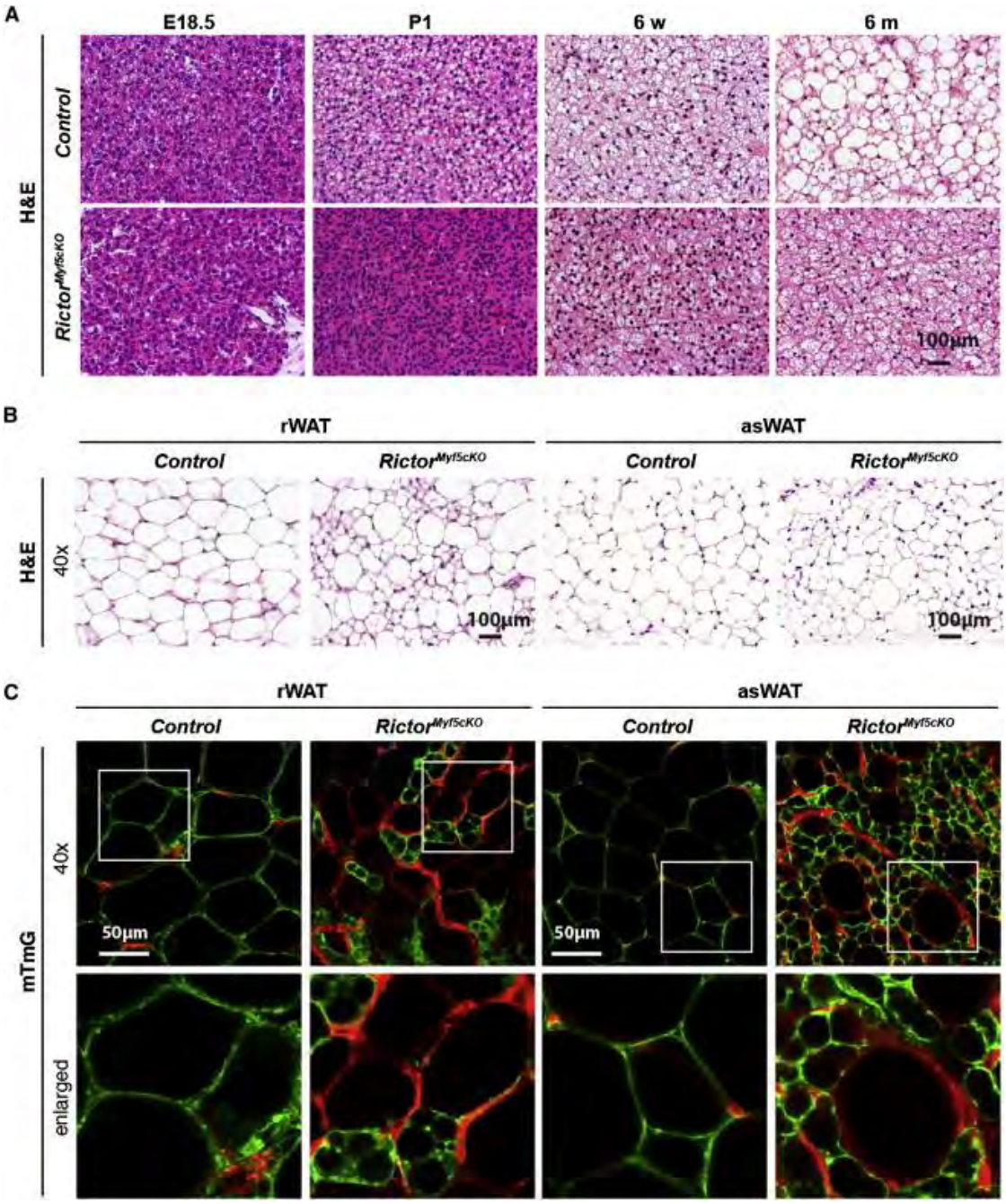

Figure 2.3 Brown and White Adipocytes Lacking Rictor Are Smaller and Multilocular

(A) H&E stains of interscapular BAT (6 weeks). (B) H&E stains of retroperitoneal and anterior subcutaneous WAT. (C) Representative images of mTFP- and mGFP-labeled adipocytes. Enlarged images indicated by white box.

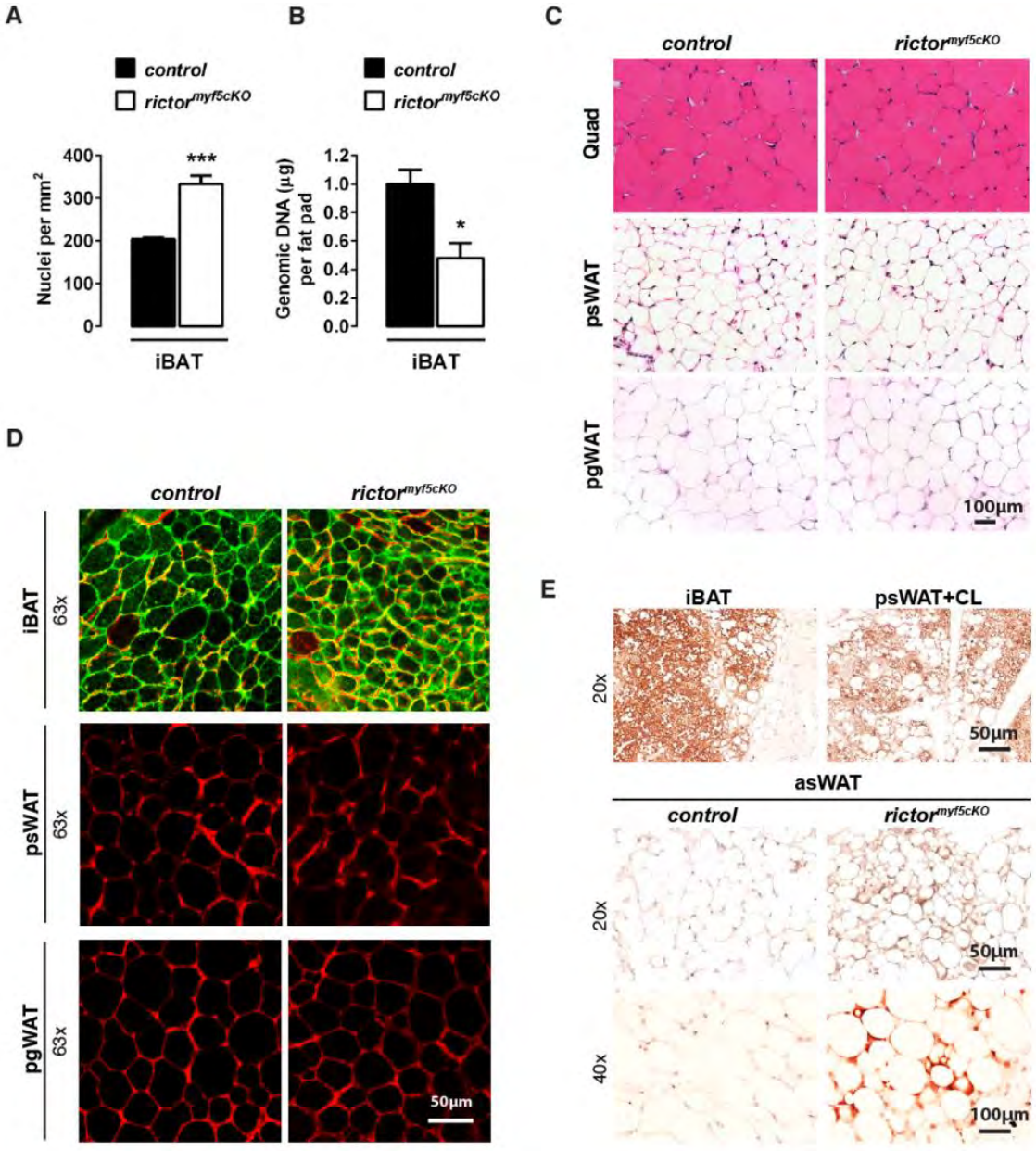
A
control
rictor myf5cKO
Nuclei per mm2
400
300
200
100
0
***
iBAT
B
control
rictor myf5cKO
Genomic DNA (µg) per fat pad
1.2
1.0
0.8
0.6
0.4
0.2
0.0
*
iBAT
C
control
rictor myf5cKO
Quad
psWAT
pgWAT
100µm
D
control
rictor myf5cKO
iBAT
63x
psWAT
63x
pgWAT
63x
50µm
E
iBAT
psWAT+CL
20x
50µm
asWAT
control
rictor myf5cKO
20x
50µm
40x
100µm

Figure 2.4 Small Adipocytes in asWAT of *Rictor*^{Myf5cKO} are UCP1+

(A) Nuclei density per mm2 of iBAT (6-wks) (n=4; bars represent mean ± SEM; t-test; ***p<0.001). (B) Qunatification of genomic DNA from iBAT (6-wks) (n=8; bars represent mean ± SEM; t-test; *p<0.05). (C) H&E stains (40x) of the quadricep (Quad) muscle and posterior subcutaneous (psWAT) and perigonadal (pgWAT) white adipose tissue (6-wks). (D) Representative images of mTFP and mGFP labeled iBAT, psWAT and pgWAT adipocytes. Note adipocytes are homogenously mGFP+ and smaller in the iBAT consistent with homogeneous Rictor loss in this tissue. (E) Top—UCP1 immunohistochemistry stains of iBAT and CL-316243 treated psWAT (20x). Botton—asWAT (20x and 40x) from control and RictorMyf5cKO mice.

Lipogenesis Is Decreased in Rictor-Deficient BAT

We hypothesized that the paucity of lipid and marked color difference between control and *Rictor*^{Myf5cKO} BAT indicates a shift from a lipogenic to oxidative state. To test this, we first examined AKT signaling in BAT, which positively regulates lipogenesis. In vivo AKT-T308 phosphorylation is intact in both fasted/refed and insulin-stimulated *Rictor*^{Myf5cKO} BAT despite ablation of pAKT S473 and pAKT T450 (which is also mTORC2 dependent) (Figures 2.5A and 2.6A), consistent with the ability of T-loop (T308) and hydrophobic motif (S473) phosphorylation to be regulated independently (Pearce et al., 2010). Surprisingly, phosphorylation of the AKT substrates FoxO1/3, GSK3β, TSC2, PRAS40, and AS160 is normal in *Rictor*^{Myf5cKO} BAT (Figure 2.5A), indicating Rictor is not essential in BAT for pan-AKT signaling. Rictor loss in BAT also does not affect phosphorylation of the SGK substrate NDRG1 (Figure 2.5A), indicating mTORC2 is not essential for SGK signaling to NDRG1 in BAT or that a compensatory pathway exists.

Next, we examined whether deleting Rictor in the *Myf5* lineage affects BAT differentiation markers. In P1 neonates, *Prdm16*, *C/ebpα*, and *C/ebpβ* expression do not differ between controls and KOs, whereas *Pparγ* and *Ucp1* levels slightly decrease (Figure 2.5B), indicating a possible delay in BAT maturation in the KOs. However, by 6 weeks, *Pparγ*, *Prdm16*, and *C/ebpα* express at control levels, whereas *C/ebpβ*, *Ucp1*, and *Dio2* express at significantly higher-than-control levels (Figure 2.5B). The mature adipocyte markers *Cidea* and *aP2* are unchanged between control and KO both at P1 and 6 weeks (Figure 2.5B). Consistent with the gene expression data, PPARγ, UCP1, and

insulin receptor beta (IRβ) proteins also express at near-control levels in *Rictor*^{Myf5cKO} BAT (Figure 2.5A). Thus, terminal differentiation per se (i.e., PPARγ, UCP1, and IRβ induction) occurs in vivo in *Rictor*^{Myf5cKO} brown adipocytes.

Next, we examined lipogenesis genes. In P1 *Rictor*^{Myf5cKO} BAT, acetyl-coA carboxylase (*Acc*), fatty acid synthase (*Fasn*), and fatty acid elongase 6 (*Elovl6*) decrease expression by 40%, 40%, and 25%, respectively (Figure 2.5C). By 6 weeks, expression of ATP citrate lyase (*Acly*) in addition to *Acc*, *Fasn*, and *Elovl6* is reduced by 90%, 75%, 80%, and 40%, respectively (Figure 2.5C), which we confirmed by western blot for ACLY and ACC (Figure 2.5A). In addition, stearoyl-CoA desaturase (*Scd1*) decreases expression by 45% in 6-week *Rictor*^{Myf5cKO} BAT (Figure 2.5C). The SREBP1c and ChREBP transcription factors regulate lipogenesis gene expression (Czech et al., 2013; Filhoulaud et al., 2013). In both P1 and 6-week *Rictor*^{Myf5cKO} BAT, the mRNA expression of SREBP1c (*Srebf1c*), which is induced by insulin, and ChREBP (α and β isoforms), which is induced by glucose, is similar (Figure 2.5D). However, there is a marked decrease in the amount nuclear SREBP1c (nSREBP1c), the transcriptionally active SREBP1c cleavage product, in Rictor-deficient BAT (Figure 2.5A) consistent with the decrease in lipogenic gene expression. The levels of insig1, another nSREBP1c target gene and negative regulator of SREBP1c processing, also decreases (Figure 2.5C). The mRNA expression of SREBP2 (which regulates cholesterol biosynthesis) slightly decreases in *Rictor*^{Myf5cKO} BAT at 6 weeks, but the SREBP2 target genes HMG-CoA synthase (*Hmg-cs*) and HMG-CoA reductase (*Hmg-cr*) express at similar levels in control and KO BAT (Figure 2.5D), and nuclear SREBP2 (nSREBP2) accumulates possibly to

higher levels in the KO BAT (Figure 2.5A). We find no difference in AMPK or hormone-sensitive lipase phosphorylation between control and *Rictor*^{Myf5cKO} BAT (Figures 2.5A and 2.6A). Together, these results indicate that despite having seemingly normal AKT signaling, de novo lipogenesis is reduced in *Rictor*^{Myf5cKO} BAT.

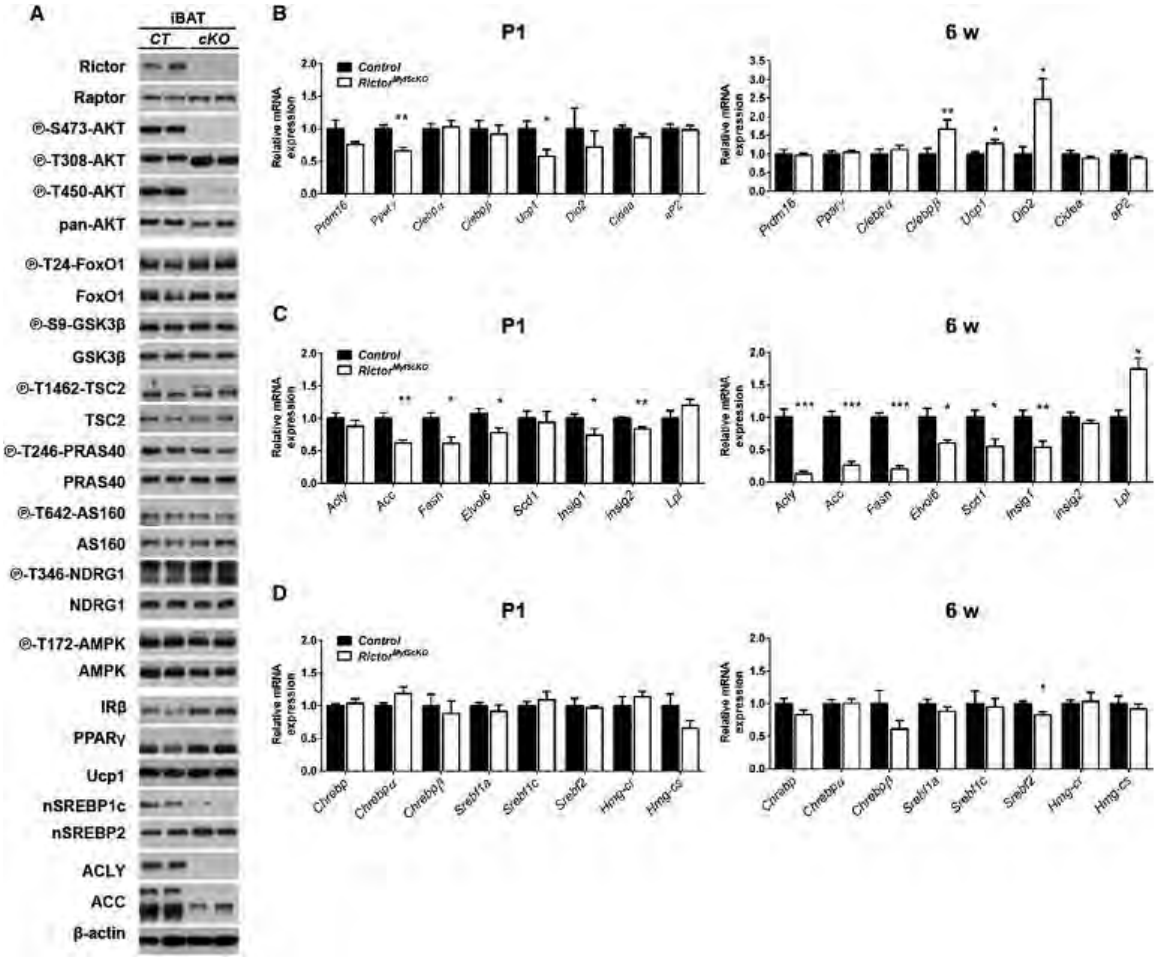

Figure 2.5. Rictor-Deficient Brown Adipocytes Have a Lipid Metabolism Defect

(A) Western blots total and phosphoproteins using 6-week iBAT lysates. Mice were fasted overnight and refed for 45 min prior to preparing lysates. (B–D) qRT-PCR of the indicated genes in P1 (n = 6) and 6-week (n = 8) iBAT (mean ± SEM; t test; $^{*}p < 0.05$,$^{**}p < 0.01$)

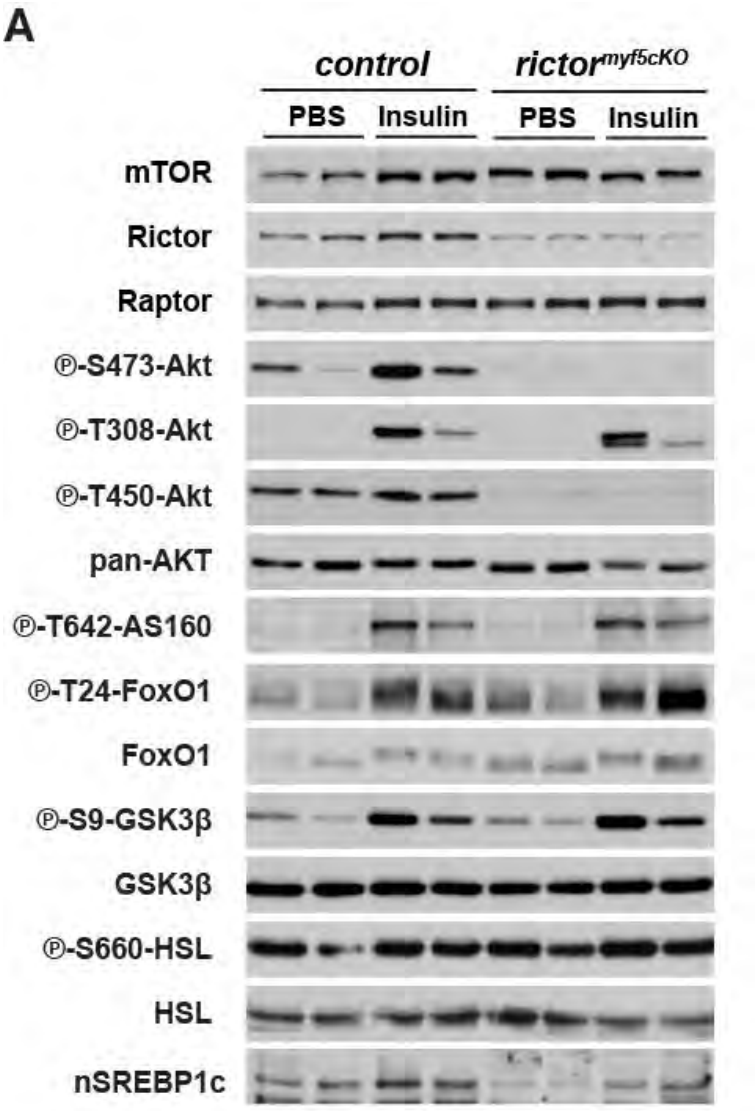

Figure 2.6 Insulin-stimulated Signaling in BAT

(A) Western blots of the indicated total and phospho-proteins using lystates prepared from the iBAT of 8-week-old mice. Overnight fasted mice were *i.p*. injected with PBS or 150U/Kg insulin and tissues were collected 15 minutes post injection.

Mitochondrial Activity Is Elevated in Rictor-Deficient BAT

To further examine the metabolic state of *Rictor*^{Myf5cKO} BAT, we examined mitochondrial activity. In P1 neonate *Rictor*^{Myf5cKO} BAT, *Pgc1a* expresses normally, whereas expression of mitochondrial transcription factor A (*Tfam*), which regulates mtDNA replication, and carnitine palmitoyltransferase 1B (*Cpt1b*), which encodes the rate-limiting enzyme in β-oxidation, slightly decreases (Figure 2.7A). In contrast, *Pgc1α*, *Tfam*, and *Cpt1b* in addition to *Ucp1* express at higher levels in the BAT of 6-week-old *Rictor*^{Myf5cKO} mice (Figures 2.7A and 2.5B), suggesting BAT mitochondrial activity progressively increases or is maintained at a higher level in *Rictor*^{Myf5cKO} mice as they age.

To explore this in more detail, we used quantitative RT-PCR (qRT-PCR) arrays to broadly measure mitochondrial gene expression in the 6-week-old BAT. Using arrays for functional genes involved in mitochondrial molecular transport and biogenesis, we detect increases in several genes indicative of increased mitochondrial activity (Figure 2.7B). Furthermore, the mitochondrial citrate and malate transporters *Slc25a1* and *Slc25a10* respectively—both of which function in fatty acid biosynthesis, the former also being an SREBP1c target gene (Infantino et al., 2007; Mizuarai et al., 2005)—significantly decrease expression in the mutant BAT. Using mitochondrial energy metabolism gene arrays, we found 58 additional genes involved in respiration (OXPHOS) are elevated in *Rictor*^{Myf5cKO} BAT (Figure 2.8A), suggesting an increase in mitochondrial mass, which we confirmed by Cox IV immunofluorescence (Figure 2.7C). Transmission electron microscopy (TEM) reveals individual mitochondria in the mutant BAT are larger and have more disorganized cristae (Figure 2.7D). To directly confirm elevated

mitochondrial activity, we measured BAT oxygen consumption rate (OCR) in a Seahorse Flux Analyzer and determined that basal and pyruvate-stimulated OCRs are elevated by around 18% in *Rictor*^{Myf5cKO} BAT (Figure 2.7E). We did not detect a significant increase in overall oxygen consumption when *Rictor*^{Myf5cKO} mice were placed in metabolic cages at 22°C, except when normalized for body weight (Figure 2.8B). Notably, however, mice are under thermal stress at this temperature, which can mask effects on BAT activity (Feldmann et al., 2009).

Interestingly, we also detect an approximate 2-fold increase in basal glucose uptake in *Rictor*^{Myf5cKO} BAT measured by ^{18}FDG positron emission tomography computed tomography scanning (Figure 2.8C) and an increase in lipoprotein lipase (*Lpl*) expression (Figure 2.5C), suggesting that *Rictor*^{Myf5cKO} BAT may consume more nutrients than age-matched control BAT. Small-metabolite profiling reveals that *Rictor*^{Myf5cKO} BAT also has elevated levels of inosine monophosphate (IMP) (Figure 2.8D), a deamination product of AMP, the accumulation of which suggests increased uncoupling (Balcke et al., 2011b). In an acute cold challenge, Rictor-deficient BAT also induces *Ucp1* expression significantly more than control BAT and the mutants have no difficulty maintaining body temperature, although body temperature regulation in an acute cold challenge is largely a function of muscle (Figure 2.7F). Finally, we see no compensatory "browning" in the psWAT as would be expected if *Rictor*^{Myf5cKO} BAT were dysfunctional (Figures 2.4C and 2.4D) (Schulz et al., 2013). These results are consistent with Rictor loss in BAT shifting metabolism to a more oxidative and less lipogenic state.

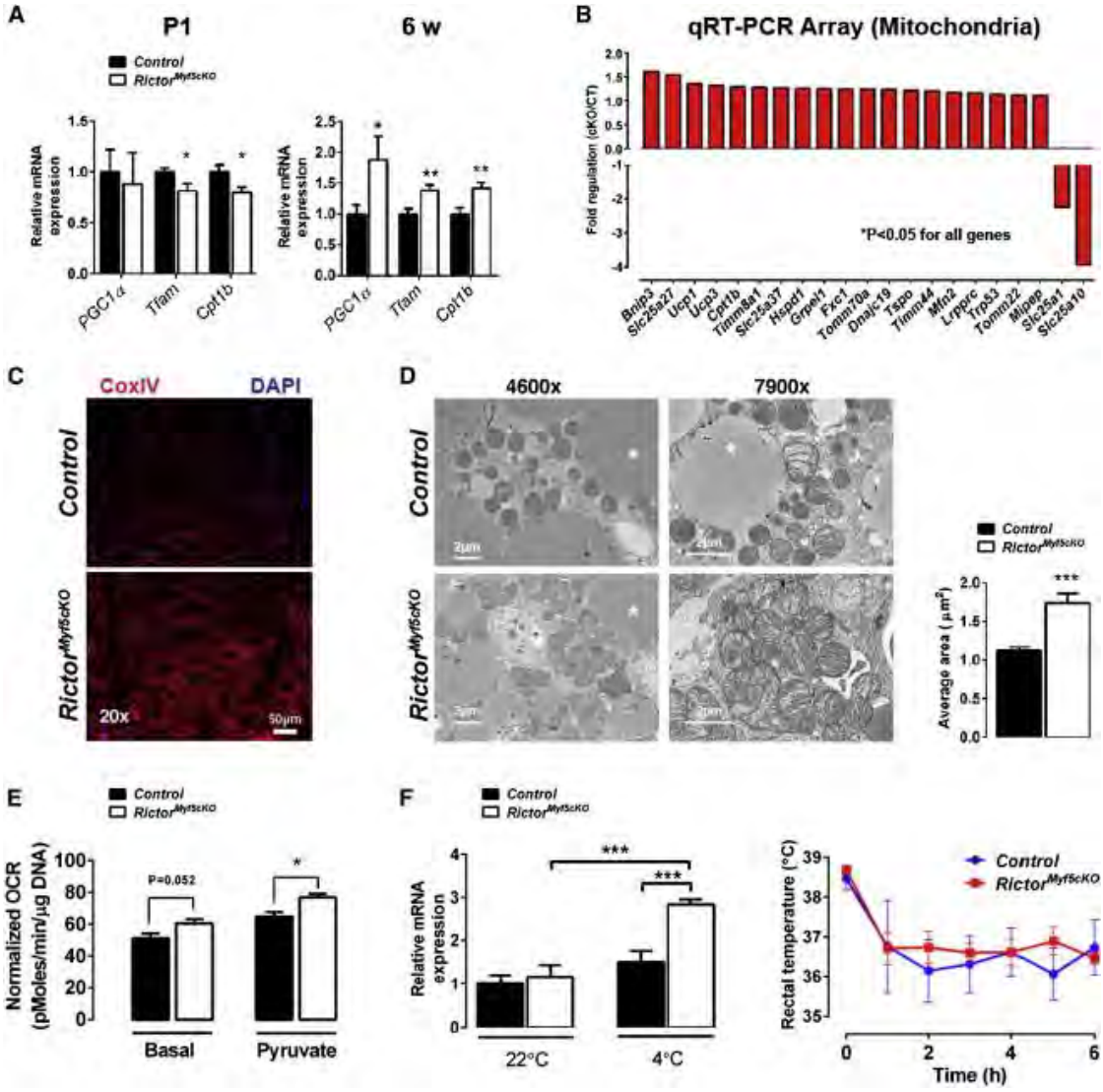
A
P1
6 w
Control
Rictor^Myf5cKO
Relative mRNA expression
PGC1α
Tfam
Cpt1b
B
qRT-PCR Array (Mitochondria)
Fold regulation (cKO/CT)
*P<0.05 for all genes
Bnip3
Slc25a27
Ucp1
Ucp3
Cpt1b
Timm8a1
Slc25a37
Hspd1
Grpel1
Fxc1
Tomm70a
Dnajc19
Tspo
Timm44
Mfn2
Lrppre
Trp53
Tomm22
Mipep
Slc25a1
Slc25a10
C
CoxIV
DAPI
Control
Rictor^Myf5cKO
20x
50μm
D
4600x
7900x
Control
Rictor^Myf5cKO
2μm
Average area (μm²)
E
Normalized OCR (pMoles/min/μg DNA)
P=0.052
Basal
Pyruvate
F
Relative mRNA expression
22°C
4°C
Rectal temperature (°C)
Time (h)

Figure 2.7 Mitochondrial Activity Is Elevated in Rictor-Deficient BAT

(A) qRT-PCR of mitochondrial genes in P1 (n = 6) and 6-week iBAT (n = 8) (mean ± SEM; t test; $^{*}p < 0.05$,$^{**}p < 0.01$) (B) Differentially expressed genes using mitochondrial qRT-PCR arrays (n = 4; t test; $p < 0.05$) (C) Representative immunofluorescence images of Cox IV staining in 6-week iBAT (n = 3). (D) Representative TEM images of 6-week iBAT (left) and mitochondria size (right) (n = 3; mean ± SEM; t test; $^{***}p < 0.001$) (E) Oxygen consumption of iBAT using a Seahorse Flux Analyzer (12 weeks, n = 5; normalized to DNA content; mean ± SEM; t test; $^{*}p < 0.05$) (F) qRT-PCR of *Ucp1* mRNA in iBAT with or without cold exposure (left) (n = 3 for 22°C; n = 4 for 4°C; mean ± SEM; two-way ANOVA; $^{***}p < 0.001$) and rectal temperature in acute cold challenge (right) (n = 4; mean ± SEM; t test; no significant difference).

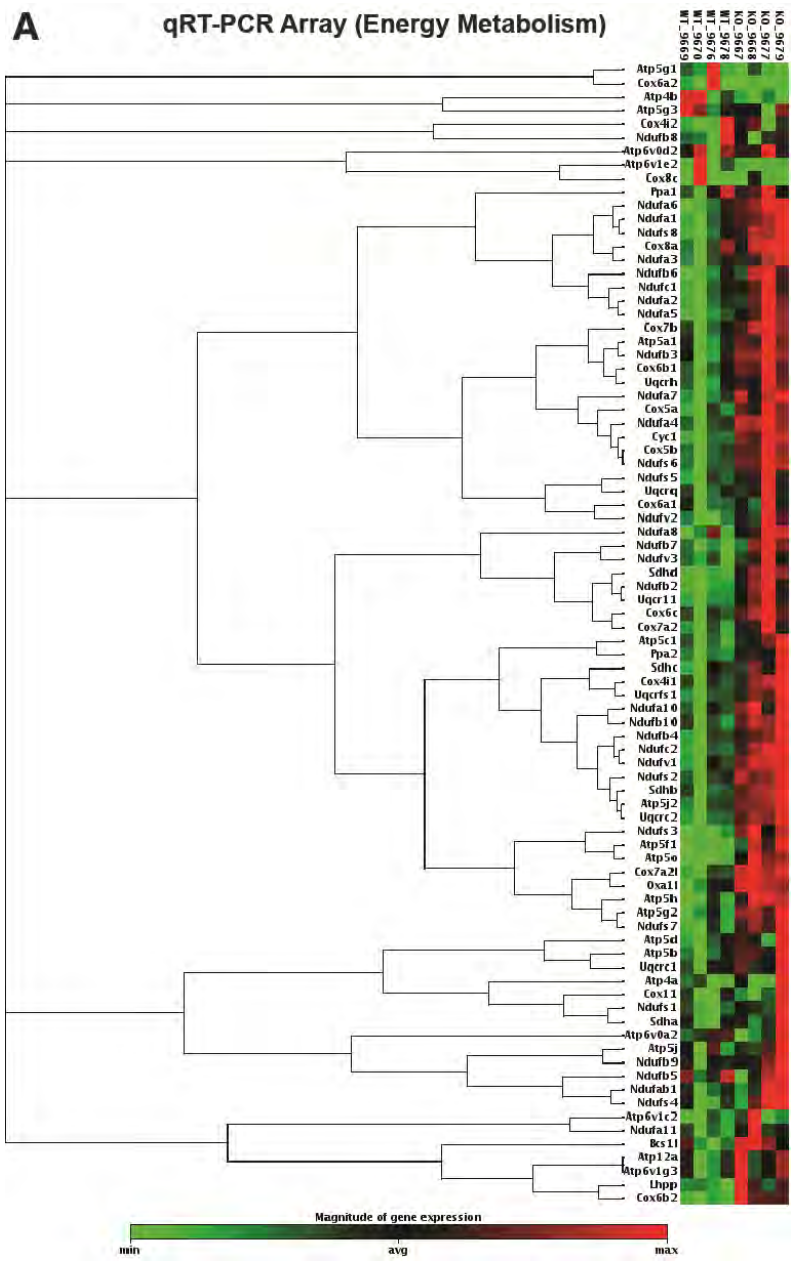
A
qRT-PCR Array (Energy Metabolism)
WT_9669
WT_9670
WT_9676
WT_9678
NO_9667
NO_9668
NO_9677
NO_9679
Atp5g1
Cox6a2
Atp4b
Atp5g3
Cox4i2
Ndufb8
Atp6v0d2
Atp6v1e2
Cox8c
Ppa1
Ndufa6
Ndufa1
Ndufs8
Cox8a
Ndufa3
Ndufb6
Ndufc1
Ndufa2
Ndufa5
Cox7b
Atp5a1
Ndufb3
Cox6b1
Uqcrh
Ndufa7
Cox5a
Ndufa4
Cyc1
Cox5b
Ndufs6
Ndufs5
Uqcrq
Cox6a1
Ndufv2
Ndufa8
Ndufb7
Ndufv3
Sdhd
Ndufb2
Uqcr11
Cox6c
Cox7a2
Atp5c1
Ppa2
Sdhc
Cox4i1
Uqcrfs1
Ndufa10
Ndufb10
Ndufb4
Ndufc2
Ndufv1
Ndufs2
Sdhb
Atp5j2
Uqcrc2
Ndufs3
Atp5f1
Atp5o
Cox7a2l
Oxa1l
Atp5h
Atp5g2
Ndufs7
Atp5d
Atp5b
Uqcrc1
Atp4a
Cox11
Ndufs1
Sdha
Atp6v0a2
Atp5j
Ndufb9
Ndufb5
Ndufab1
Ndufs4
Atp6v1c2
Ndufa11
Bcs1l
Atp12a
Atp6v1g3
Lhpp
Cox6b2
Magnitude of gene expression
min
avg
max

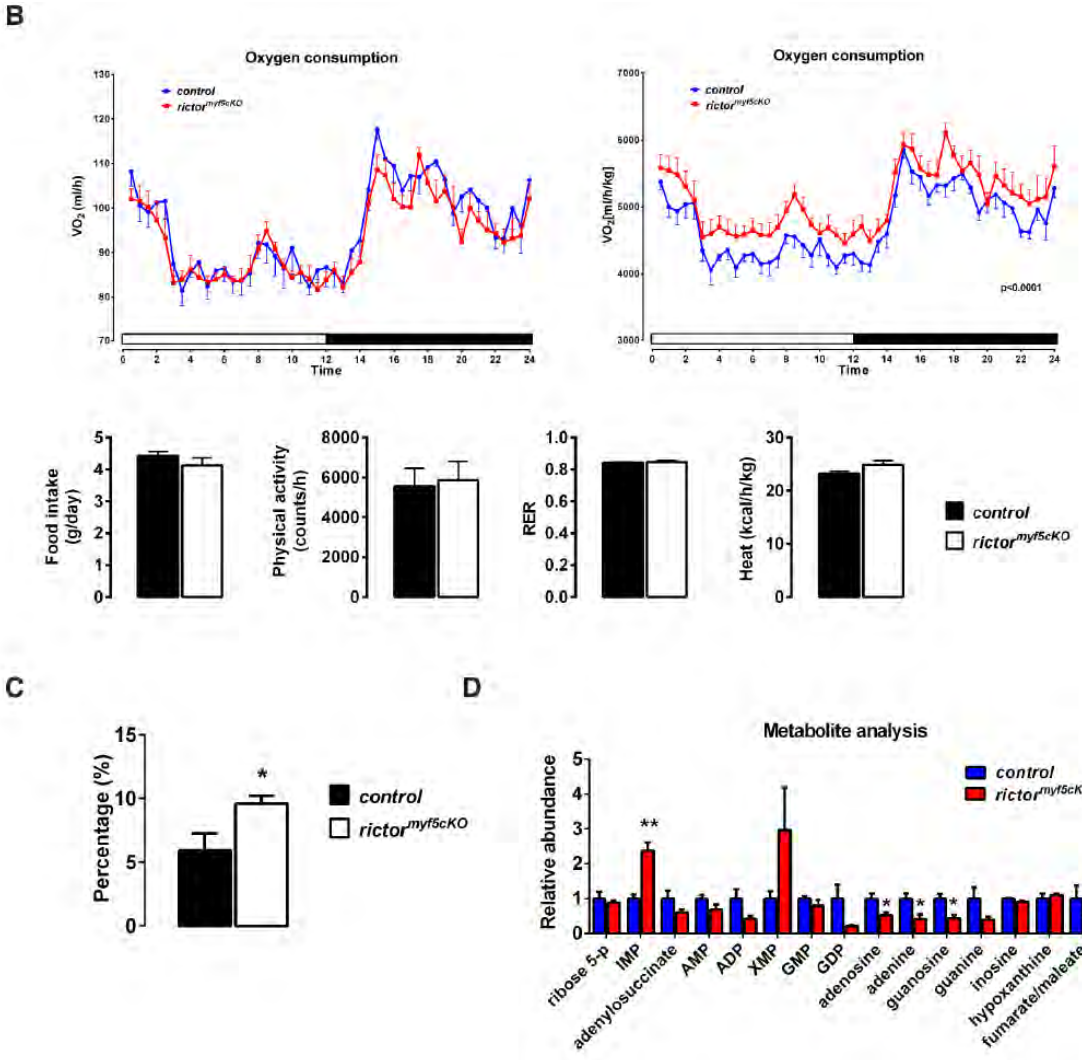
B
Oxygen consumption
control
rictor^myf5cKO
VO2 (ml/h)
Time
Oxygen consumption
VO2/[ml/h/kg]
p<0.0001
Food intake (g/day)
Physical activity (counts/h)
RER
Heat (kcal/h/kg)
control
rictor^myf5cKO
C
Percentage (%)
*
control
rictor^myf5cKO
D
Metabolite analysis
Relative abundance
control
rictor^myf5cKO
**
*
ribose 5-p
IMP
adenylosuccinate
AMP
ADP
XMP
GMP
GDP
adenosine
adenine
guanosine
guanine
inosine
hypoxanthine
fumarate/maleate

Figure 2.8 Mitochondria RT-PCR Array, Metabolic Cage Analysis and Metabolite Profiling

(A) Clustering heat map for mitochondrial genes involved in energy metabolism qRT-PCR array (n=4). **(B)** Metabolic cage analysis of 6wk-old mice under normal housing temperature (22°C): *Top Left*—whole body oxygen consumption; *Top right*—whole body oxygen consumption normalized to body weight; *Botton*—food intake, physical activity, respiratory exchange ratio (RER) and energy expenditure. (n=6) **(C)** Glucose uptake by ^{18}FDG PET-CT (n=5; bars represent mean ± SEM; t-test; *p<0.05). **(D)** Metabolite profiling was performed on 6-week control and *Rictor*^{Myf5cKO} iBAT. Note the high levels of IMP, a deamination product of AMP. AMP is formed by the adenylate kinase reaction, which produces ATP (2ADP = AMP + ATP). During metabolic stress or following treatment with chemical uncouplers, AMP is deaminated to IMP to ensure ongoing adenylate kinase activity and ATP production in order to maintain energy balance (Balcke et al., 2011a).

Brown Preadipocytes Require Rictor to Differentiate In Vitro

To examine if brown adipocyte differentiation also requires Rictor in vitro, we generated brown adipocyte precursor cells (bAPCs) harboring an inducible KO system (i.e., RictoriKO) in which Rictor deletion is triggered by 4-hydroxytamoxifen (4-OHT) (Figure 2.9A). Compared to isogenic controls, inducibly deleting Rictor rapidly and robustly depletes Rictor protein and AKT-S473 phosphorylation and, consistent with our in vivo data, leaves AKT-T308 phosphorylation intact (Figure 2.9B). Also consistent with the in vivo results, both basal and insulin-stimulated phosphorylation of FoxO1/3, GSK3β, TSC2, and PRAS40 are normal in *Rictor*^{iKO} bAPCs (Figure 2.10A). S6K1 phosphorylation is also unaffected (Figure 2.10A). Contrary to the in vivo results, acute Rictor loss in vitro decreases NDRG1 phosphorylation (Figure 2.10A). This indicates Rictor is required in cultured bAPCs for SGK activity to NDRG1, but not for pan-AKT or mTORC1 activity.

To our surprise, *Rictor*^{iKO} bAPCs are completely incapable of synthesizing lipid droplets when induced to differentiate (Figure 2.10B). This is surprising, because *Rictor*^{iKO} cells maintain normal levels of pAKT-T308, pGSK3β-S9, and pS6K1-T389 (i.e., PDK1, AKT, and mTORC1 activity, respectively) throughout the differentiation protocol (Figure 2.10C). The differentiation block occurs early as *Rictor*^{iKO} bAPCs fail to induce *C/ebpα, Pparγ, Prdm16, Pgc1α, Srebf1c, Ucp1,* and *Glut4* (Figures 2.10D and 2.9C). The expression of *C/ebpδ* and *C/ebpβ* on the other hand is induced normally and slightly higher (respectively) in the *Rictor*^{iKO} bAPCs at differentiation day 6 (Figure 2.10D). Consistent with the gene expression data, PPARγ, IRβ, UCP1, nSREBP1c, ACC,

and ACLY levels fail to increase during differentiation in *Rictor*^{iKO} bAPCs (Figure 2.10E). Notably, 4-OHT or *CreER* activation alone (i.e., in the absence of *Rictor* floxed alleles) has no effect on differentiation (not shown). Moreover, bAPCs prepared from P1 *Rictor*^{Myf5cKO} neonates also fail to differentiate, indicating that the ex vivo differentiation block is not unique to using the inducible KO system (Figure 2.9D). Importantly, expressing recombinant PPARγ in *Rictor*^{iKO} bAPCs rescues IRβ, UCP1, and nSREBP1c expression (Figure 2.10F) and lipid droplet production (Figure 2.10G), indicating Rictor promotes differentiation at least in part by facilitating PPARγ induction.

Insulin receptor substrate 1 (*Irs1*) and *Irs3* KO bAPCs also fail to induce PPARγ ex vivo (Fasshauer et al., 2001). It was later shown that *Irs1/3* KO bAPCs are unable to differentiate because they express high levels of *Pref-1*, *Wnt10a*, and *Necdin*, which encode adipogenesis inhibitors (Tseng et al., 2005). In contrast, Rictor-deficient bAPCs express normal levels of *Pref*-1, *Wnt10a*, and *Necdin* in culture, and during differentiation, *Necdin* and *Pref-1* increase, but only late in the differentiation protocol (Figure 2.9C). Thus, the mechanism by which deleting Rictor inhibits brown adipocyte differentiation differs from that of deleting *Irs1/3*.

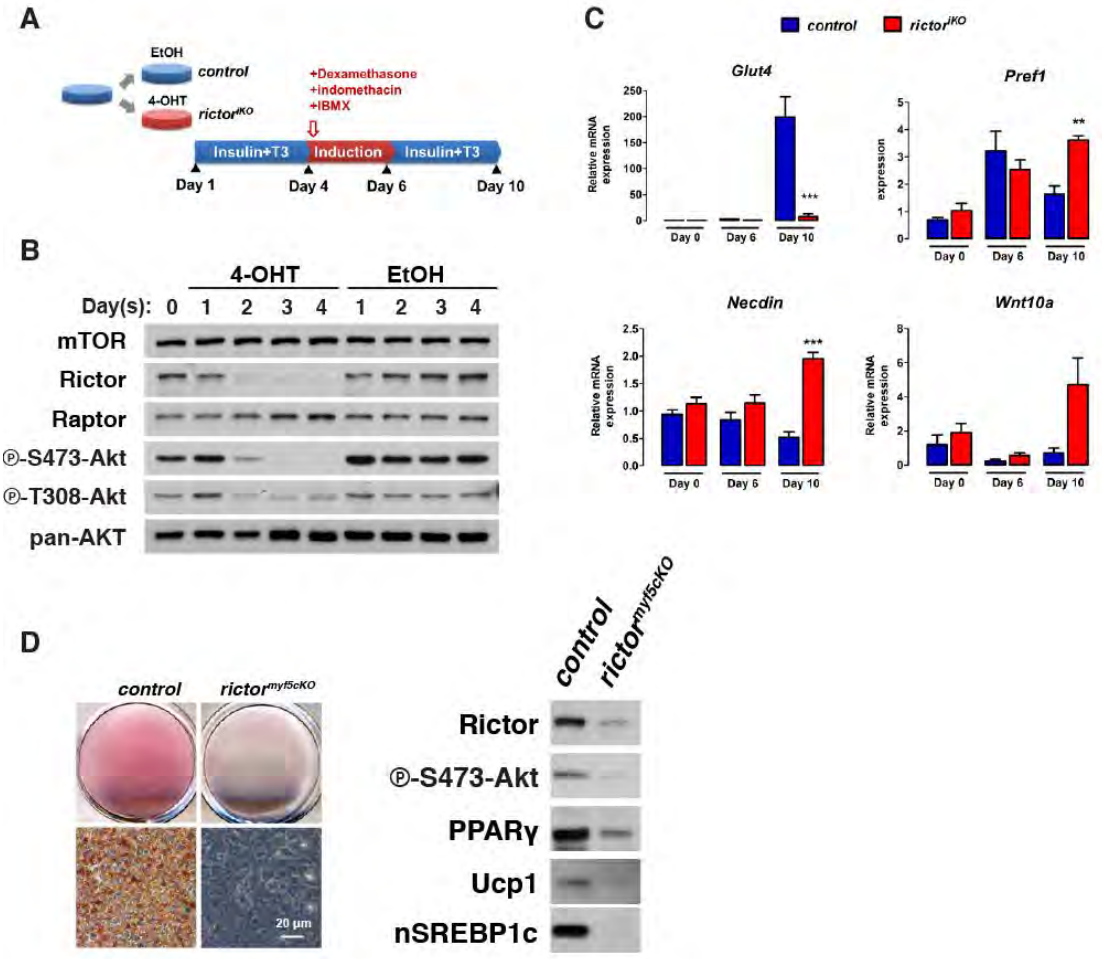
A
EtOH
control
4-OHT
rictor^iKO
+Dexamethasone
+indomethacin
+IBMX
Insulin+T3
Induction
Insulin+T3
Day 1
Day 4
Day 6
Day 10
B
4-OHT
EtOH
Day(s): 0 1 2 3 4 1 2 3 4
mTOR
Rictor
Raptor
Ⓟ-S473-Akt
Ⓟ-T308-Akt
pan-AKT
C
control
rictor^iKO
Glut4
Pref1
Necdin
Wnt10a
Relative mRNA expression
Day 0
Day 6
Day 10
D
control
rictor^myf5cKO
20 μm
Rictor
Ⓟ-S473-Akt
PPARγ
Ucp1
nSREBP1c

Figure 2.9 In Vitro Brown Adipocyte Differentiation (A) Inducible knockout differentiation protocol for comparing *Rictor*^{iKO} to isogenic control cells. Brown adipocyte precursors (bAPCs) were split from the same original dish into two dishes, one of which received vehicle (EtOH), the other 4-hydroxy-tamoxifem (4-OHT). After 3 days of treatment to induce deletion, cells were passed one time and then differentiated according to a standard 10-day brown adipocyte induction protocol (described in Experimental Procedures). **(B)** Western immunoblots showing time course following induced *Rictor* deletion in bAPCs with 4-OHT compared to vehicle (EtOH) treated isogenic controls. **(C)** qRT-PCR of mRNA levels for the indicated differentiation-related genes (n=3; bars represent mean ± SEM; t-test; *p<0.05, ***p<0.001). **(D)** *Left*—Oil Red O staining of control and *Rictor*^{Myf5cKO} bAPCs after differentiation. *Right*—Western immunoblots showing indicated differentiation markers.

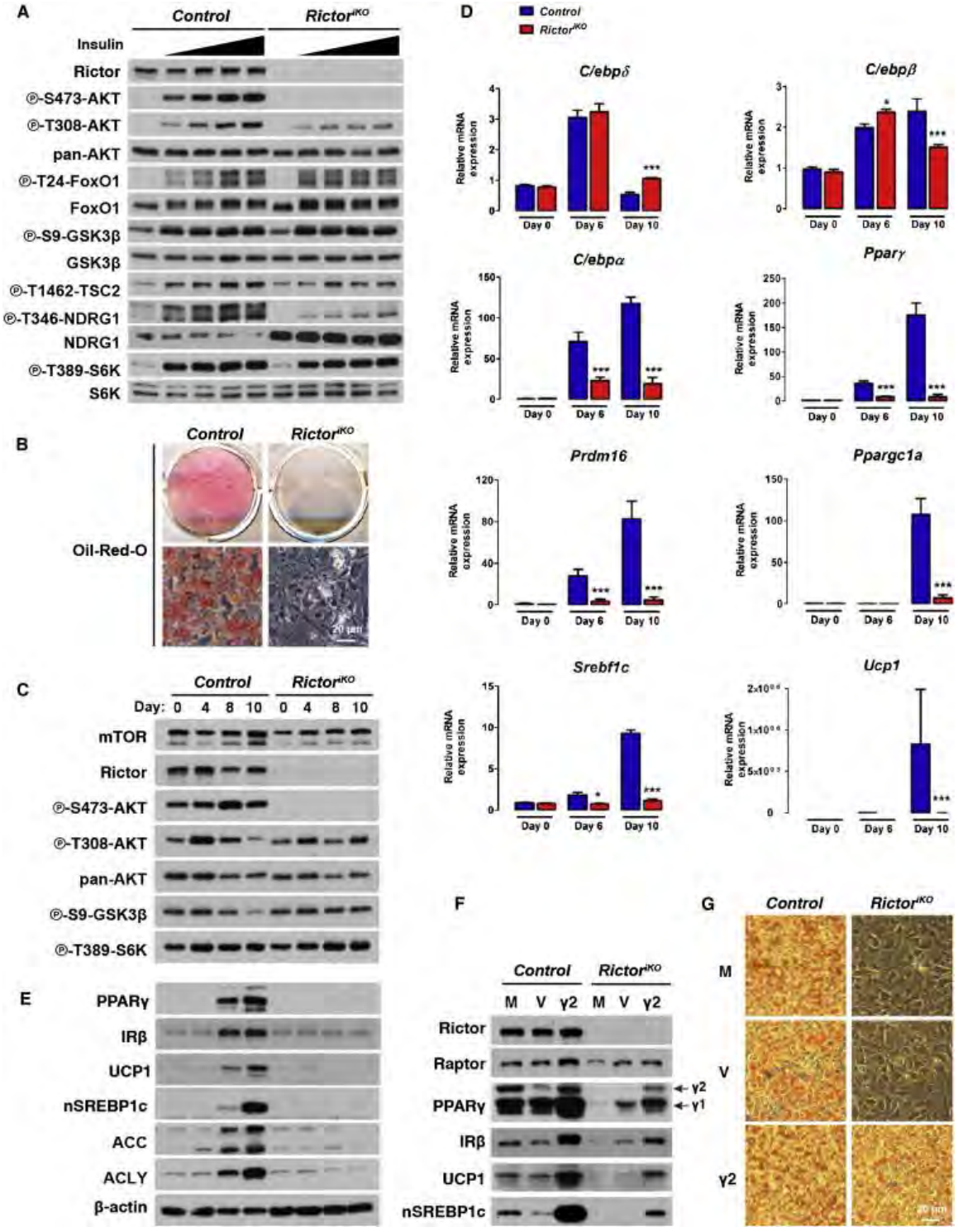
A
Control
Rictor^iKO
Insulin
Rictor
Ⓟ-S473-AKT
Ⓟ-T308-AKT
pan-AKT
Ⓟ-T24-FoxO1
FoxO1
Ⓟ-S9-GSK3β
GSK3β
Ⓟ-T1462-TSC2
Ⓟ-T346-NDRG1
NDRG1
Ⓟ-T389-S6K
S6K
B
Control
Rictor^iKO
Oil-Red-O
C
Control
Rictor^iKO
Day: 0 4 8 10 0 4 8 10
mTOR
Rictor
Ⓟ-S473-AKT
Ⓟ-T308-AKT
pan-AKT
Ⓟ-S9-GSK3β
Ⓟ-T389-S6K
E
PPARγ
IRβ
UCP1
nSREBP1c
ACC
ACLY
β-actin
D
Control
Rictor^iKO
C/ebpδ
C/ebpβ
C/ebpα
Pparγ
Prdm16
Ppargc1a
Srebf1c
Ucp1
Relative mRNA expression
Day 0
Day 6
Day 10
F
Control
Rictor^iKO
M V γ2 M V γ2
Rictor
Raptor
PPARγ
← γ2
← γ1
IRβ
UCP1
nSREBP1c
G
Control
Rictor^iKO
M
V
γ2

Figure 2.10. Rictor Is Required for Brown Adipocyte Differentiation In Vitro

(A) Western immunoblots using control and RictoriKO brown preadipocyte lysates. Cells were serum deprived 3 hr then stimulated with 0, 5, 25, 120, or 600 nM insulin for 15 min prior to lysis. (B) Oil red O staining after differentiation. (C) Western immunoblots using lysates from the indicated days of differentiation. (D) qRT-PCR for differentiation-related genes ($n = 3$; mean ± SEM; t test; $*p < 0.05$, $***p < 0.001$). (E) Same as (C). (F) Western immunoblots of cell lysates collected at day 10 of differentiation. M, mock; V, empty vector; γ2, recombinant PPARγ2. The γ1 and γ2 isoforms are indicated. (G) Oil red O staining of cells in (F).

AKT1 Functions Downstream of Rictor in Brown Adipocyte Differentiation

To further explore the mechanism by which Rictor regulates differentiation, we next asked whether an AKT or SGK pathway is required downstream of Rictor. To this end, we generated *Rictor*^{iKO} bAPCs that express hemagglutinin (HA)-SGK1, HA-AKT1, and HA-AKT2 or their phosphomimetic counterparts HA-SGK-S422D, HA-AKT1-S473D, and HA-AKT2-S474D in which a phosphomimetic residue was placed at the mTORC2 hydrophobic motif site, confirmed they were functional (Figure 2.11A), and asked whether any of these constructs rescue differentiation. Only HA-AKT1-S473D efficiently rescues lipid biosynthesis (Figure 2.12A). HA-AKT1-S473D-expressing *Rictor*^{iKO} bAPCs also induce PPARγ and restore IRβ, UCP1, nSREBP1c, ACLY, and ACC expression (Figure 2.12B). Thus, Rictor promotes differentiation as part of mTORC2 through an AKT pathway.

Our rescue experiments point to AKT1 as the isoform driving bAPC differentiation in vitro. Consistently, AKT1 is highly expressed in undifferentiated precursors and decreases expression during differentiation, whereas AKT2 expression increases during differentiation (Figure 2.11B). To further examine the role of AKT1 and AKT2 in bAPC differentiation, we generated bAPC lines that specifically lack either Akt1 or Akt2 and determined their in vitro differentiation capacity. Consistent with AKT1, but not AKT2, being required for differentiation, Akt1-deficient bAPCs cannot efficiently synthesize lipid droplets (Figure 2.12C) or upregulate PPARγ, IRβ, or UCP1 when induced to differentiate (Figure 2.12D). In contrast, Akt2-deficient bAPCs induce PPARγ, IRβ, and UCP1 normally (Figures 2.12C and 2.12D), indicating that AKT1 is

indeed the isoform required downstream of Rictor/mTORC2 for brown adipocyte differentiation. Interestingly, we noticed in our in vitro differentiation assays that although the Akt2-deficient cells differentiate, they fail to induce nSREBP1c, that ACLY and ACC express at low levels, and that lipid droplet content is reduced (Figures 2.12C and 2.12D). This suggests that although AKT2 is not essential for differentiation, it is important downstream of Rictor/mTORC2 for lipid metabolism. Indeed, when we immunoprecipitate AKT1 or AKT2 from undifferentiated bAPCs, most of the AKT phosphorylation is on AKT1, while in vivo the bulk of AKT phosphorylation shifts to AKT2 (Figures 2.11C and 2.11D). Thus, although the inability of *Rictor*^{iKO} bAPCs to differentiate in culture reflects an AKT1 deficiency, the in vivo metabolic phenotype appears to reflect an AKT2 deficiency.

BMP7 Rescues Brown Adipocyte Differentiation in the Absence of Rictor

In vitro *Rictor*^{iKO} bAPCs cannot differentiate (i.e., induce PPARγ and UCP1), but in vivo, PPARγ and UCP1-positive Rictor-deficient BAT develops. One possible explanation for this paradox is that in vivo there are developmental signals present that are missing from the artificial in vitro differentiation assay. The signals that drive brown adipocyte differentiation in vivo are poorly understood. One proposed inducer of brown adipocyte differentiation is the transforming growth factor-β superfamily member BMP7 (Schulz et al., 2013; Tseng et al., 2008). When given to control or *Rictor*^{iKO} bAPCs, BMP7 does not induce AKT phosphorylation (Figure 2.11E). However, when supplemented into the

differentiation cocktail, BMP7 restores to *Rictor*^{iKO} bAPCs their ability to synthesize lipid droplets (Figure 2.12E) and express PPARγ, IRβ, UCP1, and to a lesser extent nSREBP1c, ACLY, and ACC (Figure 2.12F). This is consistent with the in vitro differentiation assay lacking signaling molecules present in vivo and suggests BMP7 and mTORC2-AKT1 signaling converge during brown adipocyte differentiation. A model depicting the role mTORC2-AKT signaling in vitro in brown adipocyte differentiation is shown in Figure 2.12G.

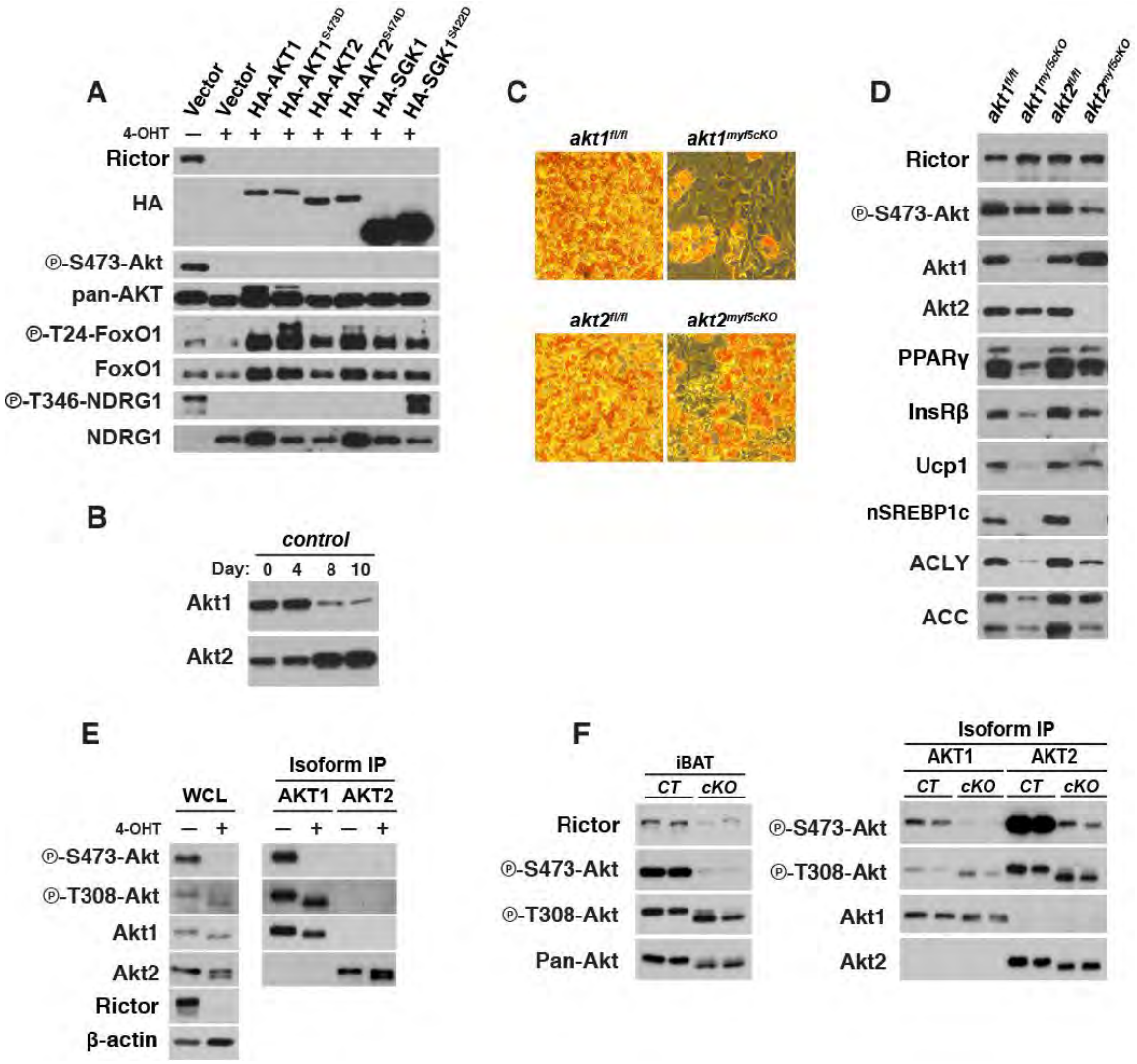

Figure 2.11 Differential Requirements for AKT Signaling In vitro and In vivo

(A) Western immunoblots of undifferentiated control and *Rictor*^{iKO} bAPCs stably expressing the indicated recombinant constructs. Cells were treated with fresh culture media before harvesting. **(B)** Western immunoblots of AKT1 and AKT2 protein expression at the indicated days during differentiation of wild type bAPCs. **(C)** Western immunoblots of lysates generated from AKT isoform-specific immunoprecipitation experiments using control or *Rictor*^{iKO} undifferentiated bAPCs. Immunoblots of the whole cell lystates (WCL) are shown to the left. **(D)** Western immunoblots of lysates generated from AKT isoform-specific immunoprecipitation experiments using iBAT dissected from 6-week-old control and *Rictor*^{Myf5cKO} mice. **(E)** Western immunoblots of lysates prepared from undifferentiated control and *Rictor*^{iKO} cells. Cells were serum deprived for 3 hours, then stimulated with FBS or BMP7 (3.2nM) for 15 minutes.

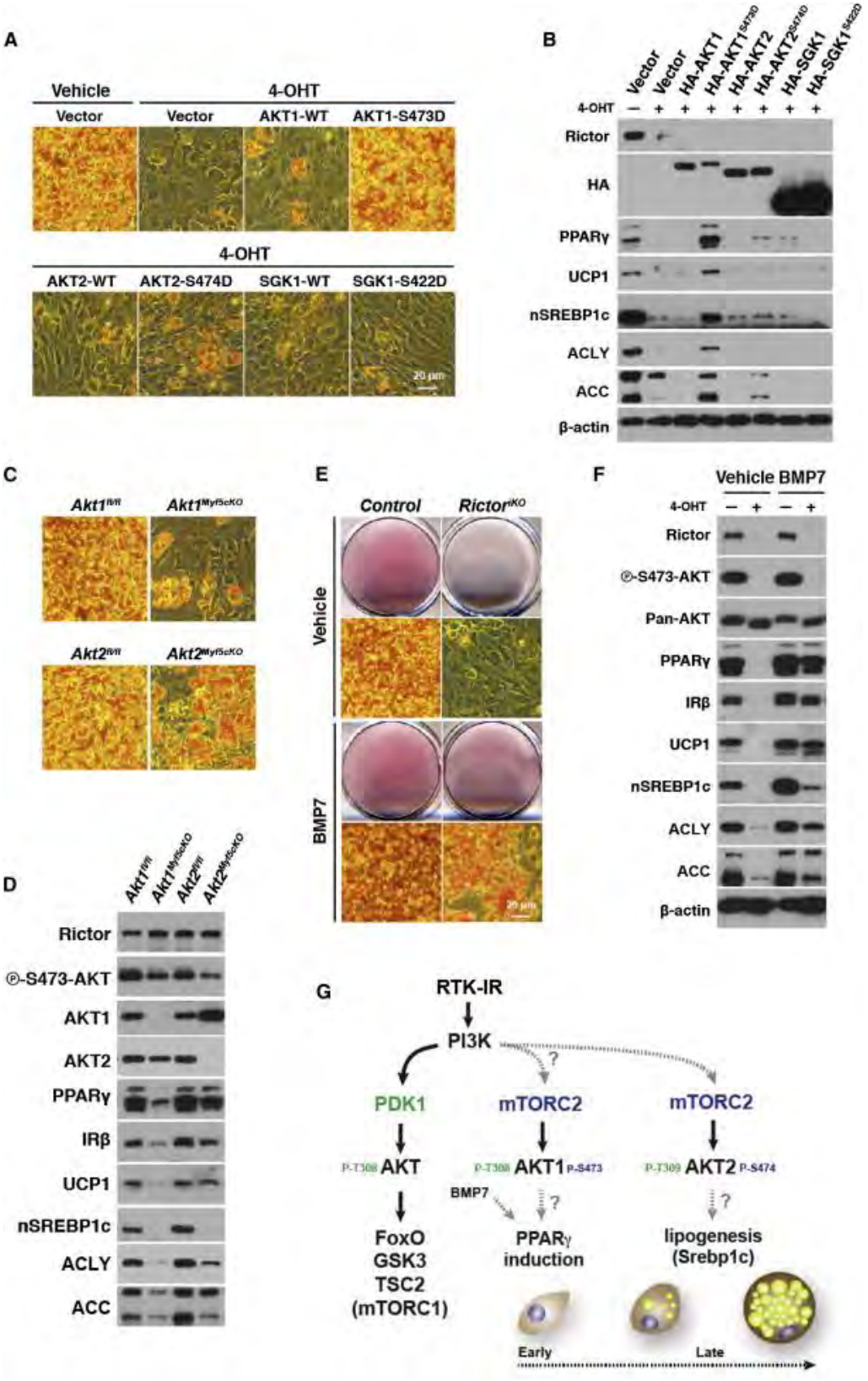
A
Vehicle
4-OHT
Vector
Vector
AKT1-WT
AKT1-S473D
4-OHT
AKT2-WT
AKT2-S474D
SGK1-WT
SGK1-S422D
20 μm
B
Vector
Vector
HA-AKT1
HA-AKT1S473D
HA-AKT2
HA-AKT2S474D
HA-SGK1
HA-SGK1S422D
4-OHT
Rictor
HA
PPARγ
UCP1
nSREBP1c
ACLY
ACC
β-actin
C
Akt1fl/fl
Akt1Myf5cKO
Akt2fl/fl
Akt2Myf5cKO
D
Akt1fl/fl
Akt1Myf5cKO
Akt2fl/fl
Akt2Myf5cKO
Rictor
Ⓟ-S473-AKT
AKT1
AKT2
PPARγ
IRβ
UCP1
nSREBP1c
ACLY
ACC
E
Control
RictoriKO
Vehicle
BMP7
20 μm
F
Vehicle
BMP7
4-OHT
Rictor
Ⓟ-S473-AKT
Pan-AKT
PPARγ
IRβ
UCP1
nSREBP1c
ACLY
ACC
β-actin
G
RTK-IR
PI3K
PDK1
mTORC2
mTORC2
P-T308 AKT
P-T308 AKT1 P-S473
P-T309 AKT2 P-S474
BMP7
FoxO
GSK3
TSC2
(mTORC1)
PPARγ
induction
lipogenesis
(Srebp1c)
Early
Late

Figure 2.12 Recombinant AKT1-S473D or BMP7 Supplementation Rescue Differentiation in the Absence of Rictor

(A) Oil red O staining of differentiated control (vehicle) and RictoriKO cells (4-OHT) cells stably expressing the indicated constructs. (B) Western immunoblots corresponding to (A). (C) Oil red O staining of differentiated Akt1 and Akt2 conditional knockout and control bAPCs. (D) Western immunoblots corresponding to (C). (E) Oil red O staining of differentiated control and RictoriKO cells in the presence or absence of BMP7 (3.2 nM added day 1 during differentiation). (F) Western immunoblots of corresponding to (E). (G) Model summarizing the role of mTORC2 in vitro in brown adipocyte differentiation.

Rictor^{Myf5cKO} Mice Are Less Susceptible to Obesity and Metabolic Disease at Thermoneutrality

The higher metabolic activity of Rictor-deficient BAT led us to wonder whether *Rictor*^{Myf5cKO} mice are resistant to obesity. Chronic consumption of a high-fat diet (HFD) triggers a phenomenon in mice called diet-induced thermogenesis, which requires UCP1 and counteracts obesity (Cannon and Nedergaard, 2010; Feldmann et al., 2009). Because BAT activity is masked by chronic thermal stress at 22°C, we conducted the following studies at thermoneutrality (30°C for mice), which exempts mice from thermal stress (Feldmann et al., 2009). When eating a normal chow diet, control and *Rictor*^{Myf5cKO} mice gain equal weight (Figure 2.13A) and consume the same total energy (Figure 2.13B) over 12 weeks. In contrast, when eating an HFD, control mice gain 14.67 ± 1.05 g whereas *Rictor*^{Myf5cKO} mice gain 10.57 ± 1.18 g (Figure 2.13A), despite both groups consuming the same energy (Figure 2.13B). Thus, controls gain 64% more weight when eating an HFD versus chow compared to *Rictor*^{Myf5cKO} mice. This suggests *Rictor*^{Myf5cKO} mice living at thermoneutrality and eating an HFD are less metabolically efficient than controls, which is indeed the case (Figure 2.13C).

The resistance to weight gain in the HFD-fed *Rictor*^{Myf5cKO} cohort is partly due to reduced growth of adipose tissue. For example, the pgWAT gains significantly less mass in the HFD-fed *Rictor*^{Myf5cKO} cohort than in HFD-fed controls (Figure 2.13D). Liver and heart also grow larger in controls eating HFD compared to chow, whereas liver and heart grow to the same mass in the *Rictor*^{Myf5cKO} cohorts regardless of diet (Figures 2.13D and 2.14A). Diet has no effect on other lean tissues in either the controls or *Rictor*^{Myf5cKO}

cohorts (Figures 2.13D and 2.14A). That pgWAT grows less in HFD-fed *Rictor*^{Myf5cKO} mice compared to HFD-fed controls indicates systemic protection against obesity is occurring because *Myf5-Cre* does not target pgWAT (Figures 2.2F and 2.4C). The reduction in pgWAT mass is due in part to smaller adipocyte size (Figure 2.13E); the livers of *Rictor*^{Myf5cKO} mice also resist hepatic steatosis (Figure 2.13E), and the HFD-fed *Rictor*^{Myf5cKO} mice perform better in a glucose tolerance test (Figure 2.14B).

In chow-fed cohorts, histology reveals that control BAT adopts a more "white adipocyte-like" appearance (Figure 2.13E). In contrast, the BAT in chow-fed *Rictor*^{Myf5cKO} mice resists the whitening effects of living at thermoneutrality and maintains a more "brown-adipocyte-like" appearance (Figure 2.13E). The resistance of *Rictor*^{Myf5cKO} BAT to whitening is reflected in the gene expression signature; for example, when normalized to BAT gene expression at 22°C, the shift to thermoneutrality decreases the expression of BAT-selective genes (*Prdm16, Sgk2, cideb, and cyp2b10*) and increases the expression of WAT-selective genes (*Dpt1, Retn, Trim14, and Nnmt*) (Harms et al., 2014) to a greater extent in control BAT than in *Rictor*^{Myf5cKO} BAT, which maintains a more BAT-like identity (Figure 2.14C).

In HFD-fed cohorts, histology reveals a large number of multilocular adipocytes in control BAT (Figure 2.13F) that are not apparent in chow-fed controls (Figure 2.13E), suggesting diet-induced thermogenesis. This is reflected in the gene expression data as Prdm16 increases in control BAT in HFD-fed mice compared to chow-fed mice (Figure 2.13G), whereas the WAT-specific genes *Retn*, *Trim14*, and *Nnmt* decrease (Figure 2.13G). Histology also reveals that *Rictor*^{Myf5cKO} BAT is even more "brown-like" in the

HFD-fed cohort, exhibiting a uniform abundance of small lipid droplets (Figure 2.13F) and a stronger BAT gene signature (i.e., elevated *Prdm16*, *Sgk2*, *Cideb*, and *Cyp2b10* and decreased *Dpt1*, *Retn*, *Trim14*, and *Nnmt*) (Figure 2.13G). Consistently, BAT functional genes (*Ucp1, Pgc1α, Cpt1β, and Dio2*) are induced to a greater extent in HFD-fed *Rictor*^{Myf5cKO} mice (Figure 2.13H), which also maintain low *Acly*, *Acc*, and *Fasn* expression (Figure 2.14D). Importantly, UCP1 protein levels are higher in the BAT of *Rictor*^{Myf5cKO} mice eating an HFD (Figure 2.13I). Notably, after 20 weeks of eating an HFD, the control BAT reverts to a more white-adipocyte-like histology; however, BAT character is preserved in *Rictor*^{Myf5cKO} mice (Figure 2.14E). Collectively, these results suggest that inhibiting mTORC2 in BAT increases diet-induced thermogenesis and, consequently, *Rictor*^{Myf5cKO} mice living without thermal stress and consuming an obesogenic diet are less susceptible to developing obesity and metabolic disease.

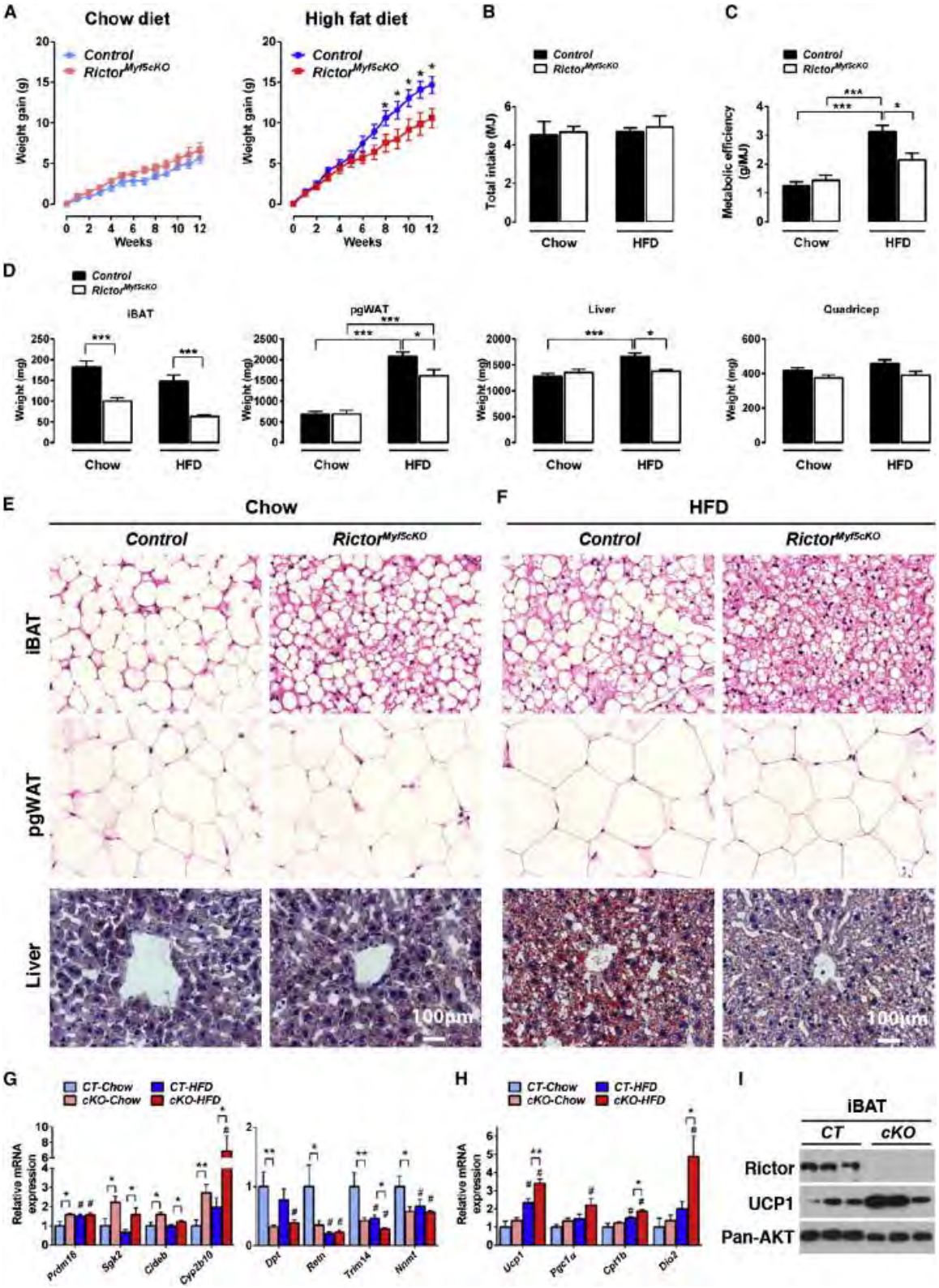
A
Chow diet
High fat diet
Control
Rictor Myf5cKO
Weight gain (g)
Weeks
B
Total intake (MJ)
Chow
HFD
C
Metabolic efficiency (g/MJ)
D
iBAT
pgWAT
Liver
Quadricep
Weight (mg)
E
Chow
F
HFD
iBAT
pgWAT
Liver
100μm
G
CT-Chow
cKO-Chow
CT-HFD
cKO-HFD
Relative mRNA expression
Prdm16
Sgk2
Cideb
Cyp2b10
Dpt
Retn
Trim14
Nnmt
H
Ucp1
Pgc1α
Cpt1b
Dio2
I
iBAT
CT
cKO
Rictor
UCP1
Pan-AKT

Figure 2.13 *Rictor*^{Myf5cKO} Mice Exempt from Thermal Stress and Consuming a High-Fat Diet Are Resistant to Obesity and Metabolic Disease

(A) Weight gain of control and RictorMyf5cKO mice during 12-weeks of normal chow (chow) or high-fat diet (HFD) (n = 8 control and n = 12 for KO in chow; n = 10 for both genotypes on an HFD; mean ± SEM; t test; ∗p < 0.05). Control mice initially weighed 21.63 ± 0.812 g in the chow group and 21.24 ± 0.621 in the HFD group. The RictorMyf5cKO mice initially weighed 19.42 ± 0.305 g in the chow group and 19.32 ± 0.348 in the HFD group. (B) Total energy intake (MJ) during the feeding regimen in (A). Control mice consumed 3.75 ± 0.56 g of chow and 2.81 ± 0.12 g of HFD; RictorMyf5cKO mice consumed 3.85 ± 0.24 g of chow and 2.95 ± 0.35 g of HFD. (C) Metabolic efficiency determined as the amount of body weight increase (g) per MJ food consumed (n = 8 control and n = 12 KO on chow; n = 10 for both genotypes on HFD; mean ± SEM; two-way ANOVA; ∗p < 0.05, ∗∗∗p < 0.001). (D) Mass (mg) of the indicated tissues collected from control and KO mice after 12 weeks on chow or an HFD (n = 8 control and n = 12 KO on chow; n = 10 for both genotypes on HFD; mean ± SEM; two-way ANOVA; ∗p < 0.05, ∗∗∗p < 0.001). (E and F) H&E staining of iBAT and pgWAT and oil red O staining of livers after 12 weeks of eating chow (E) or and HFD (F). (G) qRT-PCR of the indicated brown and white fat genes in iBAT from chow- or HFD-mice (n = 8 control and n = 12 KO on chow; n = 10 for both genotypes on HFD; mean ± SEM; two-way ANOVA; ∗p < 0.05, ∗∗p < 0.01, ∗∗∗p < 0.001; # indicates significant difference over the control chow group). (H) qRT-PCR of the

indicated metabolic genes in iBAT from chow- or HFD-mice (n = 8 control and n = 12 KO in chow; n = 10 for both genotypes in HFD; mean ± SEM; two-way ANOVA; ∗p < 0.05, ∗∗p < 0.01, ∗∗∗p < 0.001; # indicates a significant difference over the control chow group). (I) Western immunoblots of iBAT lysates.

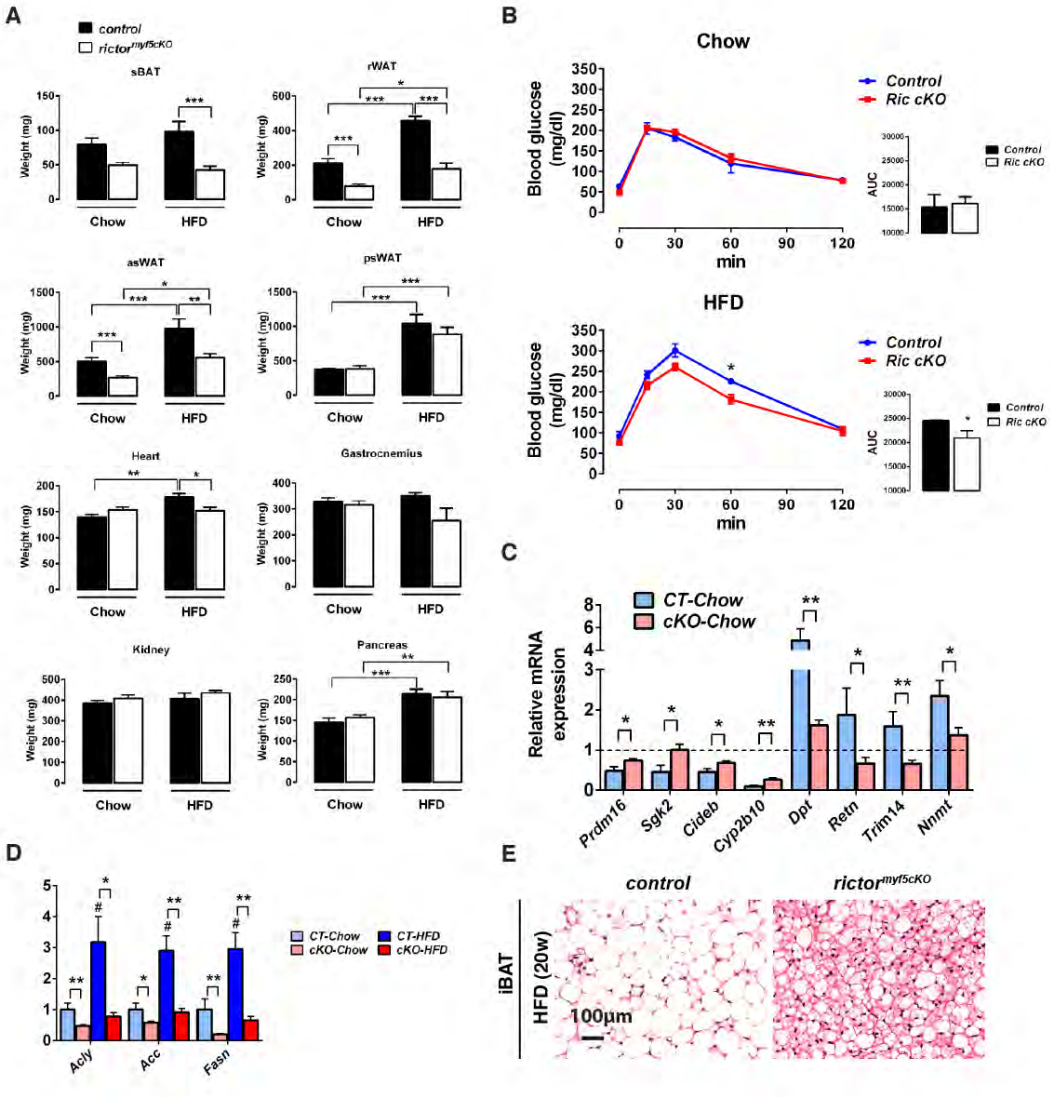

Figure 2.14 *Rictor*^{Myf5cKO} Mice Exempt from Thermal Stress and Consuming a High-Fat Diet Are Resistant to Obesity and Metabolic Disease

(A) Mass (mg) of the indicated tissues collected from control and *Rictor*^{Myf5cKO} mice living at thermoneutrality (30°C) following 12-weeks of eating chow or HFD. (n=8 for control and n=12 for KO in chow; n=10 for both genotypes in HFD; bars represent mean ± SEM; two-way ANOVA; *p<0.05, ***p<0.001) **(B)** Glucose tolerance test of control and *Rictor*^{Myf5cKO} mice on chow (top) or HFD (bottom) living at thermoneutrality. The test was performed during the 11th week of the 12-week experiment. **(C)** qRT-PCR of the indicated brown and white fat genes in iBAT from control and *Rictor*^{Myf5cKO} mice eating chow diet and living at thermoneutrality (n=8 for control and n=12 for KO in chow; bars represent mean ± SEM; two-way ANOVA; *p<0.05, **p<0.01, ***p<0.001). The expression level of each gene is normalized to the corresponding gene level in iBAT from age-matched control mice eating chow but living at the standard housing temperature (22°C). **(D)** qRT-PCR of the indicated lipogenesis genes in iBAT from chow or HFD mice (n=8 for control and n=12 for KO in chow; n=10 for both genotypes in HFD; bars represent mean ± SEM; two-way *ANOVA*; *p<0.05, **p<0.01, ***p<0.001; # indicates significant difference over the control chow group). **(E)** Representative H&E images (n=4) of control and KO mice fed with HFD at thermoneutrality for 20 weeks.

Discussion

Transcriptional regulation of BAT development has been extensively described (Kajimura et al., 2010), whereas less is known about the signaling mechanisms that regulate BAT. The control of brown fat fuel utilization is also incompletely understood (Townsend and Tseng, 2014). Previous studies reported that conditionally deleting Rictor in WAT and BAT or skeletal muscle has no effect on WAT or BAT mass or individual adipocyte or myocyte size (Bentzinger et al., 2008; Cybulski et al., 2009; Kumar et al., 2008; Kumar et al., 2010). However, these studies used Cre drivers that reportedly delete *Rictor* in mature cells, which led us to hypothesize that Rictor/mTORC2 may be more important for BAT/WAT and/or muscle development. By conditionally deleting *Rictor* in *Myf5* precursors, we discovered that Rictor is not essential in vivo for muscle development or regeneration. In contrast, *Myf5*-lineage brown and white adipocytes lacking Rictor are reduced in size. Furthermore, Rictor-deficient BAT undergoes a metabolic shift to a more oxidative and less lipogenic metabolic despite having seemingly normal pan-AKT signaling. Importantly, at thermoneutrality, this protects mice against an obesogenic diet. These findings implicate Rictor/mTORC2 as an essential signaling node in BAT that regulates the balance between fatty acid oxidation and storage. These findings could have important implications for understanding the signaling mechanisms that regulate fuel usage and metabolic activity in human BAT.

We also report that in vitro brown adipocyte differentiation requires Rictor/mTORC2. Mechanistically, Rictor/mTORC2 promotes *Pparγ* induction through AKT1 independently of pan-AKT signaling and mTORC1 activity. In vivo, however, brown adipocytes differentiate in $Rictor^{Myf5cKO}$ mice despite lacking Rictor expression. We hypothesize that this paradox indicates that the artificial in vitro culture conditions lack important signals present in vivo that overcome this deficiency. Supporting this notion, supplementing the differentiation assay with BMP7, a proposed in vivo inducer of brown adipocyte differentiation and thermogenesis (Schulz and Tseng, 2013; Tseng et al., 2008), rescues differentiation in the absence of *Rictor*. Notably, we do detect low *Pparγ* expression in $Rictor^{Myf5cKO}$ P1 BAT, which may reflect the role of Rictor/mTORC2 in early brown adipocyte differentiation and explain the mutant BAT hypoplasia. Exactly how Rictor/mTORC2 and BMP7 signaling might converge on PPARγ is not yet clear. We also show that during brown adipocyte differentiation, the major AKT isoform switches from AKT1 to AKT2; thus, although Rictor/mTORC2 may regulate differentiation through an AKT1 pathway that can be bypassed in vivo, its role in BAT metabolism is likely mediated through an AKT2 pathway that cannot be compensated for. Consistent with this idea, whole-body Akt2 KO mice among many other phenotypes have smaller BATs (Cho et al., 2001; Garofalo et al., 2003).

Why does deleting Rictor in BAT cause a metabolic shift? One possibility is that forkhead box O (FOXO) transcription factors are more active in Rictor-deficient brown adipocytes. FOXOs are regulated by multiple signals and function as cellular homeostasis regulators under stressful conditions (Eijkelenboom and Burgering, 2013).

FoxO1 and FoxO3 are AKT substrates that are partially dephosphorylated in some Rictor-deficient cells (Guertin et al., 2009; Guertin et al., 2006; Hagiwara et al., 2012; Jacinto et al., 2006; Yuan et al., 2012). When dephosphorylated, FoxO1/3 translocate to the nucleus, where they affect metabolism, survival, and cell-cycle genes and the activity of transcriptional regulators (including PPARγ and C/EBPα) (Eijkelenboom and Burgering, 2013). However, FoxO1/3 phosphorylation is not affected in Rictor-deficient BAT; thus, if the metabolic shift is driven by FoxO1/3, it may be through an alternative mechanism such as acetylation (Banks et al., 2011; Masui et al., 2013). Another possibility is that FoxC2 mediates the metabolic shift (Cederberg et al., 2001; Yao et al., 2013); however, we do not observe any change in FoxC2 expression in Rictor-deficient preadipocytes (not shown), nor do we see effects on the FoxC2 targets *C/ebpβ* or *Wnt10b* during differentiation (Gerin et al., 2009). The shift could also be mediated through unidentified AKT substrates that uniquely require hydrophobic motif phosphorylation. This is an important ongoing area of investigation.

Consistent with the *Myf5* lineage giving rise to a subset of white adipocytes, we also uncovered an essential role for Rictor/mTORC2 in white adipocyte growth in vivo. This confirms our previous discovery that some white adipocytes arise from *Myf5-Cre* expressing precursors (Sanchez-Gurmaches and Guertin, 2014b; Sanchez-Gurmaches et al., 2012). However, because in the $Rictor^{Myf5cKO}$ mice the Rictor-deficient white adipocytes are interspersed heterogeneously with nondeleted adipocytes within the same depot, we could not perform the appropriate whole-tissue biochemical studies using

Rictor-deficient WAT. We did, however, determine that RictoriKO white adipocyte precursors purified from the stromal vascular fraction of psWAT (which are not *Myf5*-lineage derived) are also defective at differentiating in vitro (not shown), indicating Rictor also has a cell-autonomous role in white adipocyte differentiation that is not dependent upon being *Myf5*-lineage derived. To determine the in vivo relevance of these findings, we will need to identify Cre drivers that express uniformly and specifically in white adipocyte precursors; however, the origins of adipocytes are just beginning to be revealed, and appropriate tools are not yet available for this line of investigation.

Is Rictor/mTORC2 a master regulator of lipid metabolism? Recent studies of liver collectively report that deleting hepatic Rictor results in a complex phenotype including increased gluconeogenesis, decreased glycolysis, and impaired lipogenesis (Hagiwara et al., 2012; Lamming et al., 2012; Yuan et al., 2012). Two studies find that hepatic Rictor loss also decreases SREBP1c activity; however, one study suggests AKT2 mediates this function (Hagiwara et al., 2012), whereas the other proposes an AKT-independent pathway (Yuan et al., 2012). These two studies are also inconsistent with respect to how Rictor loss affects AKT signaling, and thus the role of hepatic Rictor/mTORC2 is currently controversial. Nevertheless, the glucose uptake and glycolysis defect is reportedly independent of the lipogenesis defect, because restoring glucose flux in Rictor-KO hepatocytes did not rescue lipogenesis (Hagiwara et al., 2012). This study also reports that fatty acid oxidation genes are elevated in Rictor-deficient hepatocytes (Hagiwara et al., 2012). Thus, Rictor/mTORC2 may have a broad role in establishing a prolipogenic metabolic state. Going forward, it is important to determine if

Rictor/mTORC2 regulates de novo lipogenesis and β-oxidation by a common or coordinate set of mechanisms or whether one metabolic deficiency is indirectly driving the other. Notably, we detect a decrease in lipogenesis gene expression in P1 BAT lacking Rictor, but the increase in fatty acid oxidation gene expression we first detect in 6-week mutant BAT. Thus, mitochondrial activity may progressively increase in the Rictor-deficient BAT and be secondary to a lipogenesis defect. Regardless, our findings support the idea that targeting lipogenesis and/or β-oxidation pathways in adipocytes could be one approach to treating obesity and diabetes.

One prediction is that increasing BAT energy expenditure could have antiobesity therapeutic potential (Tseng et al., 2010). To achieve this goal, a deeper understanding of how BAT utilizes fuel is required (Townsend and Tseng, 2014). An important finding in our study is that *Rictor*^{Myf5cKO} mice living at thermoneutrality, when challenged with an obesogenic diet, induce higher levels of UCP1 and are more resistant to developing obesity and metabolic disease compared to HFD-fed controls. This suggests that inhibiting mTORC2 in BAT augments diet-induced thermogenesis (Cannon and Nedergaard, 2010; Feldmann et al., 2009), although we cannot yet rule out that Rictor loss in other *Myf5*-lineage tissues might also contribute to this phenotype. It is currently being debated whether humans have classic brown adipocytes or a potential third class of adipocyte called a brite/beige adipocyte (Nedergaard and Cannon, 2013). Recent work indicates that in the neck, deep fat is similar to rodent BAT and expresses high levels of UCP1, whereas more superficial fat expresses lower UCP1 levels and has more brite/beige characteristics (Cypess et al., 2013). Notably, humans typically adjust

temperature to be around thermoneutrality (Cannon and Nedergaard, 2010), and the BAT of mice living at thermoneutrality appears more "white-fat like," or perhaps more "brite/beige-fat" like (Figure 2.13). Thus, it seems likely that humans possess classic brown fat and that studies of brown fat in mice will provide important insights into human BAT regulation. Continued elucidation of mTORC2 pathways in BAT bioenergetics could therefore lead to novel antiobesity therapies that target cellular energy expenditure.

CHAPTER III:

the Role of mTORC2 Signaling in Mature Brown Adipocytes

Author contributions:
Chien-Min Hung designed the project, performed most experiments, and wrote the manuscript

David A. Guertin designed the project and edited the manuscript.

Wen-Yu Hsiao conducted *in vitro* glucose uptake assays

Introduction

By studying *in vivo* functions of mTORC2 in *Myf5*+ precursors, I previously described that mTORC2 plays a critical role in adipose tissue growth and metabolism. In particular, mTORC2 deficiency shifts BAT metabolism towards a more oxidative and less lipogenic state by enhancing mitochondrial OXPHOS genes and thermogenic program. These results are quite surprising since those phenotypes were not reported in previous studies for the role of mTORC2 in adipose tissue using *aP2* (*adipocyte protein 2*)-*Cre* (Cybulski et al., 2009; Kumar et al., 2010). The reason causing these discrepancies is not entirely clear, but the genetic tools used are very different. The Cre recombinase driven by the promoter of *Myf5* expresses in mesenchymal precursors, which give rise to myocytes, brown adipocytes and a subset of white adipocytes (Sanchez-Gurmaches and Guertin, 2014b), while the transgenic *Cre* controlled by the *aP2* promoter is presumably active only when adipocytes (includes brown and white adipocytes) become mature. However, it was recently shown that *aP2-Cre* also induces gene recombination in other cell types, including endothelial cells and heart (Lee et al., 2013). Thus, both systems are not perfect for genetic studies in mature brown adipose tissue due to concerns on tissue specificity and development. To circumvent these caveats, I utilized two different strategies in this chapter, namely *Ucp1-Cr*e and *Ucp1-CreER*, to specifically examine the role of mTORC2 in mature brown adipose tissue. Here, I demonstrated that transgenic *Ucp1-Cre* activity is mostly restricted to classical brown adipocytes, which helped clarify physiological consequences of gene disruption in a cell- and tissue-autonomous manner. Moreover, the tamoxifen-controlled CreER system allows temporal control of gene

targeting at the adult stage to avoid potential developmental issues. By using these strategies, I find here that mTORC2 has critical roles in both regulating fuel utilization and the thermogenic program in BAT. Specifically, I provide evidence supporting a model that mTORC2 has a dual role in controlling metabolic processes: it promotes glucose flux and lipid biosynthesis but negatively regulates lipid uptake and oxidation. Importantly, inhibiting mTORC2 in BAT enhances the thermogenic program even in the absence of thermal stress which profoundly protects mice against obesity and its associated metabolic syndromes, such as nonalcoholic fatty liver disease (NAFLD). Collectively, the results provide new insights into the role of mTORC2 in regulating BAT fuel utilization and thermogenesis.

Results

mTORC2 in BAT Controls Fuel Utilization

To gain insights into the role of mTORC2 in mature brown adipose tissue, I generated congenital BAT Rictor knockout mice by combining the *ucp1-cre* driver with floxed *rictor* alleles *(Ucp1-Cre;Rictor$^{fl/fl}$)*. The *Rictor$^{Ucp1\text{-}cKO}$* mice are born at expected ratios and grow normally under standard vivarium conditions (normal chow diet; 22°C) (Figure 3.1A). Gross tissue mass of all classical BATs, like interscapular BAT (iBAT), subscapular BAT (sBAT) and cervical BAT (cBAT) are reduced ~50% in *Rictor$^{Ucp1\text{-}cKO}$* mice compared to BATs in control mice (Figure 3.1B). The reduction in tissue mass is, at least partially, due to a reduction in lipid storage as shown by histological analysis

(Figure 3.1C). Except for a modest decrease in liver and anterior subcutaneous WAT (asWAT) mass, all other tissues are of normal size (Figure 3.1D and 3.1E). As expected, Rictor protein levels are decreased in iBAT, and the lack of mTORC2 signaling in Rictor-deficient BATs is confirmed by the reduction in both AKT S473 and T450 phosphorylation (Figure 3.1F). In contrast, there is no decrease in either Rictor protein or AKT phosphorylation in posterior subcutaneous WAT (psWAT), perigonadal WAT (pgWAT) and liver (Figure 3.1G). Thus, under standard conditions (mild cold stress at 22°C) *Ucp1-Cre* mostly restricts *Rictor* deletion to classic brown adipocytes where the mTORC2 signaling is required to maintain intracellular lipid stores.

Importantly, the paucity of lipid storage is almost identical to the previous findings in $Rictor^{Myf5cKO}$ mice, suggesting mTORC2 signaling is directly involved in regulating the homeostasis of lipid metabolism. Hence, I thought to examine how molecular markers and pathways affected by mTORC2 inhibition in mature brown adipocytes by quantitative real-time PCR (qRT-PCR). First, adipocyte markers (*C/ebpα*, *C/ebpβ*, *Pparγ1/2*, *Fabp4* and *Adipoq*) (Figure 3.1H) and BAT identity genes (*Ucp1*, *Elovl3*, *Dio2*, *Prdm16* and *Pgc1α*) (Figure 3.1I) express normally in $Rictor^{Ucp1\text{-}cKO}$ BAT, indicating BAT development is not affected by mTORC2 loss. Interestingly, *interferon regulatory factor 4* (*Irf4*) is highly induced in Rictor-deficient BAT (Figure 3.1I). Irf4 is a newly identified activator of BAT thermogenic program, which cooperates with PGC1α to regulate *Ucp1* expression (Kong et al., 2014). However, higher *Irf4* levels are not paralleled by a higher *Ucp1* mRNA expression, although UCP1 protein levels are slightly

elevated in Rictor-deficient BAT (Figure 3.1F and 3.1J). The discrepancy in *Ucp1* expression between the result here and the previous *Myf5* model is needed to be clarified.

On the other hand, an elevation in lipolysis (i.e. the breakdown of triglycerides) activity could also result in a decrease of lipid content in adipocytes. Adipose triglyceride lipase (ATGL) and hormone-sensitive lipase (HSL), two essential lipases mediating lipolysis, express at similar mRNA and protein levels in both control and Rictor-deficient BAT. Also, the phosphorylation levels of two regulatory sites on HSL (S565 site by AMPK; S660 site by PKA) are also not perturbed by mTORC2 inhibition, suggesting lipolysis is not a primary cause for the reduction in lipid stores. Our lab has previously shown that mTORC2 signaling promotes lipid biosynthetic pathways in brown (Hung et al., 2014) and white adipose tissue (Tang et al., 2016). Consistent with this notion, the mRNA (Figure 3.2A) and protein (Figure 3.1F) levels of *Acly*, *Acc*, and *Fasn* are decreased in the BAT of $Rictor^{Ucp1\text{-}cKO}$ mice. Importantly, *Chrebpβ*, which encodes a transcriptional activator for DNL genes (Herman et al., 2012), but not *Srebf1c,* is severely reduced in mRNA levels (Figure 3.2A). The expression of *Agpat1* and *Agpat2*, which function in *de novo* phospholipid and triacylglycerol biosynthesis, are also modestly reduced (Figure 3.2B). Therefore, the reduction in lipid production pathways could partially explain the low lipid content observed in Rictor-deficient BAT. These results from BAT-specific knockout mice corroborate with the previous findings in $Rictor^{Myf5cKO}$ mice and suggest that mTORC2 signaling intrinsically (or cell-autonomously) regulates the expression of *de novo* lipogenesis pathway.

When BAT is activated, intracellular lipid storage is rapidly mobilized to provide fatty acids as a major fuel source for thermogenesis. Meanwhile, large amount of glucose and lipids are withdrawn from the circulation into BAT, where they are further processed to replenish the lipid storage. The high glucose flux and high lipid oxidation are hallmarks of BAT metabolism during thermogenesis. However, it is still not entirely clear about the signaling pathways coordinating glucose and fatty acid utilization. Our previous report (Tang et al., 2016) has made a connection between the mTORC2 signaling and glucose uptake in white adipocytes. Given the DNL pathway is compromised in KO BAT, I thus hypothesized that glucose uptake could be affected by mTORC2 loss. As expected, BAT incorporates a much higher amount of glucose than pgWAT, but it is surprising that mTORC2 deficiency does not impair basal glucose uptake (i.e. without stimulation) in BAT (Figure 3.2C). To further examine the role of mTORC2 in glucose uptake, I thus utilized the culture system mentioned previously to measure glucose consumption of brown adipocytes under different stimuli. Likewise, basal glucose uptake in cultured brown adipocytes is also not altered by mTORC2 inhibition. However, Rictor-deficient adipocytes show mild reductions in glucose uptake in response to acute (15mins) insulin treatment and prolonged (2hrs) CL-316,243, a β-adrenergic agonist, stimulation (~30% and ~25%, respectively) (Figure 3.2D). Notably, acute CL-316,243 treatment does not stimulate glucose uptake in brown adipocytes. The difference in kinetics indicates that distinct regulatory mechanisms may exist between insulin- and CL-316,243-stimulated glucose incorporation. These data also support a few

other studies showing that mTORC2 is required for the β-adrenergic receptor (β-AR)–dependent glucose uptake (Albert et al., 2016; Sato et al., 2014).

In addition to glucose, circulating fatty acids and triglycerides can also be taken up by brown adipose tissue at very high rates. As shown in Figure 3.2E, Rictor-deficient BAT demonstrates a ~64% higher uptake of free fatty acids than the uptake of control BAT. In accordance, *lipoprotein lyase* (*Lpl*), which encodes an enzyme hydrolyzing triglycerides in lipoproteins, and several PPARα-target genes, which are involved in mitochondrial or peroxisomal lipid oxidation pathways, are upregulated in knockout BAT (Figure 3.2F). Overall, the inhibition of mTORC2 reprograms BAT metabolism, thus favoring lipid utilization and oxidation over glucose-mediated lipogenesis.

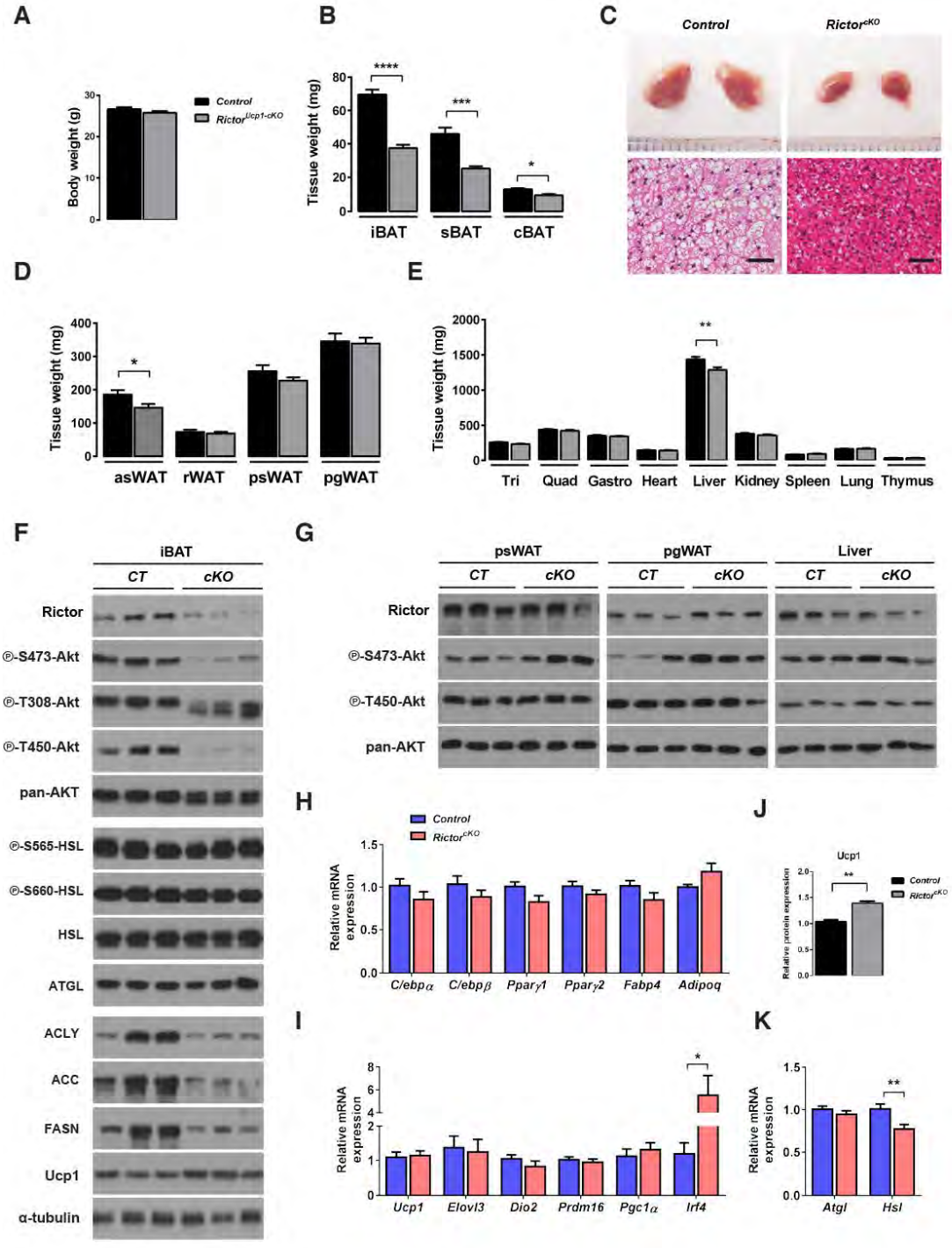
A
Body weight (g)
Control
Rictor Ucp1-cKO
B
Tissue weight (mg)
iBAT
sBAT
cBAT
C
Control
Rictor cKO
D
Tissue weight (mg)
asWAT
rWAT
psWAT
pgWAT
E
Tissue weight (mg)
Tri
Quad
Gastro
Heart
Liver
Kidney
Spleen
Lung
Thymus
F
iBAT
CT
cKO
Rictor
Ⓟ-S473-Akt
Ⓟ-T308-Akt
Ⓟ-T450-Akt
pan-AKT
Ⓟ-S565-HSL
Ⓟ-S660-HSL
HSL
ATGL
ACLY
ACC
FASN
Ucp1
α-tubulin
G
psWAT
pgWAT
Liver
CT
cKO
Rictor
Ⓟ-S473-Akt
Ⓟ-T450-Akt
pan-AKT
H
Control
Rictor cKO
Relative mRNA expression
C/ebpα
C/ebpβ
Pparγ1
Pparγ2
Fabp4
Adipoq
J
Ucp1
Relative protein expression
Control
Rictor cKO
I
Relative mRNA expression
Ucp1
Elovl3
Dio2
Prdm16
Pgc1α
Irf4
K
Relative mRNA expression
Atgl
Hsl

Figure 3.1 mTORC2 Deficiency in Mature Brown Adipocytes Reduces Tissue size and Lipid stores

(A) Body weight of 14wks mice (male, n=11) (B) Brown adipose tissue mass (14wks, male, n=11) (C) Top: Gross appearance of iBAT; Bottom: representative H&E staining sections (14wks, male, the scale bar represents 100μm) (D) White adipose tissue mass (14wks, male, n=11) (E) Liver and other lean tissue mass (14wks, male, n=11) (F) Western blots for interscapular BAT lysates (overnight fasting with 1h refeeding) (G) Western blots for psWAT, pgWAT and liver (overnight fasting with 1h refeeding). (H) qRT-PCR of adipocyte differentiation markers (I) qRT-PCR of thermogenesis-related genes (14wks, male, n=8) (J) Densitometric analysis of UCP1 expression levels (n=4) (K) qRT-PCR of *Atgl* and *Hsl* (14wks, male, n=8) (Bars represent mean ± SEM; t-test; *p<0.05, **p<0.01, ***p<0.001)

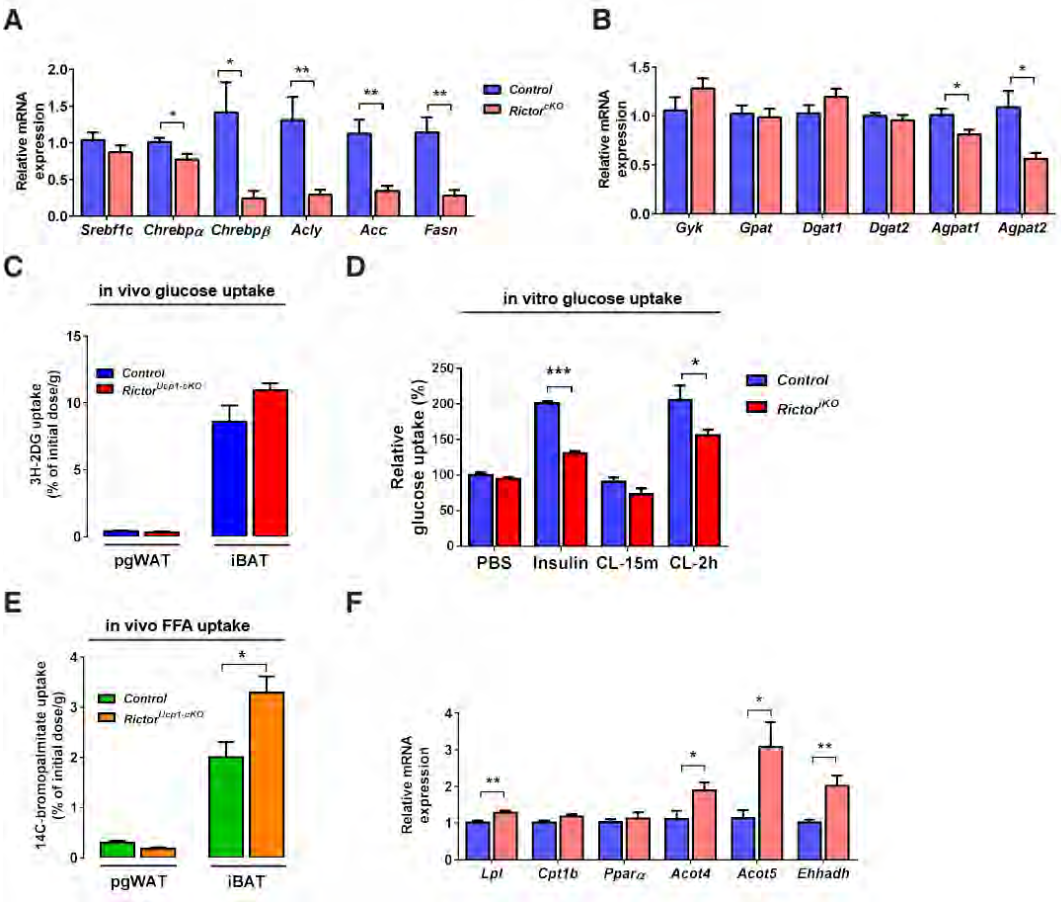

Figure 3.2 Rictor-deficient brown fat displays a metabolic shift from lipogenesis to lipid oxidation

(A) qRT-PCR of de novo lipogenesis genes (14wks, male, n=8) (B) qRT-PCR of phospholipid and triglyceride synthesis genes (14wks, male, n=8) (C) In vivo assay for ^{3}H-2-deoxy-glucose uptake (10wks, male, n=6) (D) In vitro assay for ^{3}H-2-deoxy-glucose uptake, differentiated brown adipocytes at day 11 (n=3) (E) In vivo assay for ^{14}C-bromo-palmitate uptake (10wks, male, n=6) (F) qRT-PCR of lipid uptake and oxidation genes (14wks, male, n=8) (Bars represent mean ± SEM; t-test; *p<0.05, **p<0.01, ***p<0.001)

BAT *Rictor* KO Mice Are Cold Tolerant

UCP1-mediated "non-shivering" thermogenesis which maintains the homeostasis of body temperature during cold exposure is accompanied by elevated glucose and lipid consumption. Since mTORC2 deficiency changes fuel utilization, it is obligatory to determine whether *Rictor*$^{Ucp1\text{-}cKO}$ mice can maintain euthermia under acute and chronic cold conditions. When mice were acutely challenged with an extreme cold (6°C) condition, both control and *Rictor*$^{Ucp1\text{-}cKO}$ mice drop their body temperature similarly in the first three hours; however, the KO mice maintain their body temperature at slightly higher levels at the end of the experiment (Figure 3.3A). By contrast, the fasted mice exhibit much rapid rates of decrease in body temperature than the mice supplied with food (Figure 3.3B). Under this condition, the body temperature of *Rictor*$^{Ucp1\text{-}cKO}$ mice is trending towards lower levels after 5 hours in cold (Figure 3.3B), which could be due to the limited lipid storage in KO BAT. However, mice living at a chronic cold condition (6°C for two weeks) exhibit no difference in body temperature between two groups (Figure 3.3C), suggesting that the disruption of mTORC2 in BAT does not impede the ability of mice to defend body temperature under cold stresses. In addition, the BAT thermogenesis can be directly measured by the heat released from brown fat. An infrared thermo-imager was used to detect skin surface temperature of mice. As shown in Figure 3.3E, higher maximal and average temperatures of the interscapular region are recorded in the cold-adapted *Rictor*$^{Ucp1\text{-}cKO}$ mice compared to controls, indicating high heat production from Rictor-deficient brown fat. In contrast, there is no difference in heat output and rectal temperature between two groups at room temperature (Figure 3.3D). In

agreement with high heat production, key regulators of thermogenesis (*Prdm16*, *Pgc1α* and *Irf4*) are significantly upregulated in Rictor-deficient BAT compared to control in chronic cold conditions (Figure 3.3 G).

It is known that the processes in lipid turnover (lipid biosynthesis and mobilization) are highly induced in activated BAT (Townsend and Tseng, 2014). Consistent with this notion, there is 1.5 to 2 fold induction of DNL genes (*Chrebpβ*, *Acly*, *Acc* and *Fasn*) in wildtype cold-adapted BAT compared to the ones at 22°C (Figure 3.3H). Interestingly, despite lower in overall levels, DNL genes are also highly induced (3 to 6 fold changes compared to 22°C) (Figure 3.3H) in the BAT of $Rictor^{Ucp1\text{-}cKO}$ mice after cold acclimation. Examined by hematoxylin and eosin (H&E) stain, both control and $Rictor^{Ucp1\text{-}cKO}$ BATs exhibit similar morphology with brown adipocytes containing lipid droplets that are small, but uniform, in size (Figure 3.3F) after two-week habitation at 6°C. These data indicate that additional signals/mechanisms exist to compensate the requirement of mTORC2 signaling for glucose metabolism and lipid synthesis when BAT is chronically stimulated. Also, glycerol kinase (Gyk) (Figure 3.3I) and lipid oxidation pathways (*Lpl*, *Cpt1a*, *Acot4*, *Acot5* and *Ehhadh*) are also upregulated in $Rictor^{Ucp1\text{-}cKO}$ BAT to greater extents (Figure 3.3J), supporting augmented lipid usage in KO BAT. In conclusion, Rictor-deficient BAT is fully functional in thermogenesis when nutrient supply is sufficient; given it has defects in lipogenesis.

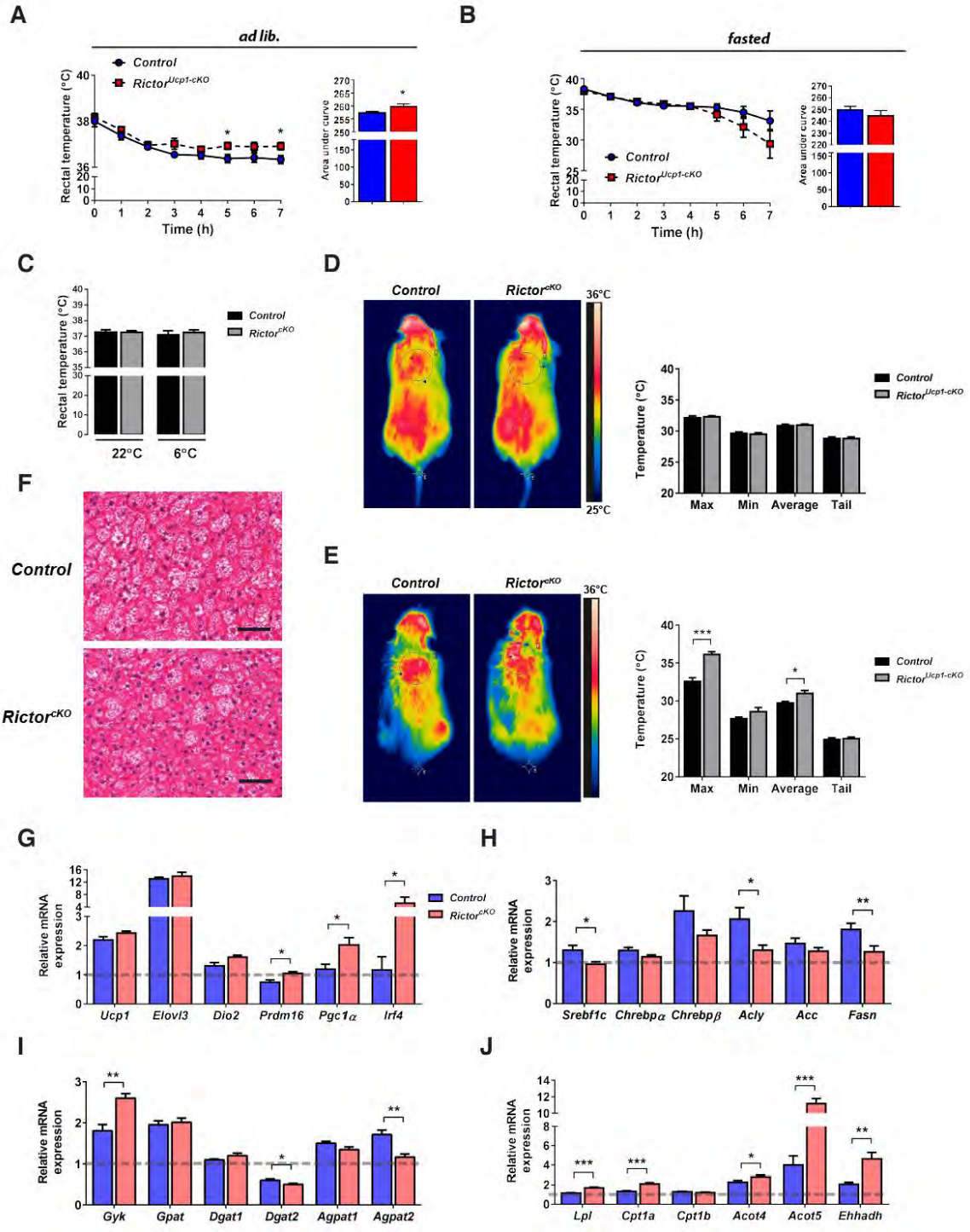
A
ad lib.
Control
Rictor Ucp1-cKO
Rectal temperature (°C)
Time (h)
Area under curve
B
fasted
C
Control
Rictor cKO
22°C
6°C
D
Control
Rictor cKO
36°C
25°C
Temperature (°C)
Max
Min
Average
Tail
E
F
Control
Rictor cKO
G
Relative mRNA expression
Ucp1
Elovl3
Dio2
Prdm16
Pgc1α
Irf4
H
Srebf1c
Chrebpα
Chrebpβ
Acly
Acc
Fasn
I
Gyk
Gpat
Dgat1
Dgat2
Agpat1
Agpat2
J
Lpl
Cpt1a
Cpt1b
Acot4
Acot5
Ehhadh

Figure 3.3 *Rictor*$^{Ucp1\text{-}cKO}$ mice are cold tolerant with enhanced heat production

(A) Rectal temperature for ad libitum mice are exposed to cold (10wks, male, n=9-10) (B) Rectal temperature for fasted mice are exposed to cold (10wks, male, n=9-10) (C) Rectal temperature for resting mice housed at 22°C and 6°C (10wks, male, n=11 at 22°C n=5-6 at 6°C) (D) Infrared thermography of skin surface temperature (22°C, n=8-9) (E) Infrared thermography of skin surface temperature (6°C, n=4) (F) Representative H&E staining sections for iBAT from 2-week adapted mice (14wks, male, n=8) (G) qRT-PCR of thermogenic genes (14wks, male, n=8) (H) qRT-PCR of lipogenesis genes (14wks, male, n=8) (I) qRT-PCR of triglyceride synthesis genes (14wks, male, n=8) (J) qRT-PCR of lipid uptake and oxidation genes (14wks, male, n=8) (All genes are present as relative levels to the ones in room temperature control BAT; Bars represent mean ± SEM; t-test; *p<0.05, **p<0.01, ***p<0.001)

Enhanced Browning in Beige/Brite Adipocytes of *Rictor*$^{Ucp1\text{-}cKO}$ Mice

In contrast to classical brown adipocytes, beige or brite adipocytes express very low levels of *Ucp1* when mice are housed at room temperature; however, the formation of beige/brite adipocytes and their *Ucp1* expression can be drastically induced by chronic cold stimulation. Since mTORC2 loss enhances BAT thermogenesis upon cold exposure, I would like to further investigate whether mTORC2 play a similar role in beige/brite adipocytes. To visualize and quantify the abundance of beige/brite adipocytes, I crossed *Ucp1-Cre* control mice or *Ucp1-Cre;Rictor*$^{fl/fl}$ mice with the *Rosa26-mTmG* mice (Muzumdar et al., 2007), which carry a dual color reporter allele that consists of member-targeting fluorescent reporters. All Cre-positive cells and their descendants are irreversibly labeled with membrane-targeted GFP (mGFP), whereas all Cre-negative cells express membrane-targeted Tomato (mTFP). As expected, at 22°C, the presence of GFP-labelled (green) adipocytes is mostly restricted to classical brown fat depots (iBAT, sBAT, and rBAT (renal BAT)), while adipocytes in white fat depots (pgWAT and rWAT) are exclusively marked by mTFP (red) (Figure 3.4A). Interestingly, chronic cold exposure increases the percentage of mGFP+ cells in rBAT, but not, in the other depots (Figure 3.4A). Again, the mTmG labeling results in agreement with the loss of Rictor protein detected by western blots (Figure 3.1F&G) demonstrated the tissue-specificity of *Ucp1-Cre* transgene.

On the other hand, small proportions of mGFP+ cells can be spotted in psWAT even at 22℃ (Figure 3.5A). By contrast, numerous clusters of mGFP+ adipocytes, presumed beige/brite adipocytes, emerge in psWAT after chronic cold exposure (Figure

3.5A). The percentage of mGFP+ adipocytes within the cluster/patch rises from 14% at 22°C to 47% at 6°C in control mice, and the percentage goes from 5% to 56.7% in *Rictor*$^{Ucp1\text{-}cKO}$ mice (Figure 3.5B and 3.5C). Thus the abundance of beige/brite adipocytes is quantitatively similar between wildtype and *Rictor*$^{Ucp1\text{-}cKO}$ mice. Notably, those mGFP+ cells in *Rictor*$^{Ucp1\text{-}cKO}$ mice are smaller than the neighboring mTFP+ cells (Figure 3.5B), which is similar to *Rictor* knockout phenotypes in BAT. Histological analysis also reveals the formation of multilocular brown-like adipocytes in psWAT after cold acclimation (Figure 3.5D), and psWAT from *Rictor*$^{Ucp1\text{-}cKO}$ mice exhibits a profound "browning" morphology compared to control. Accordingly, thermogenic program genes (*Ucp1*, *Pgc1α* and *Dio2*) are upregulated in control psWAT and to greater extents in tissues from *Ucp1-Cre;Rictor* mice (Figure 3.5E). Conversely, there is no difference in differentiation or lineage markers (*Cd137*, *Pparγ1*, *Pparγ2*, *Prdm16* and *Zfp423*) among different groups (Figure 3.5E). The enhanced browning phenotype in inguinal WAT (psWAT) argues that the signaling cascades elicited by mTORC2 have a similar role in both brown and beige adipocytes for regulating the thermogenic program.

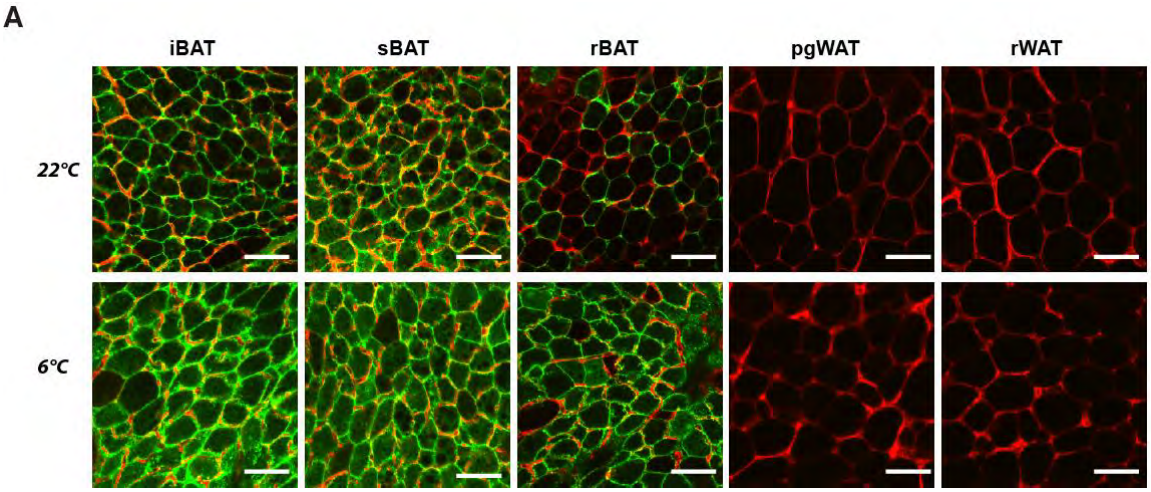

Figure 3.4 Lineage-tracing by *Ucp1-Cre-mTmG reporter*

(A) Representative confocal microscopy images of mTFP- and mGFP-labelled adipocytes in the indicated fat depots. (Top panels: mice housed at room temperature, Bottom panels: mice housed at 6°C for 2 weeks, the scale bar represents 50μm)

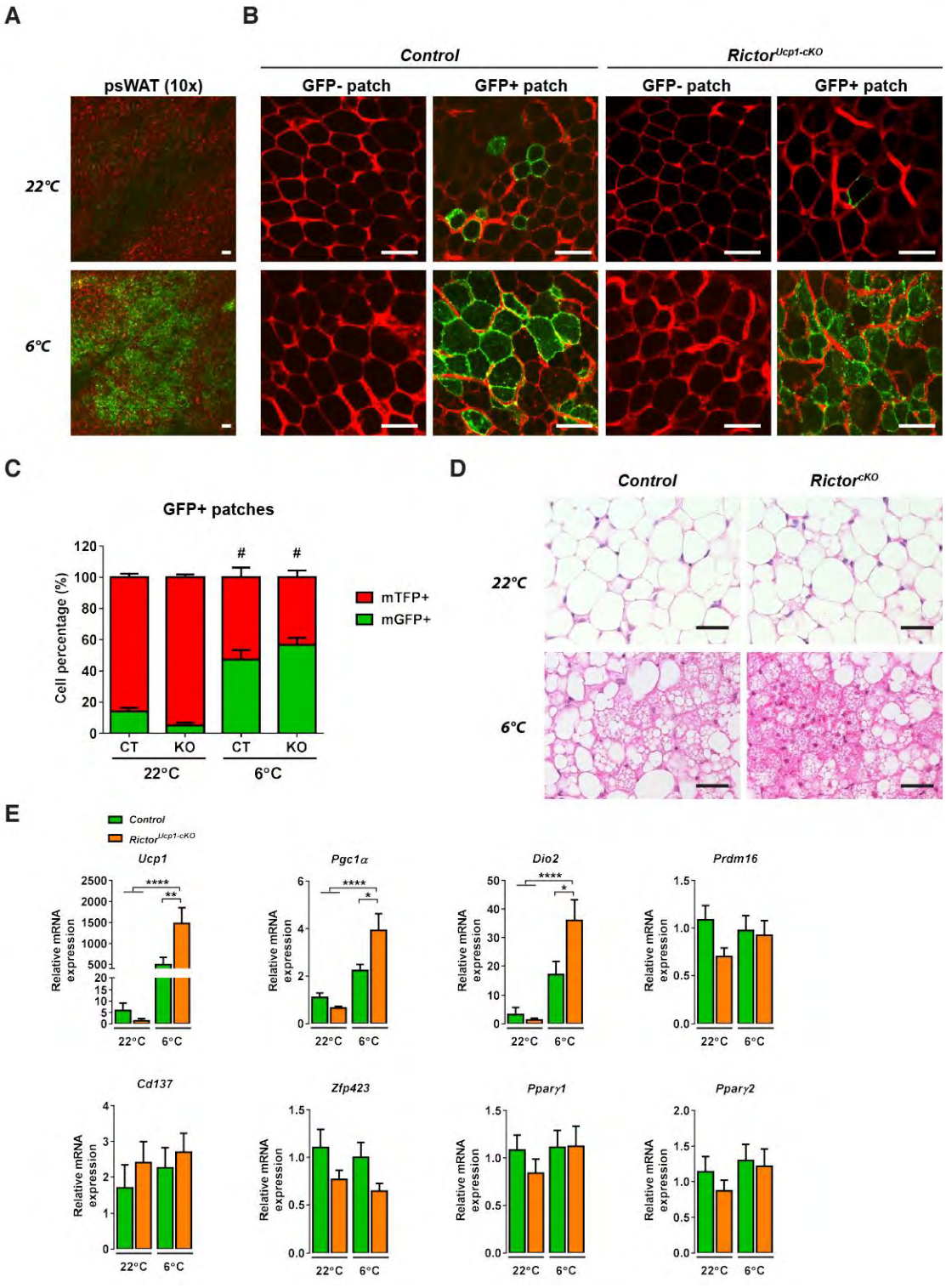
A
B
Control
Rictor Ucp1-cKO
psWAT (10x)
GFP- patch
GFP+ patch
GFP- patch
GFP+ patch
22°C
6°C
C
GFP+ patches
Cell percentage (%)
mTFP+
mGFP+
CT
KO
CT
KO
22°C
6°C
D
Control
Rictor cKO
22°C
6°C
E
Control
Rictor Ucp1-cKO
Ucp1
Pgc1α
Dio2
Prdm16
Cd137
Zfp423
Pparγ1
Pparγ2
Relative mRNA expression
22°C
6°C

Figure 3.5 Enhanced browning in psWAT of *Rictor*$^{Ucp1\text{-}cKO}$ mice

(A) Confocal microscopy images of psWAT showing GFP+ patches (the scale bar represents 50μm) (B)Representative confocal microscopy images of mTFP- and mGFP-labelled adipocytes in psWAT. (Top panels: mice housed at room temperature, Bottom panels: mice housed at 6°C for 2 weeks, the scale bar represents 50μm) (C) Quantification of mGFP+ versus mTFP+ cells in the GFP+ clusters (D) Represntative H&E stains for psWAT from room temperature or cold-adapted mice (E)qRT-PCR of thermogenic and differentiation/lineage markers (14wks, male, n=8) (Bars represent mean ± SEM; t-test; *p<0.05, **p<0.01, ***p<0.001)

BAT *Rictor* KO Mice Are Resistant to Obesity at Thermoneutrality

Small rodents, like mice, housed at standard vivarium conditions (room temperature, 21~22°C) are, in fact, under a chronic thermal stress (i.e. the animals are compelled to increase their metabolic rates to maintain euthermia) (Cannon and Nedergaard, 2011). By contrast, living at 22°C is considered as a thermoneutral condition for most people because we wear clothing. To rule out cold stress as the driving factor accounting for brown fat phenotypes, I next investigated the role of mTORC2 in BAT by housing mice at thermoneutrality (30°C for mice), which is more close to the physiological conditions of humans. Six-week-old young mice were acclimated to a thermoneutral room for eight weeks and fed with standard chow diet. Strikingly, wildtype brown adipocytes completely lose their brown adipocyte morphology as each of them contains a large unilocular lipid droplet similar to white adipocytes (Figure 3.6A). This phenomenon has been described as "whitening" and it is accompanied by diminished brown fat marker genes and increased white marker genes (Harms et al., 2014). By contrast, Rictor-deficient brown adipocytes are resistant to the whitening effect of thermoneutrality, as evidenced by multilocular morphology and by better preserved brown characteristics in gene expression (*Ucp1*, *Elovl3*, *Prdm16*, *Irf4*, *Cideb* and *Sgk2*) (Figure 3.6B and 3.6C). Of note, white selective markers (*Dpt* and *Retn*) and DNL pathway genes (*Srebf1c*, *Chrebpβ*, *Acly*, *Acc* and *Fasn*) express at lower levels in Rictor-deficient BAT. These data again suggest that mTORC2 activity normally suppresses the thermogenic program, and importantly this phenotype is not dependent on cold stimulation.

Evidence from both rodent and human studies have clearly demonstrated that brown adipose tissue significantly contributes to whole body energy expenditure and thus enhancing brown fat activity could have protective effects against obesity and diabetes (Bartelt and Heeren, 2014). To further examine the responses of mice to obesogenic diet, mice were given with a 45% high-fat diet (HFD) for 16 weeks in thermoneutral conditions. As the end of diet-experiment, *Rictor*$^{Ucp1\text{-}cKO}$ mice gain significantly less body weight (Figure 3.6 E and 3.6F), while the food consumption is not different between two groups (Figure 3.6 G). Importantly, *Rictor*$^{Ucp1\text{-}cKO}$ mice also show protection from increased adiposity (asWAT, rWAT and pgWAT) and hepatomegaly, which are caused by excess lipid deposition in these tissues (Figure 3.6 H). Therefore, *Rictor*$^{Ucp1\text{-}cKO}$ mice are resistant to HFD-induced obesity at thermoneutrality.

Inducible Deletion of *Rictor* in BAT Augments Diet-induced Thermogenesis

Unlike white adipose tissue which mostly forms postnatally, mouse BAT is fully mature and functional at birth allowing newborns to adapt to the cold environment. Because the expression of Ucp1 is initiated in utero between embryonic day (E) 18.5 and E19.5, the deletion of *Rictor* gene by *Ucp1-Cre* mediated recombination is expected to occur around this period. Therefore, it was difficult to rule out the possibility that beneficial effects elicited by congenital *Rictor* knockout are secondary to developmental defects. On the other hand, pharmacological agents for acute inhibition of mTORC2 signaling in BAT are highly desirable to investigate the therapeutic application of mTORC2 inhibition. Unfortunately, such inhibitors that specifically and potently inactivate mTORC2 are yet

to be discovered. To overcome these issues, I further generated an inducible knockout model for *Rictor* deletion by crossing *Rictor* floxed mice with *Ucp1-CreER*^{T2} transgenic mice. The CreER recombinase consists of Cre protein fused to the hormone-binding domain of estrogen receptor. The recombinase remains inactive until it binds to estrogen receptor ligands, like tamoxifen (TAM), thus allowing a temporal control of gene deletion. Rictor protein can be rapidly eliminated in BAT after six-day tamoxifen treatment (data not shown) and remains at low levels for at least ten weeks post injection (Figure 3.8D). Again, inhibition of mTORC2 activity is confirmed by reduction in phosphorylation of AKT-T450 (Figure 3.8D). Then I designed an experiment to test whether induced *Rictor* deletion in BAT of middle-aged mice (20 weeks old) could still provide beneficial effects on HFD (Figure 3.7A). After TAM treatment, control (Cre-negative mice) and inducible BAT-KO (*Rictor*$^{Ucp1\text{-}iKO}$) mice were first transferred to a thermoneutral room for one-week adaptation and then the mice were fed either with chow diet or 45% HFD for nine weeks. Remarkably, in HFD-fed cohorts, *Rictor*$^{Ucp1\text{-}iKO}$ mice exhibit a less increase in body weight than control mice do (Figure 3.7B and 3.7C). After HFD feeding, the average body weight of control mice is 44.4 ± 1.4g, whereas that of *Rictor*$^{Ucp1\text{-}iKO}$ mice is only 38.0 ± 1.2g (Figure 3.7B). Importantly, the difference in body weight is not due to changes in food consumption (Figure 3.7D), but it is mainly due to reduction in adipose tissue mass, especially in pgWAT (Figure 3.7E). Interestingly, while gross liver weight is only modestly changed, livers from *Rictor*$^{Ucp1\text{-}iKO}$ mice are protected from lipid deposition (liver steatosis) caused by HFD feeding (Figure 3.7G). Importantly, mice with HFD-feeding usually develop progressive glucose intolerance and

insulin resistance. In accordance with the protection from obesity, *Rictor*$^{Ucp1\text{-}iKO}$ mice conserve efficient glucose clearance (glucose tolerance test) on HFD than control mice (Figure 3.7H and 3.7I); however, I did not observe any difference in insulin sensitivity (Figure 3.7J and 3.7K). In addition, all metabolic parameters tested here are similar between the chow cohorts. Altogether, these results suggest that mTORC2 inhibition in BAT demonstrates similar favorable effects on whole body metabolism regardless of mouse age.

It has been described that the energy expenditure of BAT can be stimulated when mice fed with high-calorie diet, which is called diet-induced thermogenesis (DIT). However, the molecular basis of DIT in BAT has not been fully characterized. I next investigated whether brown fat activity changes in response to different diets. In the chow-diet cohorts, histology reveals a higher percentage of multilocular adipocytes in Rictor-deficient BAT, whereas adipocytes in control BAT mostly consist of unilocular and "white adipocyte-like" cells. Interestingly, HFD treatment is able to reverse the whitening effect of warm environment, as judged from increased abundance of multilocular cells in control BAT (Figure 3.8A). In contrast, Rictor-deficient BAT exhibits a stronger response to HFD (Figure 3.8A). This morphological browning is also paralleled by the UCP1 protein levels (Figure 3.8B) with highest UCP1 expression in Rictor-deficient BAT from the HFD cohorts. Consistently, a panel of thermogenic genes (*Ucp1*, *Pgc1α*, *Irf4*, *Cidea*, *Dio2* and *Elovl3*) are either significantly or trending towards higher levels in Rictor-deficient BAT (Figure 3.8C and 3.8D). These results strongly agree with our previous findings in the *Rictor*^{Myf5cKO} model, suggesting that inhibition of

mTORC2 signaling enhances diet-induced thermogenesis in BAT. Moreover, Rictor-ablated BAT also has higher expression of *Lpl* and *Cpt1b* (Figure 3.8D), which might correlate with increased lipid usage under these conditions. Thus, I examined serum levels of nutrients in both chow-fed and HFD-fed groups. While serum levels of glucose and cholesterol significantly increase in the HFD cohorts of both genotypes, *Rictor*$^{Ucp1\text{-}iKO}$ mice are able to maintain lower levels of triglycerides (TAG) and free fatty acids (FFA) on HFD compared to control mice (Figure 3.8E). These data collectively suggest that Rictor-deficient BAT protects mice from HFD-induced lipotoxicity and obesity at thermoneutrality possibly due to augmented diet-induced thermogenesis.

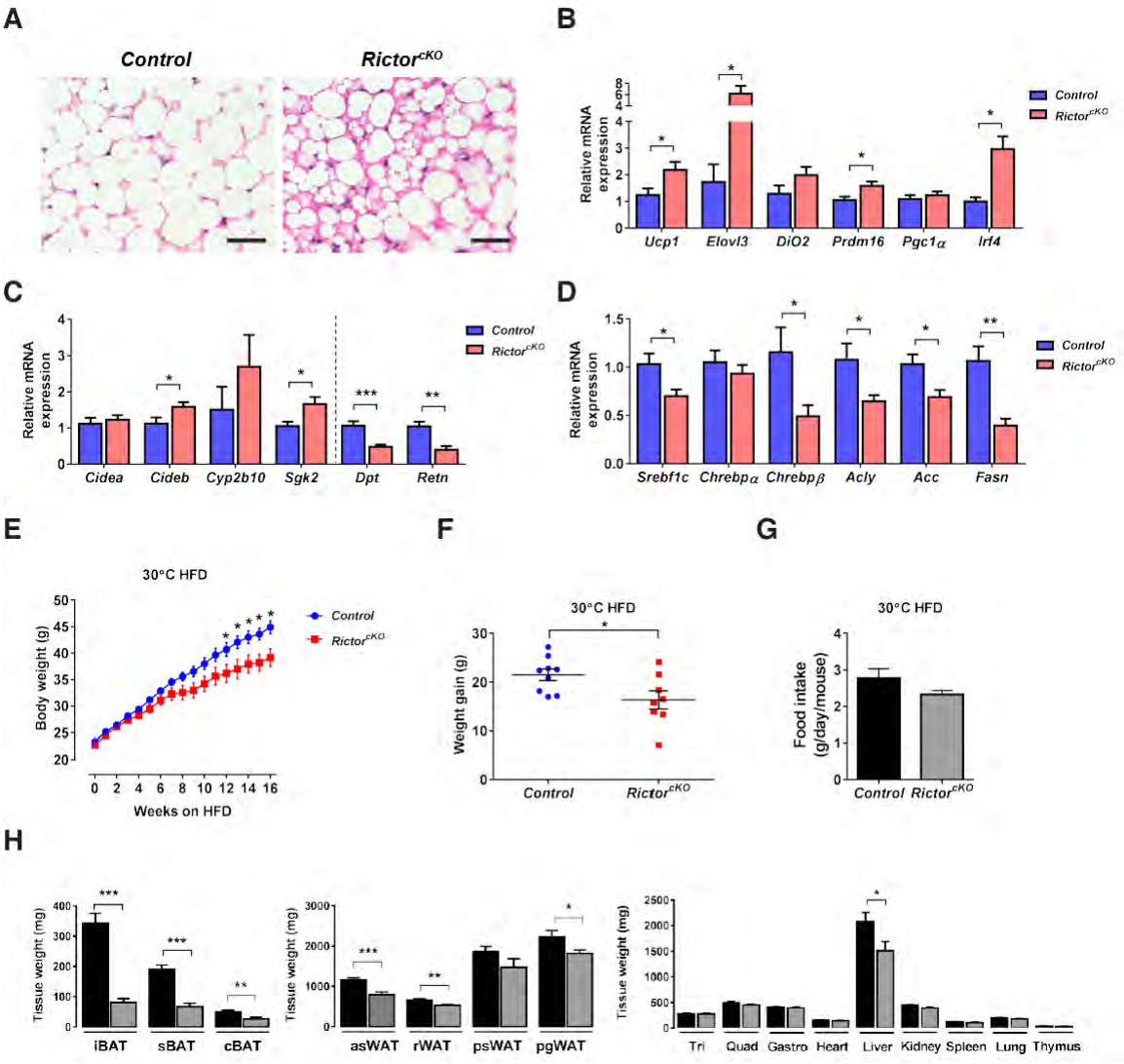

Figure 3.6 *Rictor*$^{Ucp1\text{-}cKO}$ BAT is resistant to the "whitening" effect

(A) Represntative H&E stains for iBAT (14wks, male, n=8, the scale bar represents 100μm) (B-D) qRT-PCR of thermogenic, BAT-selective, WAT-selective and lipogenic genes (14wks, male, n=8) (E) Growth curves for HFD-fed mice at thermoneutrality (10-26 weeks, male, n=8-9) (F) Net weight gain from initial body weight (26 weeks, male, n=8-9) (G) Food consumption during HFD (n=4-5) (H) Tissue mass of HFD-

fed mice (26 weeks, male, n=8-9) (Bars represent mean ± SEM; t-test; *p<0.05, **p<0.01, ***p<0.001)

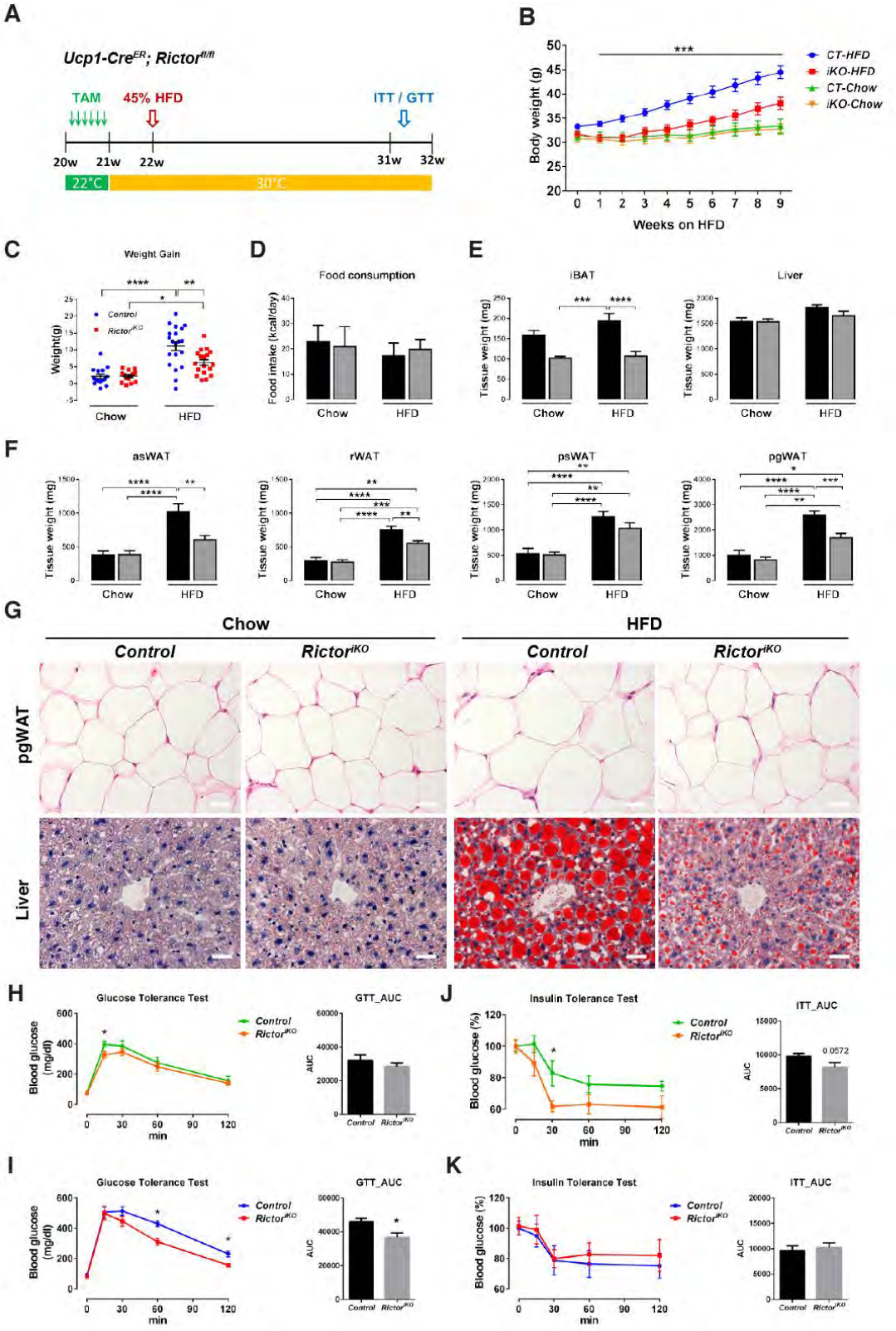
A
Ucp1-Cre^ER; Rictor^fl/fl
TAM
45% HFD
ITT / GTT
20w
21w
22w
31w
32w
22°C
30°C
B
Body weight (g)
Weeks on HFD
CT-HFD
iKO-HFD
CT-Chow
iKO-Chow
C
Weight Gain
Weight(g)
Control
Rictor^iKO
Chow
HFD
D
Food consumption
Food intake (kcal/day)
E
iBAT
Liver
Tissue weight (mg)
F
asWAT
rWAT
psWAT
pgWAT
G
Chow
HFD
Control
Rictor^iKO
pgWAT
Liver
H
Glucose Tolerance Test
Blood glucose (mg/dl)
min
GTT_AUC
AUC
I
J
Insulin Tolerance Test
Blood glucose (%)
ITT_AUC
0.0572
K

Figure 3.7 Mice with Rictor inducible knockout in BAT are less susceptible to obesity and metabolic disease

(A) Diagram for the HFD experiment (B) Growth curve for chow-fed and HFD-fed cohorts (male, n=13-18) (C) Net weight gain from initial body weight (male, n=13-18) (D) Food consumption during HFD (n=3-4) (E) Tissue mass for iBAT and liver (male, n=13-18) (F) Tissue mass for white fat depots (male, n=13-18) (G) Represntative H&E stains for pgWAT and liver (the scale bar represents 100μm) (H&I) Glucose tolerance test for (H) chow-fed cohorts (n=7-9) and (I) HFD-fed cohorts (n=7-8) (J&K) Insulin tolerance test for (J) chow-fed cohorts (n=7-9) and (K) HFD-fed cohorts (n=7-8) (Bars represent mean ± SEM; t-test; *p<0.05, **p<0.01, ***p<0.001)

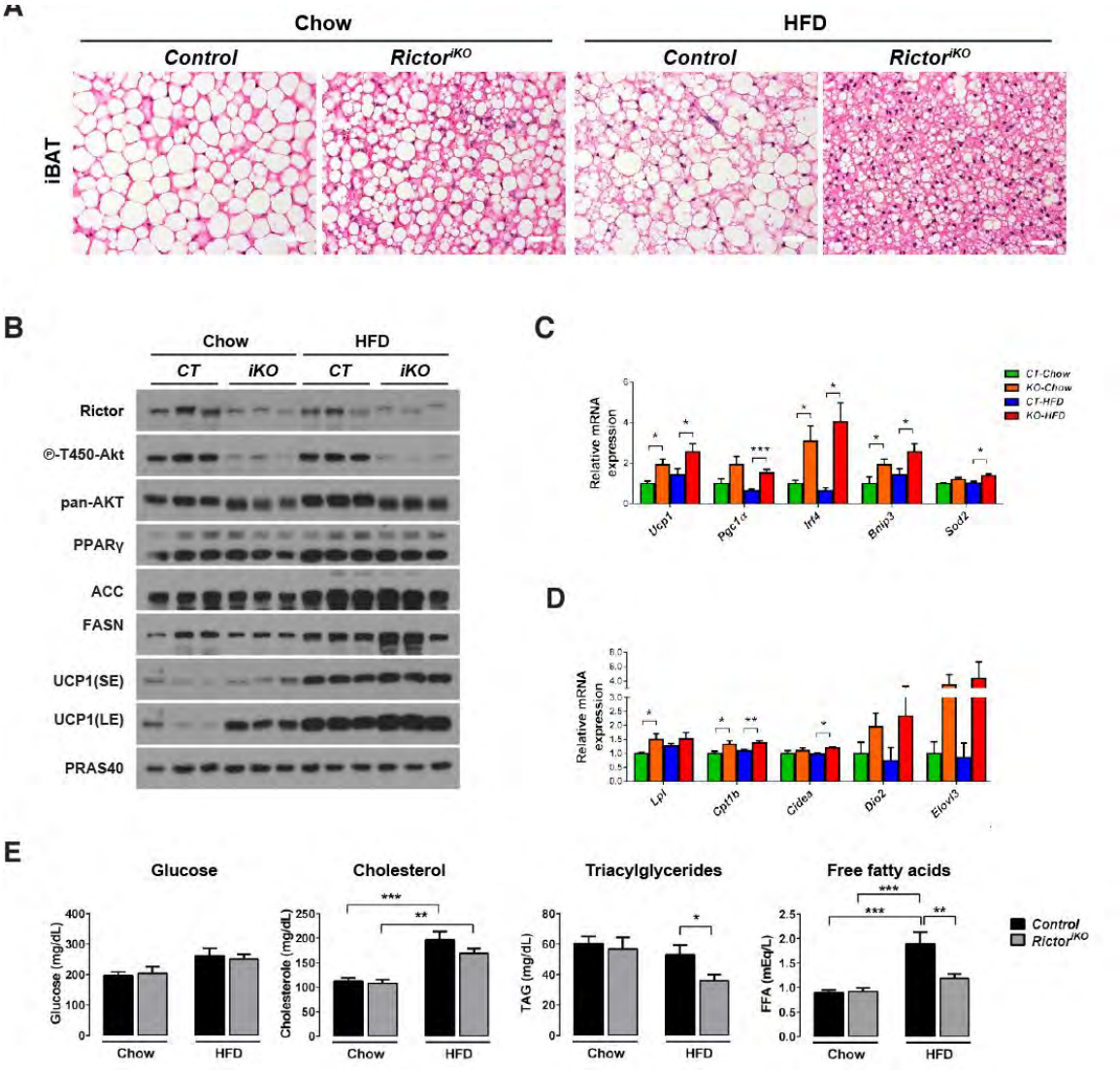

Figure 3.8 Inducible *Rictor* KO BAT shows enhanced diet-induced thermogenesis

(A) Represntative H&E stains for iBAT (the scale bar represents 100μm) (B) Western blots for iBAT from chow-fed and HFD-fed mice (C) (D) qRT-PCR of thermogenic genes (male, n=8) (E) Serum chemistry for glucose, cholesterol, triacylglycerides and free fatty acids (Bars represent mean ± SEM; t-test; *p<0.05, **p<0.01, ***p<0.001)

Discussion

It is widely appreciated that activating brown adipose tissue could be a potential therapeutic strategy to combat obesity and type II diabetes. When BAT thermogenesis is fully activated, high amounts of glucose and fatty acids are taken up by brown adipose tissue to fulfill its metabolic and energetic demands during uncoupled respiration. The tremendous oxidative capacity is not only a hallmark of BAT metabolism but also provides the basis for developing novel therapies to treat metabolic disease in humans. Therefore, understanding molecular events and signaling pathways that govern fuel utilization and thermogenesis is unequivocally important. Glucose uptake measurement has been used as a marker for brown fat activity, especially the ^{18}F-FDG-PET/CT scan for measuring human BAT. However, the role of glucose and glucose-driven lipogenesis in thermogenesis has not been conclusively illustrated. By contrast, many regulatory molecules or metabolic enzymes involved in lipolysis and lipid oxidation are shown to be

essential for the activation of UCP1-mediated thermogenesis (Ahmadian et al., 2011; Lee et al., 2016; Lee et al., 2015). It is estimated that intracellular TAG pools contribute to up to ~84% and ~74% respiration during acute and chronic cold exposure, respectively (Labbe et al., 2015). Here, by using novel genetic models, I demonstrate the critical role of mTORC2 in regulating BAT metabolism and thermogenesis. Specifically, inactivation of mTORC2 in BAT enhances fatty acid utilization and oxidation but reduces glucose uptake and *de novo* lipogenesis. Importantly, the defects in glucose metabolism do not impede BAT thermogenesis upon cold exposure. Instead, loss of mTORC2 augments BAT thermogenic responses to counteract deleterious consequences of HFD-feeding at thermoneutrality, thus protecting mice from developing obesity and metabolic disease. Given humans prefer to live in a thermoneutral environment, the results shown here might be highly relevant and applicable to human BAT studies.

CHAPTER IV:

mTORC2 Signaling Suppresses Ucp1 expression through promoting FoxO1 acetylation

Author contributions:
Chien-Min Hung designed the project, performed most experiments, and wrote the manuscript

David A. Guertin designed the project and edited the manuscript.

SuMyung Jung conducted qRT-PCR of Figure 4.1C

Introdcuation

In previous chapters, the *in vivo* models of mTORC2-ablation in BAT demonstrated a remarkable enhancement in BAT metabolism and activity, which protects mice from HFD-induced obesity and metabolic disease. However, the mechanism by which mTORC2 regulate BAT thermogenic program is remain elusive. Recent studies suggested FoxO1 is a critical mediator of mTORC2 signaling, which regulates FoxO1 through AKT-dependent (Yuan et al., 2012) and AKT-independent mechanisms (Masui et al., 2013). Interestingly, one study showed that FoxO1 can bind and activate *Ucp1* promoter, thus increasing *Ucp1* expression (Ortega-Molina et al., 2012). Therefore, I would like to specifically examine whether mTORC2 could regulate *Ucp1* expression through modulating FoxO1 activity. I report here that mTORC2 functions through FoxO1 activity to negatively regulate BAT thermogenic program. Mechanistically, mTORC2 inhibition reduces the acetylation levels of on FoxO1 without affecting canonical AKT-mediated phosphorylation. Intriguingly, FoxO1 deacetylation can be also induced by β-adrenergic signaling, suggesting such regulatory mechanism could be involved in normal BAT activation. Last, both pharmacological and genetic approaches further confirm that FoxO1 activity is essential for the induction of thermogenic program genes, such as *Ucp1*, *Pgc1α* and *Irf4*, in cultured brown adipocytes. In addition, I also provide evidence showing that mTORC2 signaling could also play a suppressive role in the PKA-mediated signaling. Collectively, these findings suggest that mTORC2

signaling regulate *Ucp1* and the BAT thermogenic program in part through modulating FoxO1 activity.

Results

mTORC2 Cell-autonomously Regulates *Ucp1* Expression

It is well-recognized that insulin signaling can antagonize β-adrenergic signaling in certain metabolic processes, and *vice versa*. For example, insulin has an inhibitory effect on catecholamine-induced lipolysis in part through diminishing cAMP levels. However, it is unclear whether insulin signaling also exerts an adverse effect on *Ucp1* induction by β_3-adrenergic signaling. According to the results shown in previous sections, mTORC2 inhibition appears to augment the gene expression of thermogenic program in both brown adipocytes and brite/beige adipocytes. Given that mTORC2 is one of the key mediators downstream of the insulin receptor signaling, I thus hypothesized that mTORC2 could negatively regulate *Ucp1* expression through cell-autonomous mechanisms. To test this hypothesis, I took advantage of the inducible cell line system (*Ubc-CreER*^{T2};*Rictor*$^{fl/fl}$ brown preadipocytes). As shown in Chapter II, mTORC2 activity is required for brown adipocyte differentiation in culture. Herein I took a different strategy by inducing *Rictor* deletion after PPARγ induction (Figure 4.1A) to avoid interference with differentiation. Indeed, when 4-hydroxytamoxifen (4-OHT) is given at Day 6 to induce *Rictor* deletion, the blockage of mTORC2 signaling does not impede PPARγ expression (Figure 4.1 B). CL-316,243 (a β_3-adrenergic agonist) and forskolin (an activator of cAMP production)

can potently upregulate thermogenic genes, such as *Ucp1*, in mature brown adipocytes. Consistent with the *in vivo* data, loss of mTORC2 activity potentiates UCP1 induction by CL-316,243 and forskolin (Figure 4.1B). Notably, these changes can be at least partially explained by increased *Ucp1* transcription levels (Figure 4.1C). Thus, these data support the hypothesis that mTORC2 cell-autonomously regulates *Ucp1* expression in response to β_3-adrenergic signaling stimuli.

To further gain insights into the mechanisms implicated here, I then compared the signaling responses of control and Rictor-deficient cells to insulin and CL-316,243 stimulation. Control and Rictor-deficient cells have similar responses to insulin stimulation, as judged by the activation of AKT downstream effectors (phosphorylation of AS160 and S6K) (Figure 4.1D). Interestingly, CL-316,243 treatment modestly activates mTORC1 signaling (p-S6K-T389) but does not stimulate mTORC2 signaling (p-AKT-S473). CL-316,243 stimulation leads to activation of PKA and its downstream effectors, including HSL and p38-MAPK (mitogen-activated protein kinase). Both control and *Rictor* knockout cells display similar responses to CL-316,243 in as judged from the phosphorylation of PKA substrates, while HSL-S660, a PKA phosphorylation site, remains a higher level after 30 mins. Moreover, Rictor-deficient adipocytes have higher p38-MAPK (T180) phosphorylation across all the conditions tested, indicating enhanced p38-MAPK activity in KO cells. It is noteworthy that p38-MAPK signaling plays an important role in *Ucp1* transcription in response to β_3-adrenergic stimulation (Collins et al., 2010). In contrast, mTORC2 inhibition does not alter the phosphorylation of ERK1/2 after insulin or CL-316,243 treatment (Figure 4.1D), suggesting mTORC2

specifically regulates p38-MAPK activity. Intriguingly, there is one proposed mechanism by which mTORC2 negatively regulate p38-MAPK activity through stabilizing a phosphatase, DUSP10 (dual specificity phosphatase 10), which normally dephosphorylates and shuts down p38-MAPK (Benavides-Serrato et al., 2014). However, whether this is the case here still needs to be clarified.

Given AKT and mTORC1 function downstream of mTORC2 in response to growth factor stimulation, it is possible that AKT or mTORC1 mediate the Ucp1 regulation by mTORC2. As shown in Figure 4.1D, the inhibition of mTORC2 signaling partially affects AKT (p-AKT-T308), but not mTORC1 (p-S6K-T389), activation. To find out which signaling molecules are involved in *Ucp1* regulation, I additionally employed inducible *Akt1/2* DKO and *Raptor* KO brown preadipocyte lines (Figure 4.2A). Noticeably, deletion of *Akt1* and *Akt2* blocks brown adipocyte differentiation with low PPARγ expression and absence of mature markers, like UCP1 and lipogenic enzymes (ACLY, ACC, and FASN) (Figure 4.2A and 4.2B). On the contrary, inducible deletion of *Raptor* does not affect differentiation *per se,* but it interferes with *Ucp1* mRNA expression upon CL-316,243 stimulation (Figure 4.2A and 4.2B), indicating that mTORC1 activity is required for *Ucp1* maximal induction. This finding is quite interesting and in line with a recent study (Liu et al., 2016) which reported that adipocytes lacking mTORC1 are refractory to β-AR-dependent *Ucp1* induction. Thus, mTORC2 regulates *Ucp1* expression possibly through AKT/mTORC1-independent mechanisms.

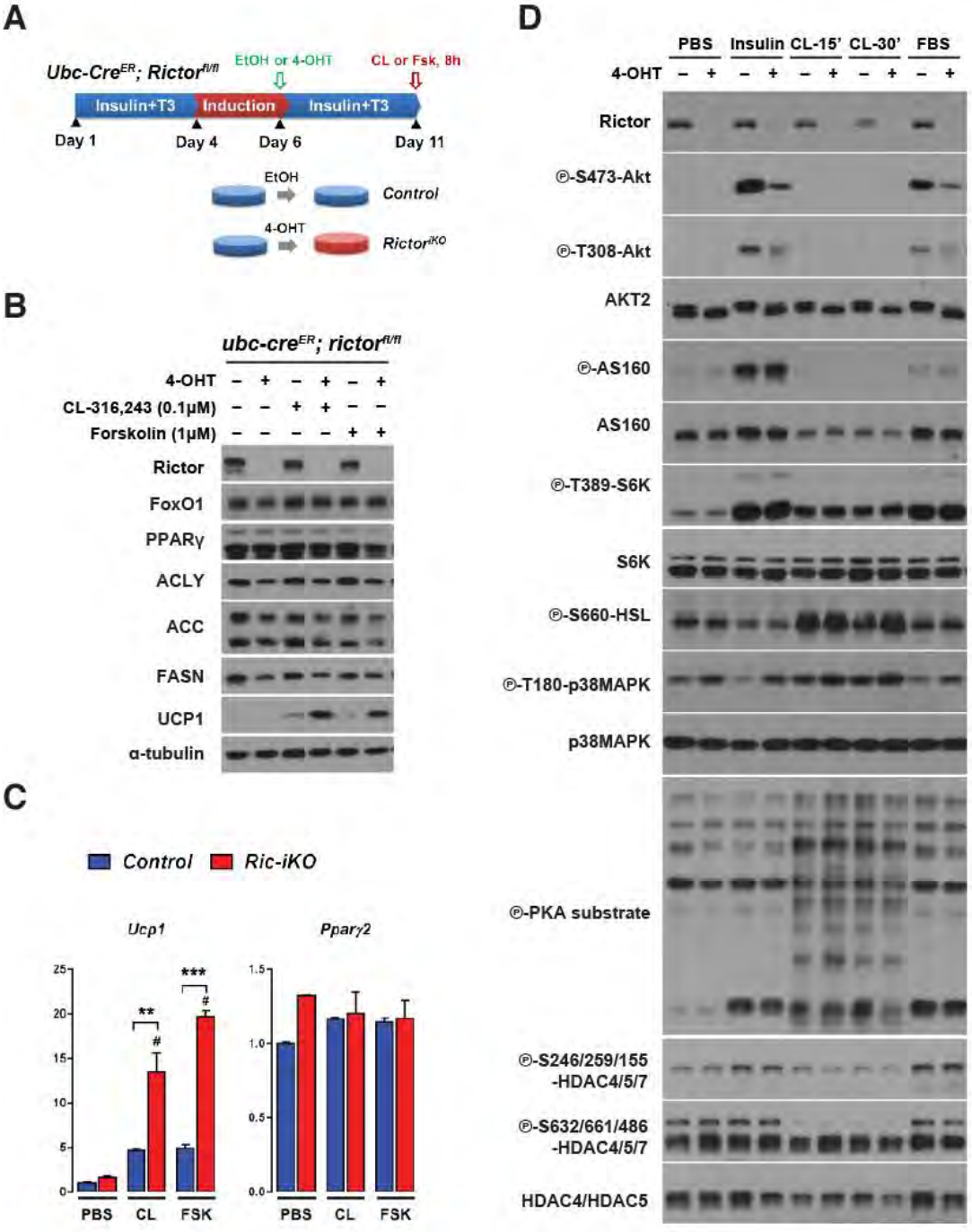
A
Ubc-Cre^ER; Rictor^fl/fl
EtOH or 4-OHT
CL or Fsk, 8h
Insulin+T3
Induction
Insulin+T3
Day 1
Day 4
Day 6
Day 11
EtOH
Control
4-OHT
Rictor^iKO
B
ubc-cre^ER; rictor^fl/fl
4-OHT
CL-316,243 (0.1μM)
Forskolin (1μM)
Rictor
FoxO1
PPARγ
ACLY
ACC
FASN
UCP1
α-tubulin
C
Control
Ric-iKO
Ucp1
Pparγ2
PBS
CL
FSK
D
PBS
Insulin
CL-15'
CL-30'
FBS
4-OHT
Rictor
Ⓟ-S473-Akt
Ⓟ-T308-Akt
AKT2
Ⓟ-AS160
AS160
Ⓟ-T389-S6K
S6K
Ⓟ-S660-HSL
Ⓟ-T180-p38MAPK
p38MAPK
Ⓟ-PKA substrate
Ⓟ-S246/259/155 -HDAC4/5/7
Ⓟ-S632/661/486 -HDAC4/5/7
HDAC4/HDAC5

Figure 4.1 mTORC2 inhibition potentiates UCP1 induction by β_3-adrenergic signals

(A) Experiment scheme for in vitro differentiation : 4-OHT was added at Day6 to induce gene deletion, CL-316,243 or forskolin was added at Day 11 for 8 hrs (B) Western blots for CL-316,243 and forskolin-stimulated UCP1 induction in *Ubc-CreER;Rictor* cells (C) qPCR for CL-316,243 and forskolin -stimulated UCP1 induction in *Ubc-CreER;Rictor* cells (D) Western blots for cellular signaling (cells are serum-deprived for 4h, then stimulated with 150nM insulin for 15mins, 1μM CL-316,243 for 15 and 30 mins and FBS for 1hr)

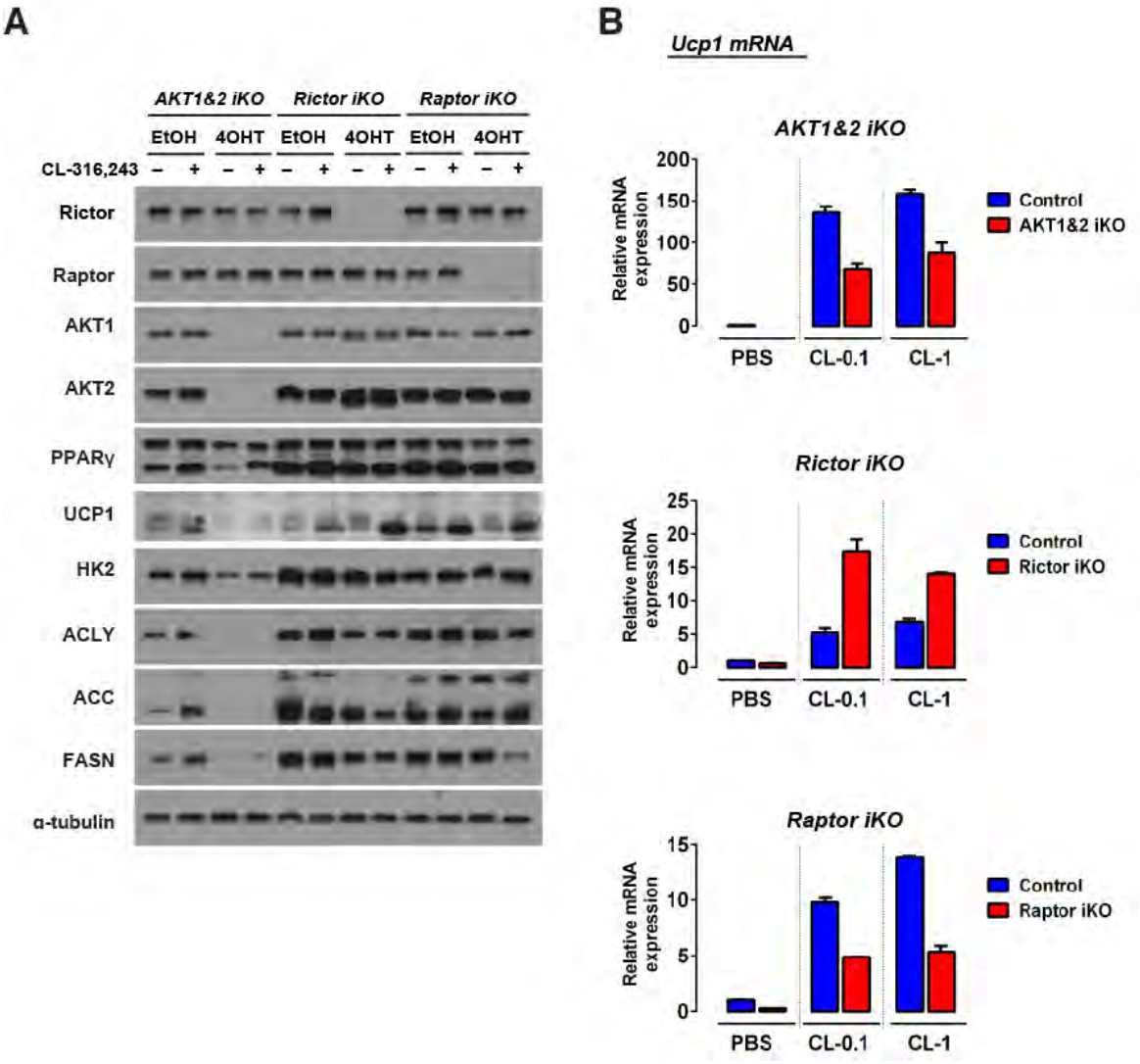

Figure 4.2 mTORC2 regulates UCP1 induction independently of AKT/mTORC1 signaling

(A) Western blots for CL-316,243 (0.1μM, 8h) stimulated UCP1 induction (B) qRT-PCR for *Ucp1* expression (cells harvested 8h after CL-316,243 treatment, n=2) (Bars represent mean ± SEM; t-test; *p<0.05, **p<0.01, ***p<0.001)

mTORC2 Suppresses *Ucp1* Expression through FoxO1 Activtiy

FoxO1 has been characterized as a critical downstream mediator of mTORC2 functions through AKT-dependent (Hagiwara et al., 2012) or AKT-independent (Masui et al., 2013) pathways. As shown in Figure 3.8C (Chapter III), I observed several FoxO target genes [*Ucp1(Ortega-Molina et al., 2012)*, *Pgc1α* (Daitoku et al., 2003), *Irf4* (Eguchi et al., 2011)*, Bnip3* (Mammucari et al., 2007) and *Sod2* (Kops et al., 2002)] upregulated in mTORC2-deficient BAT. Hence, I tested the hypothesis that FoxO1 conveys mTORC2 signaling in *Ucp1* regulation by using pharmacological and genetic approaches. AS1842856 is a cell-permeable inhibitor that directly binds to the active form (unphosphorylated) of FoxO1 and thus blocks its transcription activity (Nagashima et al., 2010), and it has high selectivity and high binding affinity (IC_{50}=33nM) to FoxO1 over other FoxO proteins. In Figure 4.3A, AS1842856 at 1μM effectively reduces UCP1 induction by CL-316,243 in mTORC2 deficient brown adipocytes but minimally affects UCP1 levels in control cells, even though, at higher doses, the inhibitor exerts the same efficacies in both control and KO cells. Paralleled results are also obtained in *Ucp1* mRNA levels (Figure 4.3B). Of note, the inhibitor also partially suppresses *Pgc1α* and *Pdk4*, which have been implicated as FoxO1 target genes, but not *Pparγ*. Similarly, the FoxO1 inhibitor also blocks UCP1 induction by forskolin stimulation (Figure 4.3C).

To avoid off-target effects of the inhibitor, I next designed specific guide RNA sequences to target endogenous *Foxo1* alleles using a lentiviral CRISPR/Cas9 system (Sanjana et al., 2014; Shalem et al., 2014). After stable selection, CRISPR-mediated recombination efficiently eliminates FoxO1 expression in wild-type brown preadipocytes

(not shown) and it does not affect differentiation (Figure 4.4A), suggest FoxO1 is dispensable for differentiation. In contrast, FoxO1 deficiency blocks UCP1-induction by the β-AR signaling (Figure 4.4A). Remarkably, in addition to *Ucp1* levels, FoxO1 depletion also abolishes the transcription of *Pgc1α, Atgl,*and *Pdk4* induced by CL-316,243 in both control and Rictor-deficient cells without affecting *Pparγ2* expression (Figure 4.4B).

In line with the CRISPR-mediated knockdown, brown preadipocytes with *Foxo1* deletion driven by *Adipoq-Cre* also differentiate normally (e.g. equal PPARγ expression to tcontrol), but these knockout cells are completely refractory to the β-AR signaling (CL-316,243 and isoproterenol), PPARγ-agonist (rosiglitazone) and cAMP stimulation (Forskolin) towards activating BAT-enriched genes (*Ucp1*, *Pdk4*, and *Atgl*) expression (Figure 4.5B). Of note, although the expression of *Pgc1α* and *Irf4* is still controlled by FoxO1, they do not increase in response to stimuli in these cell lines. In summary, both *in vivo* and *in vitro* data collectively suggest that mTORC2 negatively regulates *Ucp1* and possibly several other genes (*Pgc1a*, *Pdk4*, *Atgl, Irf4*…etc.) through modulating FoxO1 activity.

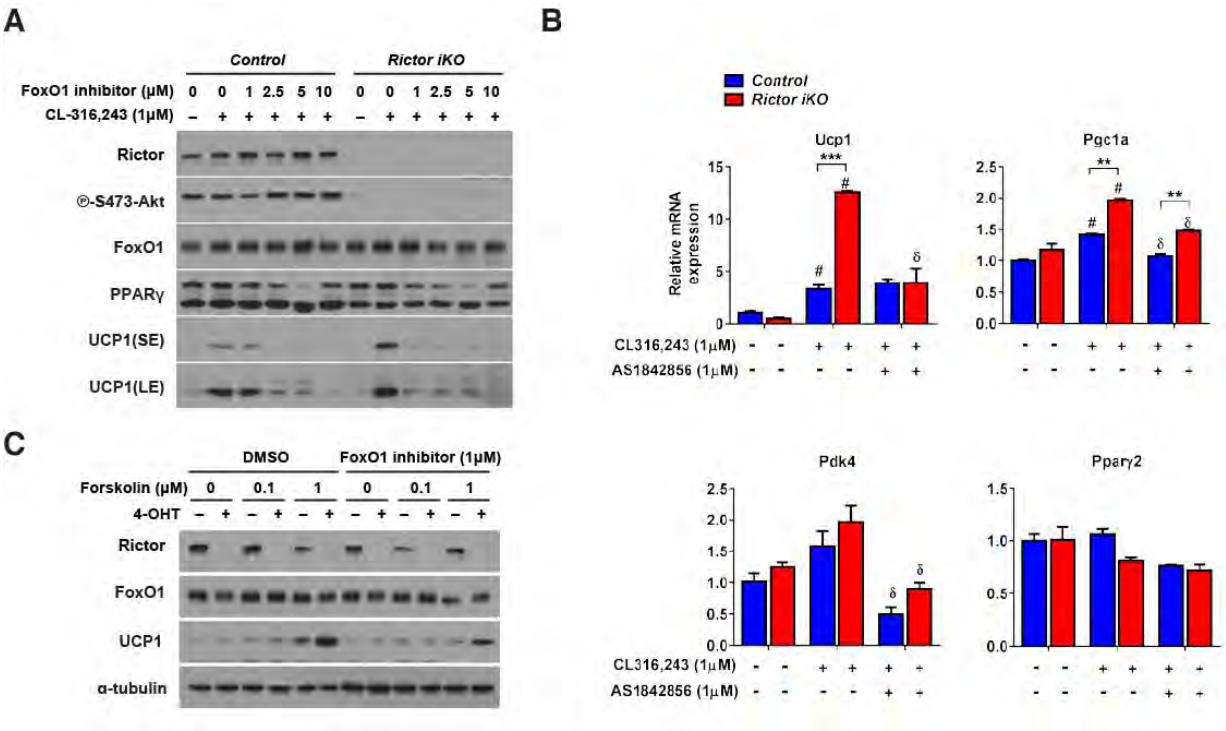

Figure 4.3 Inhibition of FoxO1 blocks UCP1 induction by β_3-adrenergic signaling

(A) Western blots for the effects of a FoxO1 inhibitor, AS1842856, on UCP1 induction (B) qRT-PCR for *Ucp1, Pgc1α, Pdk4 and Pparγ2* expression (cells harvested 8h after drug treatment, n=2) (C) Western blots for the effects of the FoxO1 inhibitor on forskolin-stimulated UCP1 expression (Bars represent mean ± SEM; t-test; *p<0.05, **p<0.01, ***p<0.001)

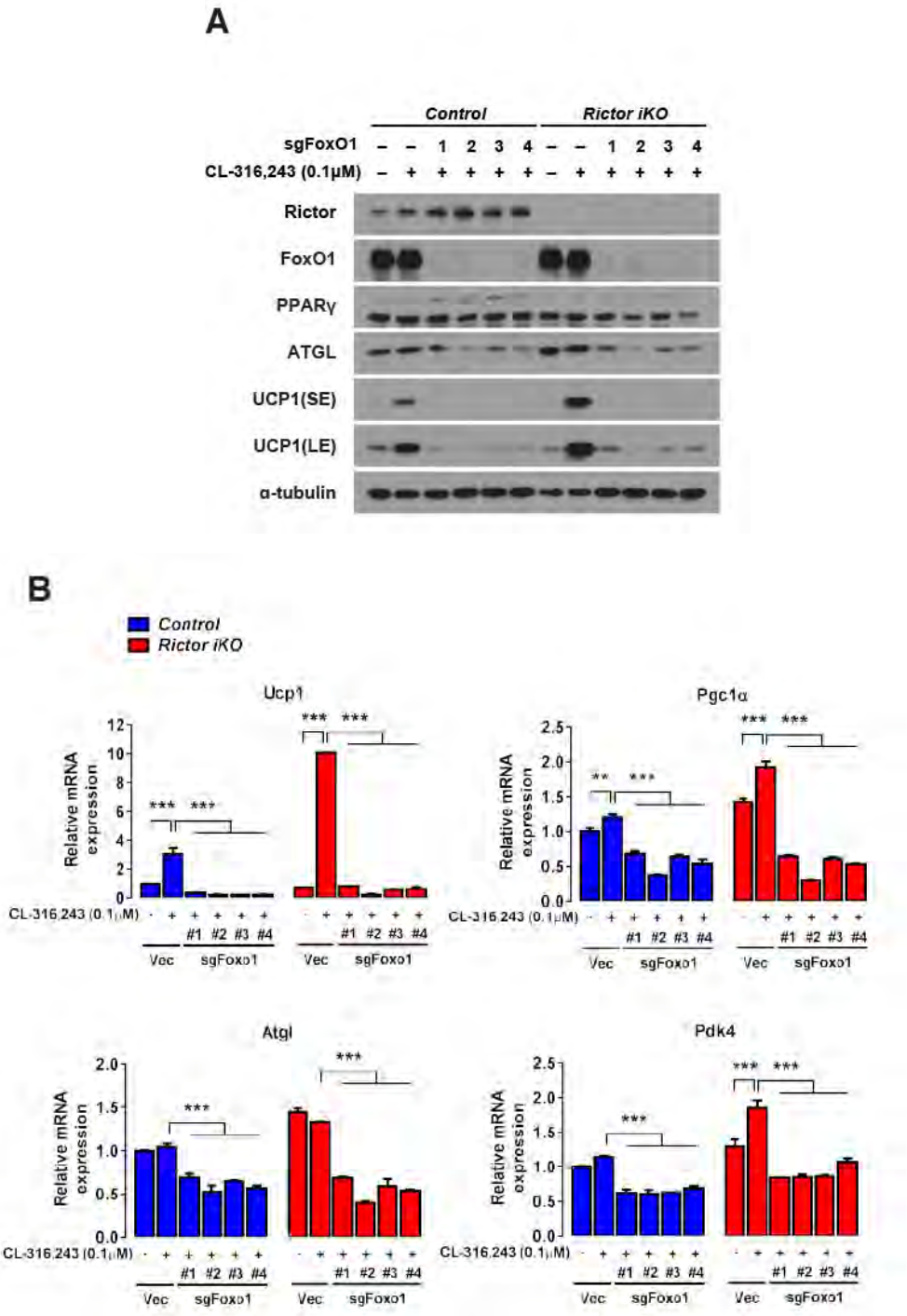
A
Control
Rictor iKO
sgFoxO1 – – 1 2 3 4 – – 1 2 3 4
CL-316,243 (0.1μM) – + + + + + – + + + + +
Rictor
FoxO1
PPARγ
ATGL
UCP1(SE)
UCP1(LE)
α-tubulin
B
Control
Rictor iKO
Ucp1
Pgc1α
Atgl
Pdk4
Relative mRNA expression
CL-316,243 (0.1μM)
#1 #2 #3 #4
Vec
sgFoxo1

Figure 4.4 FoxO1 is required for UCP1 induction by β_3-adrenergic signaling

(A) Western blots for the effects of CRISPR-mediated *Foxo1* knockout on UCP1 induction by CL-316,243 (B) Corresponding qRT-PCR for the experiment in (A) (cells harvested 8h after CL-316,243 treatment, n=2) (cells harvested 8h after drug treatment, n=2) (Bars represent mean ± SEM; t-test; *p<0.05, **p<0.01, ***p<0.001)

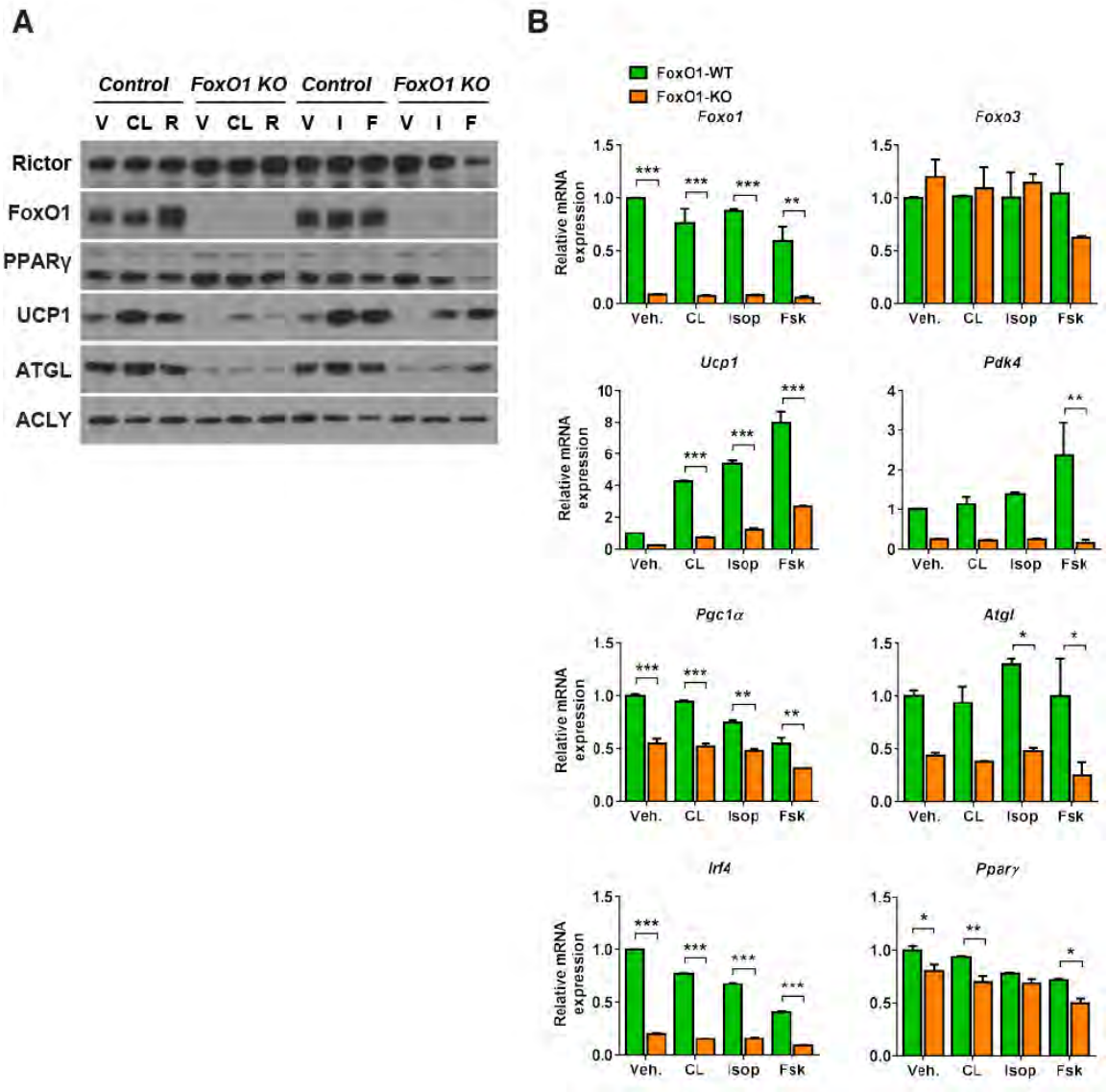

Figure 4.5 FoxO1 is essential for the expression of BAT-enriched genes

(A) Western blots for the effects of conventional *Foxo1* knockout on UCP1 induction

(B) Corresponding qRT-PCR for the experiment in (A) (cells harvested 8h after drug treatment, n=2) (Bars represent mean ± SEM; t-test; *p<0.05, **p<0.01, ***p<0.001)

mTORC2 Regulates FoxO1 Activity by Affecting Its Acetylation

FoxO transcription factors, in general, are regulated by various post-translational modifications, including phosphorylation, acetylation, glycosylation and ubiquitination [reviewed in (Daitoku et al., 2011; Huang and Tindall, 2011; Klotz et al., 2015; Wang et al., 2014)]. Insulin signaling inhibits FoxO through AKT-mediated phosphorylation at T24, S256 and S319, which promotes it nuclear exclusion and subsequent ubiquitination-mediated degradation. In contrast, the acetylation status of FoxO affects its transcriptional activity. The effects of FoxO acetylation on target genes appear to be context-dependent; however, many studies demonstrated that acetylation of FoxO1 compromises its DNA-binding ability (Daitoku et al., 2004; Kitamura et al., 2005; Masui et al., 2013; Matsuzaki et al., 2005). Thus I further examined whether mTORC2 controls FoxO1 acetylation and phosphorylation states *in vivo*. Remarkably, acetylation levels are much reduced in Rictor-deficient brown fat, whereas two AKT phosphorylation sites (T24 and S256) are not affected by mTORC2 inhibition (Figure 4.6A). Together with FoxO1, phosphorylation of other AKT substrates, such as AS160 and PRAS40, are all preserved even when mTORC2 activity is compromised, suggesting classical AKT pathways are rather normal. The changes in FoxO1 acetylation prompted me to search protein deacetylases that are controlled by mTORC2 signaling. A recent study argued that mTORC2 inhibits class IIa HDACs (HDAC4, 5, 7 and 9) through direct phosphorylation and thus prevents FoxO1 deacetylation (Masui et al., 2013). Interestingly, by screening small molecule inhibitors of HDACs, I found both pan-HDAC inhibitors (Sodium butyrate,Trichostatin A and SAHA) and a specific HDAC4/5 inhibitor

(LMK-235) can block CL-316,243 induced UCP1 expression *in vitro* (Figure 4.6C and 4.6D). However, in contradictory to that report, I observed no difference in these inhibitory phosphorylation sites on HDAC4, 5, 7 in the cell culture system and mouse tissues analyzed here (Figure 4.1C; Figure 4.6A and 4.6B). Therefore, our results do not support the notion that class IIa HDACs mediate mTORC2 signaling towards FoxO1 regulation. On the other hand, sirtuin family proteins have been implicated in FoxO1 regulation (Jing et al., 2007; Wang and Tong, 2009). It is interesting that a pan-sirtuin inhibitor (Nicotinamide), but not the Sirt1 inhibitor (EX-527), can suppress UCP1 induction (Figure 4.6C), suggesting that sirtuin family deacetylases could be involved (e.g. Sirt2 and Sirt3). Nonetheless, the exact mechanism underlying how mTORC2 regulates FoxO1 acetylation state still requires further investigation.

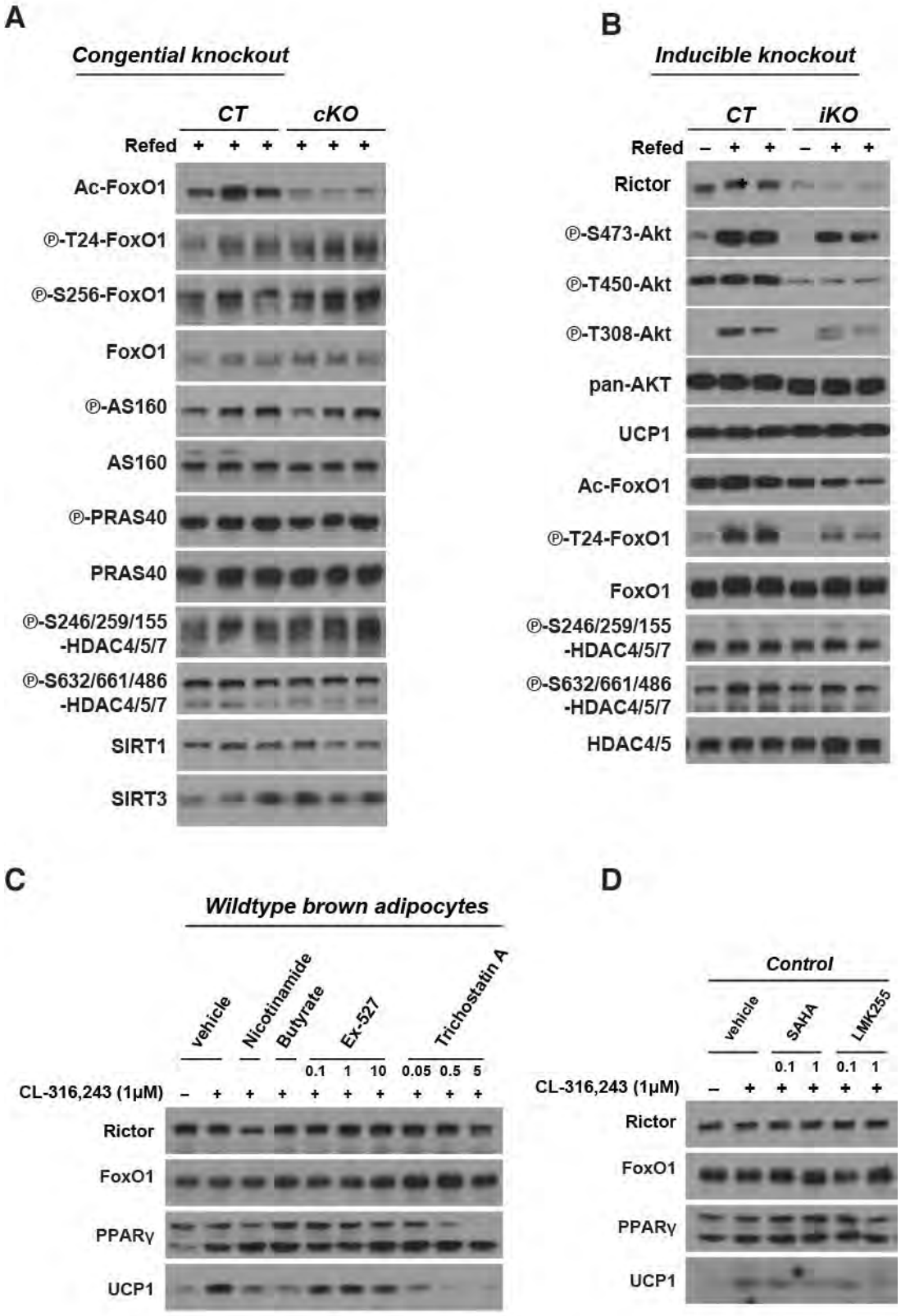
A
Congential knockout
CT
cKO
Refed + + + + + +
Ac-FoxO1
Ⓟ-T24-FoxO1
Ⓟ-S256-FoxO1
FoxO1
Ⓟ-AS160
AS160
Ⓟ-PRAS40
PRAS40
Ⓟ-S246/259/155 -HDAC4/5/7
Ⓟ-S632/661/486 -HDAC4/5/7
SIRT1
SIRT3
B
Inducible knockout
CT
iKO
Refed – + + – + +
Rictor
Ⓟ-S473-Akt
Ⓟ-T450-Akt
Ⓟ-T308-Akt
pan-AKT
UCP1
Ac-FoxO1
Ⓟ-T24-FoxO1
FoxO1
Ⓟ-S246/259/155 -HDAC4/5/7
Ⓟ-S632/661/486 -HDAC4/5/7
HDAC4/5
C
Wildtype brown adipocytes
vehicle
Nicotinamide
Butyrate
Ex-527
Trichostatin A
0.1 1 10
0.05 0.5 5
CL-316,243 (1μM) – + + + + + + + + +
Rictor
FoxO1
PPARγ
UCP1
D
Control
vehicle
SAHA
LMK255
0.1 1
0.1 1
CL-316,243 (1μM) – + + + + + +
Rictor
FoxO1
PPARγ
UCP1

Figure 4.6 FoxO1 is hypo-acetylated in Rictor-deficient BAT

(A) Western blots for iBAT lysates from control and *Rictor*$^{Ucp1\text{-}cKO}$ mice (mice were fasted overnight, refed 1hr before dissection) (B) Western blots for iBAT lysates from control and *Rictor*$^{Ucp1\text{-}iKO}$ mice (mice were fasted overnight, refed 1hr before dissection) (C) Western blots for cell lysates from wild-type brown adipocytes (10mM Nicotinamide, 1mg/ml Sodium butyrate, 0.1~10μM Ex-527, 0.05~5μM Trichostatin A) (D) Western blots for cell lysates from wild-type brown adipocytes (0.1, 1 μM SAHA; 0.1, 1 μM LMK-235)

FoxO1 Acetylation Can Be Triggered by β_3-Adrenergic Activation

Since I provide extra data to support that FoxO1 could be a critical transcription regulator of the thermogenic program, it becomes important to know whether FoxO1 can be activated by β-AR signaling *in vivo*. To this end, thermoneutral animals were injected with β_3-adregneric receptor ligand, CL-316,243, for three days to activate BAT thermogenesis. CL-316,243 treatment completely reverses the whitening effect of thermoneutrality on control BAT but to a greater extent on Rictor-deficient BAT (Figure 4.7B). As expected, UCP1 protein levels are greatly induced after β-AR stimulation (Figure 4.7A), indicative of BAT activation. Remarkably, FoxO1 acetylation is dramatically reduced in CL-316,243-activated BAT compared to saline-treated ones, while neither phosphorylation sites (T24 and S256) on FoxO1 nor global lysine acetylation are affected by CL-316,243 (Figure 4.7A). Comparable changes in UCP1

expression and FoxO1 acetylation also occur in Rictor-deficient BAT. It is noteworthy that the basal (saline) levels of FoxO1 acetylation in Rictor knockout BAT are already lower than control, which may explain higher *Ucp1* levels in KO BAT in the basal state (saline) (Figure 4.7A). Finally, the lower basal levels of FoxO1 acetylation in Rictor KO BAT inversely correlates with a greater response of thermogenic genes induction (*Pgc1α*, *Irf4* and *Elovl3*) towards an acute CL-316,243 treatment (6 hours) (Figure 4.7C). These results together suggest that loss of mTORC2 signaling increases the sensitivity of brown adipocytes to β_3-adrenergic signaling, which is in line with the cell culture results.

Finally, I would like to determine whether FoxO1 acetylation is also regulated *in vitro*. Consistent with the findings in BAT, nuclear FoxO1 of Rictor-deficient cells displays lower acetylation levels in a FBS-stimulated condition (Figure 4.8A). More importantly, CL-316,243 treatment drastically induces FoxO1 deacetylation within a few hours, while it does not affect FoxO1 phosphorylation (Figure 4.8B, 4.8D, and 4.8E). Again, FoxO1 acetylation levels in Rictor knockout cells are already lower in the basal (unstimulated) state than control and only display a modest decrease in response to β_3-adrenergic activation. The fact that β_3-adrenergic signals can induce FoxO1 deacetylation is coincident with the previous finding that β-AR signaling induces PGC1α deacetylation through PKA-mediated Sirt1 activation (Gerhart-Hines et al., 2011). In addition, PPARγ was also reported to be a Sirt1 substrate, and the Sirt1-mediated deacetylation promotes the association of PPARγ and Prdm16, which results in an enhancement of the thermogenic program in white adipocytes (Qiang et al., 2012). Interestingly, I also find that the acetylation level of PPARγ is lower in Rictor knockout

adipocytes compared to control adipocytes at the basal levels, and CL-316,243 treatment also triggers PPARγ deacetylation in control cells, but not in Rictor-deficient cells (Figure 4.8F). Altogether, there is an emerging scenario that the β-adrenergic signaling concurrently activates key regulators of thermogenesis, including FoxO1, PGC1α and PPARγ, through Sirt1-mediated deacetylation in adipocytes. However, whether mTORC2 exploits the same sirtuin-dependent mechanism or even mTORC2 directly mediates β-AR signaling to regulate these factors requires further elaborate examination.

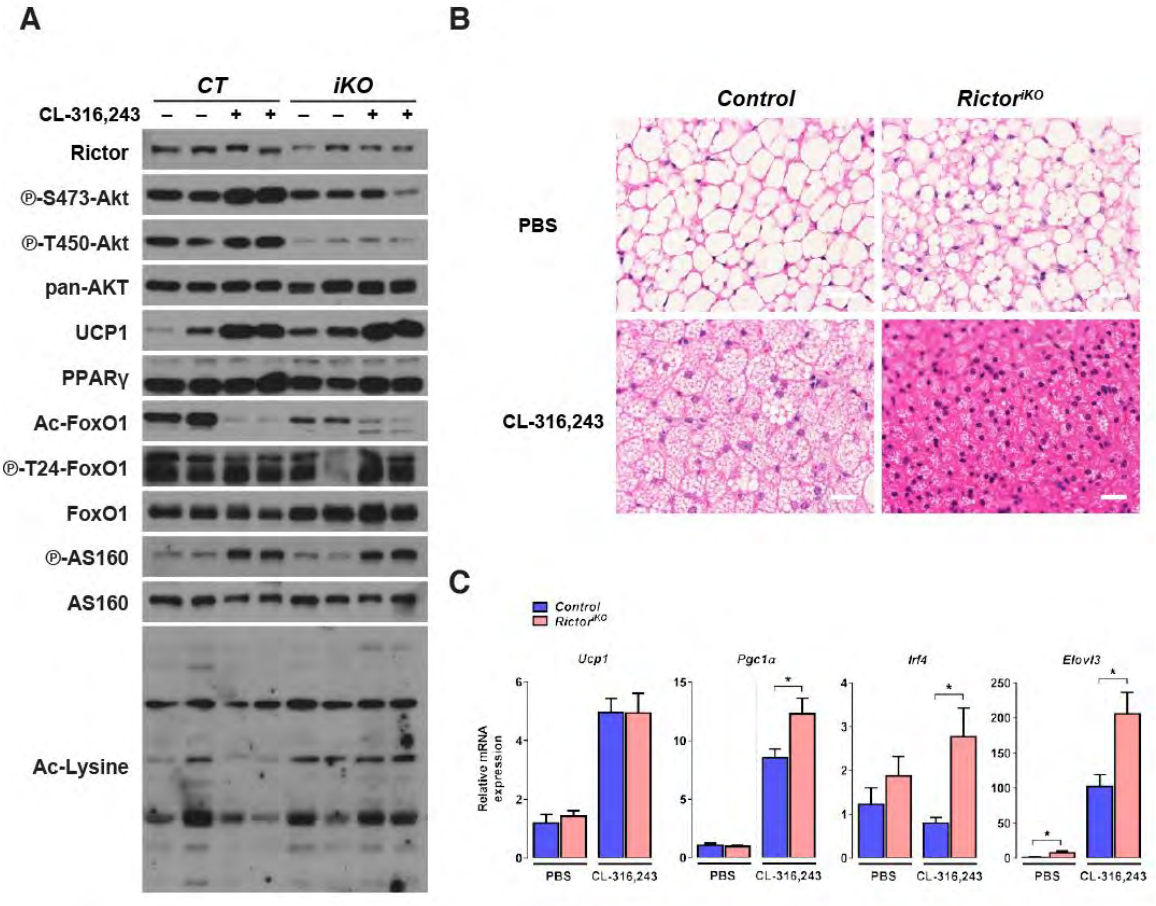

Figure 4.7 β_3-adrenergic signaling triggers deacetylation of FoxO1 *in vivo*

(A) Western blots for iBAT lysates from control and *Rictor*$^{Ucp1\text{-}cKO}$ mice (mice were fasted overnight, refed 1hr before dissection) (B) Western blots for iBAT lysates from control and *Rictor*$^{Ucp1\text{-}iKO}$ mice (mice were fasted overnight, refed 1hr before dissection) (C) Western blots for iBAT lysates from mice treated with PBS or CL-316,243 for three days (D) qRT-PCR for iBAT samples from mice treated with PBS or CL-316,243 for 6hrs (n=6, Bars represent mean ± SEM; t-test; *p<0.05, **p<0.01, ***p<0.001)

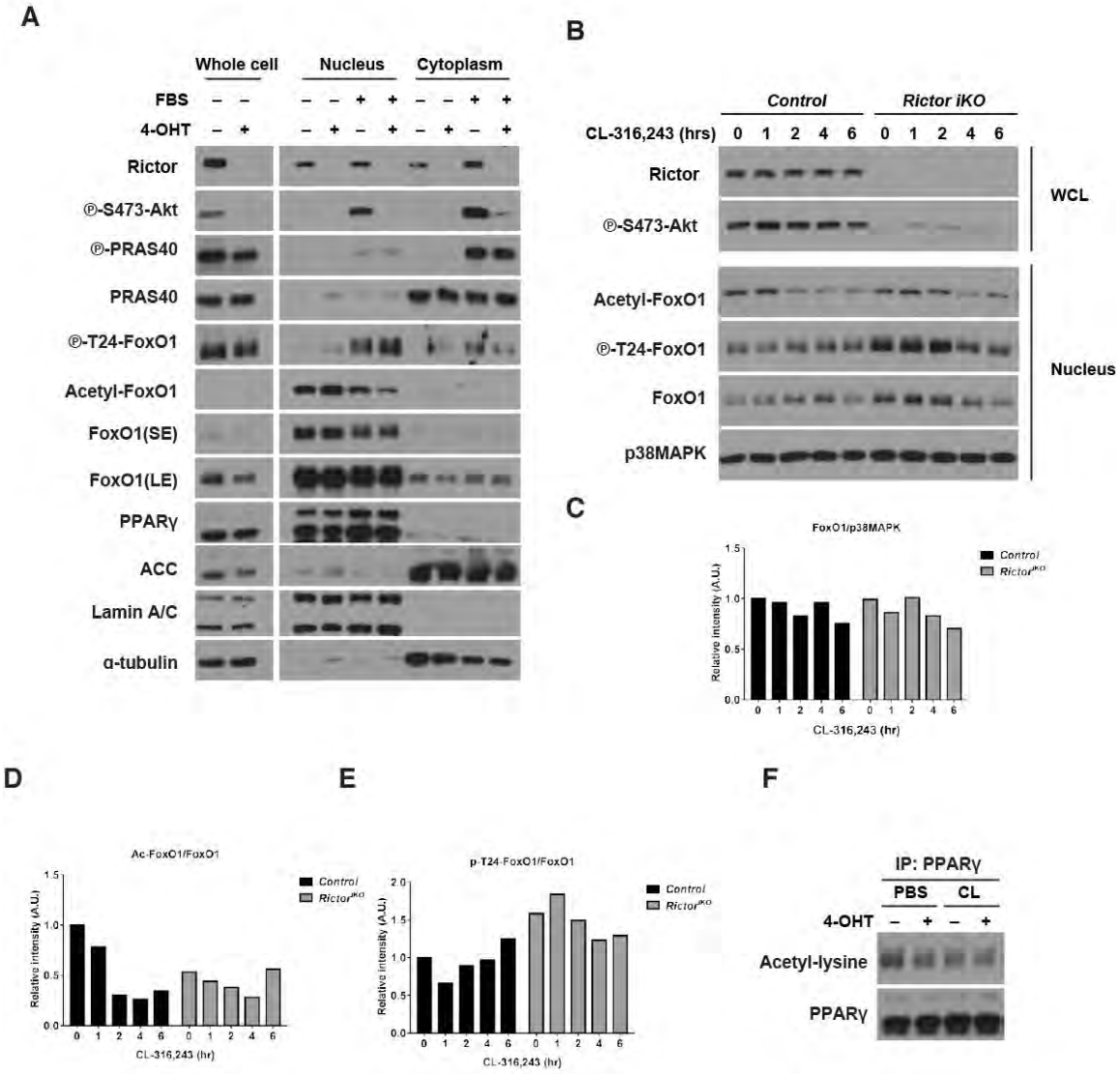
A
Whole cell
Nucleus
Cytoplasm
FBS
4-OHT
Rictor
Ⓟ-S473-Akt
Ⓟ-PRAS40
PRAS40
Ⓟ-T24-FoxO1
Acetyl-FoxO1
FoxO1(SE)
FoxO1(LE)
PPARγ
ACC
Lamin A/C
α-tubulin
B
Control
Rictor iKO
CL-316,243 (hrs)
0 1 2 4 6 0 1 2 4 6
Rictor
Ⓟ-S473-Akt
WCL
Acetyl-FoxO1
Ⓟ-T24-FoxO1
FoxO1
p38MAPK
Nucleus
C
FoxO1/p38MAPK
Control
Rictor iKO
Relative intensity (A.U.)
CL-316,243 (hr)
D
Ac-FoxO1/FoxO1
Control
Rictor iKO
Relative intensity (A.U.)
CL-316,243 (hr)
E
p-T24-FoxO1/FoxO1
Control
Rictor iKO
Relative intensity (A.U.)
CL-316,243 (hr)
F
IP: PPARγ
PBS
CL
4-OHT
Acetyl-lysine
PPARγ

Figure 4.8 FoxO1 acetylation state in response to different treatments

(A) Western blots for cell fractionation experiment (feeding and fasting induced FoxO1 acetylation changes in the nuclear fraction and the cytoplasmic ftaction) (B) Western blots for differentiated brown adipocytes treated with CL-316,243 for 1,2,4, and 6hrs. (C) (D) (E) Quantification of band density in (B) (F) Western blots for lysates with PPARγ immunoprecipitation and then probed with pan-acetylation antibody.

Discussion

Here, I find that mTORC2 controls BAT thermogenic program through regulating FoxO1 activity. Most importantly, this regulation seems to be independent of classical AKT-mediated phosphorylation. As mentioned before, FoxO1 activity is modulated by a variety of post-translational modifications, including phosphorylation and acetylation. AKT-mediated phosphorylation sites on FoxO1 are largely intact when *Rictor* is deleted *in vitro* and *in vivo*. However, other stress kinases, like AMPK, JNK, and MAPK, are also known to regulate FoxO1 at different sites (Asada et al., 2007; Yun et al., 2014), which also need to be characterized in the future. Interestingly, I observed that p38-MAPK is more active in Rictor KO brown adipocytes than that in control cells *in vitro*. Since p38-MAPK is reported to phosphorylate FoxO1 and promote its activity, I could not entirely exclude the possibility that mTORC2 exploits other AKT-independent mechanisms that affect FoxO1 phosphorylation and activity. Conversely, FoxO1 is clearly hypo-acetylated in Rictor-deficient BAT. Therefore, modulating FoxO1 acetylation state could be a likely mechanism that allows mTORC2 to fine-tune FoxO1 activity. A recent study suggests that mTORC2 negatively regulates class IIa HDACs by direct phosphorylation in glioblastoma cells, which, in turn, regulate FoxO1 acetylation (Masui et al., 2013). However, in contrast to this study, I did not find evidence supporting that mTORC2 controls class IIa HDACs activity through phosphorylation in the cell culture system and mouse tissues analyzed here. Instead, it is equally possible that mTORC2 directly or indirectly regulates sirtuins activity. Since sirtuin activity can be triggered by low energy state and high cellular NAD+ (nicotinamide adenine

dinucleotide) levels, it would be necessary to determine whether mTORC2 inhibiton could affect the NAD+/NADH ratio or related signaling pathways (e.g. AMPK signaling) in the future. Alternatively, removing individual lysine deacetylases by CRISPR or RNAi would be another approach to determine whether mTORC2 controls FoxO1 acetylation through a specific deacetylase.

In addition, I also discovered the β-adrenergic agonist (CL-316,243) treatment robustly triggers deacetylation of FoxO1 in BAT without affecting FoxO1 phosphorylation. Consistently, CL-316,243-induced FoxO1 deacetylation can also be observed in the culture system. Since it has been reported that PKA signaling can directly activate Sirt1 via phosphorylation (Gerhart-Hines et al., 2011), it is likely that the β-AR induced deacetylation of FoxO1 could be also mediated by Sirt1 or other sirtuin family members. Nevertheless, these findings provide some clues leading to a novel mechanism by which FoxO1 is regulated upon cold exposure to activate *Ucp1* expression. Again, it is necessary to determine whether mTORC2 mediates or exploits this regulatory mechanism towards controlling FoxO1.

CHAPTER V:

Significance and concluding remarks

The physiological function of FoxO1 in adipose tissue

The physiological role of FoxO1 in brown or white adipose tissue remains enigmatic because contradictory results have been reported in the literature. In an earlier study, Nakae and colleagues (Nakae et al., 2008) first reported the ectopic expression of a dominant-negative FoxO1 in adipose tissue enhances browning and *Ucp1* expression. By contrast, two independent groups showed *Pten* overexpression increases energy expenditure through hyperactivation of FoxO1 in BAT (Garcia-Cao et al., 2012; Ortega-Molina et al., 2012). Interestingly, Nakae (Nakae et al., 2012) later identified a novel repressor of FoxO1, called FoxO corepressor (FCoR), whose overexpression reduces *Ucp1* and *Pgc1α* expression by interrupting Sirt1-mediated FoxO1 deacetylation. Conversely, FCoR depletion in adipose tissue enhances oxygen consumption and lipid usage, which is presumably caused by FoxO1 activation. Other studies also suggest FoxO1 regulates lipolysis in fat tissues through promoting the transcription of *Atgl* and lysosomal lipase (*Lipa*), implying that FoxO1 is involved in lipid mobilization (Chakrabarti et al., 2011; Chakrabarti and Kandror, 2009; Lettieri Barbato et al., 2013). Furthermore, FoxO1 is also shown to positively regulate *Irf4* expression in the adipose tissue (Eguchi et al., 2011), and IRF4 was discovered to enhance BAT thermogenesis through interacting and collaborating with PGC1α (Kong et al., 2014). In line with the literature, I demonstrate here that FoxO1 is required for the expression of several genes involved in thermogenesis (*Ucp1*, *Pdk4*, *Irf4* and *Cidea*) and lipolysis (*Atgl*) in cultured brown adipocytes (Figure 3.11C and 3.11D). Collectively, FoxO1 appears to play a pivot role in adipose tissue by coupling intracellular fatty acid availability and thermogenesis

together in fat tissues. This mechanism is crucial for brown adipose tissue since lipolysis (i.e. releasing free fatty acids) is prerequisite for thermogenic function (Ahmadian et al., 2011; Lee et al., 2016; Lee et al., 2015). Nonetheless, how the mTORC2-FoxO1 axis integrates different physiological signals in adipose tissue remains elusive.

How does mTORC2 integrate signals in different physiological states?

Based on the results in this dissertation, I conclude that mTORC2 seems to serve as a pivotal signaling switch between energy storage and expenditure states by regulating two important functions—lipid biosynthesis and thermogenesis—in brown adipose tissue. First, mTORC2 promotes de novo lipogenesis by facilitating glucose uptake and utilization through AKT-mediated pathways, which is essential for adipocyte differentiation and growth. Second, mTORC2 suppresses BAT thermogenic program via regulating FoxO1 activity through a novel mechanism that involves modulating lysine acetylation status of FoxO1. Although the detailed mechanism by which mTORC2 regulate FoxO1 acetylation is not completely understood, β_3-adrenergic receptor activation also triggers FoxO1 deacetylation, suggesting the mTORC2-mediated signaling and the β-AR signaling might converge on FoxO1 regulation (Figure 5.1). Thus, elucidating how mTORC2 reacts and integrates various signals (especially insulin versus norepinephrine) in different physiological states could be one of the future directions.

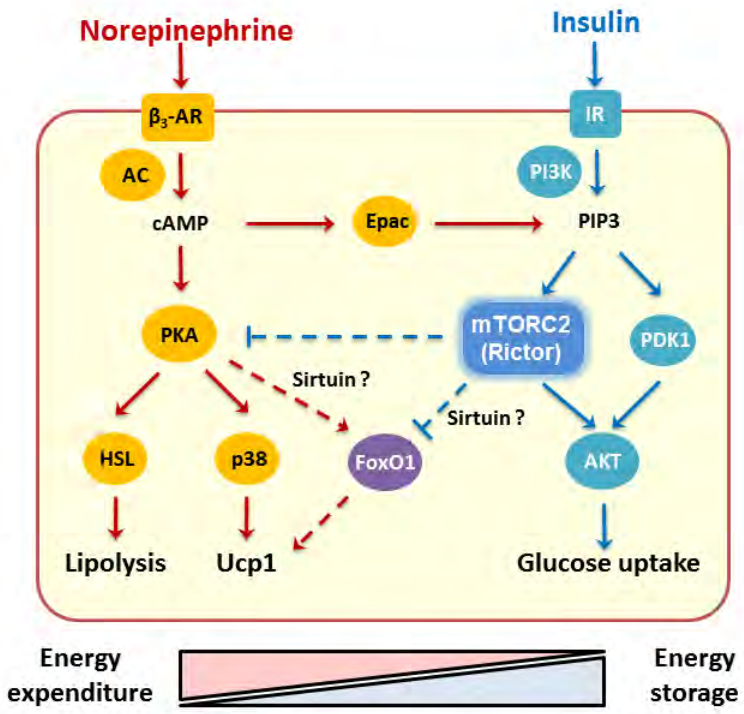

Figure 5.1 mTORC2 Helps Maintain a Balance between Energy Expenditure and Energy Storage

According to the literature and our findings, mTORC2 serves as an important regulator of BAT energy homeostasis downstream of both insulin and norepinephrine signaling. When activated by these two signals, mTORC2 facilitates glucose uptake and subsequent lipogenesis. Conversely, mTORC2 also has a novel function in suppressing the PKA signaling and FoxO1 activity, which are required for BAT thermogenesis.

As discussed in Chapter I, BAT metabolism and activity are regulated by insulin and adrenergic receptor signaling pathways, and cross-talk between these two systems could ultimately lead to opposing or synergic effects on different cellular processes. For example, FoxO1 is typically inhibited by insulin signaling, but the mechanism I elucidated here by which the β_3-adrenergic signaling modulates FoxO1 acetylation states might provide a novel mechanism that counteracts inhibitory phosphorylation by insulin. Indeed, most of the acetylation sites on FoxO1 surround a conserved AKT serine phosphorylation site (S256 in human FoxO1a) localized to a region containing the nuclear localization signal motif (Obsil and Obsilova, 2008). This may imply a regulatory link between acetylation modification and the phosphorylation-mediated nuclear/cytoplasmic shuttle mechanism. On the other hand, acetylation states of FoxO1 can also be modulated by cellular Redox states. Sirt1 is known to be activated by oxidative stress and thus catalyzes FoxO3a deacetylation (Brunet et al., 2004). As a result, deacetylated FoxO3a turns on the expression of genes encoding antioxidant enzymes such as SOD2. Also, UCP1 and other uncoupling proteins (UCP2 and UCP3) have been ascribed for the role in defending against oxidative stress (Mailloux and Harper, 2011; Mailloux et al., 2011). Importantly, a substantial amount of reactive oxygen species (ROS) can be generated by high mitochondrial respiration in BAT. Therefore, the original role of FoxO1 on *Ucp1* expression could be an evolutionally conserved function, as part of a cellular defense system to neutralize oxidative stress. To test this hypothesis, a genetic model with BAT-specific FoxO1 ablation would be crucial to reveal specific functions of FoxO1 in follow-up studies.

From an energetics perspective, cells or tissues receive hormonal signals which reflect systemic energy status to adjust cellular metabolic processes. In a fed state, insulin and growth factors promote anabolic pathways, such as lipogenesis and glycogenosis, which lead to energy conservation or growth. Conversely, in an energy-deprived state, serum catecholamines are elevated and stimulate the PKA signaling pathway, which usually activates catabolic pathways, such as lipid oxidation. These mechanisms are conserved in many tissues and cell types during the fasting-feeding cycle. However, a complex interplay between the insulin and β-adrenergic receptor signaling is found in brown adipose tissue, and the findings here might be useful to understand some of these interactions (Figure 5.1). Besides activating the canonical PKA pathways, catecholamine-induced cAMP production has been shown to activates PI3K through Epac1 (exchange factor directly activated by cAMP 1) in many cell types. A recent study suggested mTORC2 is involved in the Epac1-mediated glucose uptake, which is induced by β-adrenergic receptor activation. Consistent with this notion, I also observed that mTORC2 inhibition partially reduces CL-316,243-induced glucose uptake. This connection may explain how β-adrenergic signaling can trigger both catabolic and anabolic processes simultaneously during thermogenic metabolism in BAT. Nonetheless, I also notice that mTORC2 has a suppressive role on p38-MAPK signaling (or even upstream PKA signaling) in conjunction with inhibitory regulation on FoxO1. While the existence of these feedback mechanisms is seemingly paradoxical, mTORC2 could function as a circuit breaker to prevent "overheating" and nutrient depletion. Indeed, in mTORC2-deficient BAT, there are enhancements in UCP1 expression and lipid oxidation

with a severe reduction in lipogenic functions, collectively causing BAT in an unbalanced state (i.e., loss of metabolic flexibility) marked with deprivation of intracellular lipid store (Figure 5.2).

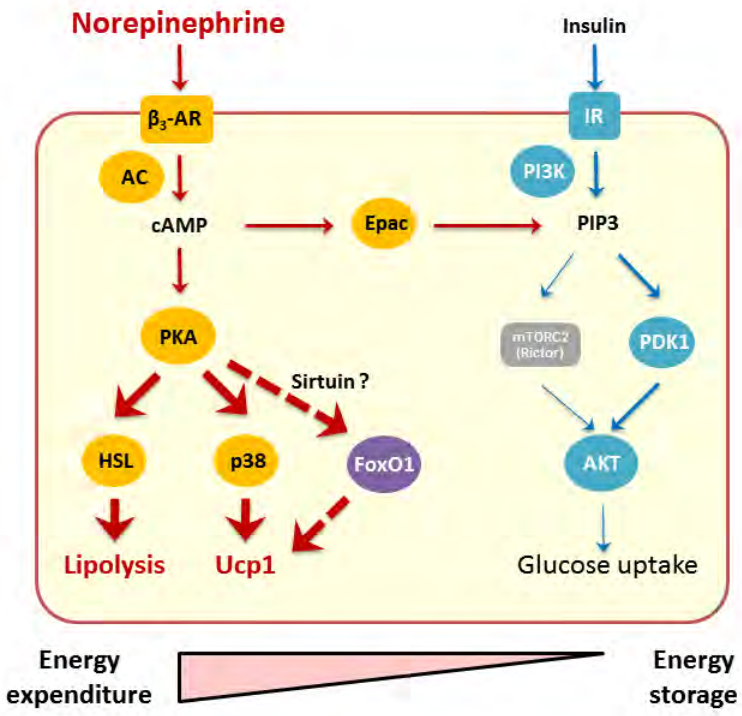

Figure 5.2 mTORC2 Deficiency Causes an Unbalanced State of BAT metabolism

When mTORC2 is ablated, BAT metabolism is shifted from glycolysis and lipogenesis towards lipid oxidation and thermogenesis. Although lipogenesis is not essential for the activation of thermogenesis, but it is important for the replenishment of intracellular TG pools. Therefore, mTORC2-deficient BAT could lose the metabolic flexibility to adapt extreme conditions, such as acute cold challenge.

Interestingly, the BAT phenotypes caused by mTORC2 inhibition are highly paralleled by some aspects of Sirt1 hyperactivation BAT. Sirtuins are NAD+ dependent metabolic/energy sensors, and they can be activated at low energy states such as fasting or calorie restricted conditions. Administration of Sirt1 activator or Sirt1 transgenic expression stimulates energy expenditure and lipid oxidation pathways in BAT (Boutant et al., 2015; Canto et al., 2012; Feige et al., 2008; Xu et al., 2016). Importantly, Sirt1 activation also enhances transcriptional induction of *Ucp1* to β-adrenergic stimulation. In these studies, FoxO1 hypo-acetylation was commonly observed in Sirt1-activated cells or tissues; however, no functional assays were done to address the role of FoxO1 in Sirt1-mediated phenotypes. Although a direct connection between mTORC2 and Sirt1 has not been reported, I purpose a more rigorous examination regarding any function link between the two molecules. In addition, other Sirt1 substrates, such as PGC1α and PPARγ, should also be examed in Rictor-deficient BAT. Furthermore, several key transcription factors that drive lipogenesis have been described to be regulated by acetylation modification (Wang et al., 2015). For example, Sirt1 can directly deacetylate SREBP and diminish its activity during fasting, resulting in down-regulation of lipogenesis (Walker et al., 2010). We do not know whether mTORC2 also regulates these lipogenic factors in a similar fashion, but it is possible that mTORC2 function as a part of signaling circuits that coordinatingly control key transcriptional factors to facilitate a tight regulation of both gene expression and metabolism in response to nutrient and energy fluctuations.

The functional uniqueness of brown adipose tissue

For the majority of organisms, their body temperatures and metabolic rates are greatly impacted by the ambient temperature; most animals are thus ectotherms. Conversely, birds and mammals have the endogenous capacity to maintain their thermal balance and core temperatures through insulation layers and thermogenic organs; therefore, they are endothermic organisms. The mechanisms of thermogenesis have been extensively documented in mammals compared to very few studies in birds (Cannon and Nedergaard, 2011). When exposed to the cold environment, the mammals tend to shiver initially to increase heat production; however, shivering can not endure for an extended period. It was then realized that, after prolonged cold exposure, these animals ceased to shake but, paradoxically, still retained high metabolic rates and normothermia. This high energy expenditure is due to the recruitment of tissues capable of non-shivering thermogenesis, and brown adipose tissue is the primary organ for this function.

Brown adipose tissue has been evolved relatively late in the evolutionary history, and it is almost exclusively found in the mammals. BAT metabolism can be rapidly activated whenever the animals are in need of extra heat production, like neonates after birth or during arousal from hibernation. The functional uniqueness of BAT comes from the existence of UCP1 protein, which is not present or expresses at very low levels in other non-adipose tissues. *Ucp1* is the first member of uncoupler protein (UCP) family identified in Mammals. There are four homologs identified later: UCP2 is ubiquitously expressed, UCP3 exists only in skeletal muscle and the heart, UCP4 and UCP5 (or brain mitochondrial carrier protein-1, BMCP-1) are principally expressed in the brain.

However, all these UCP-like proteins (UCP2-5) are thought to be physiologically irrelevant to the thermogenesis function because of their low abundance in mitochondrial membrane and lacking the same biochemical properties of UCP1(Nedergaard and Cannon, 2010).

Interestingly, some earlier reports suggested the expression of *Ucp1* in non-adipocytes tissues (Cannon and Nedergaard, 2004). For example, there are studies showing that chronic treatment of β_3-AR agonists leads to UCP1 expression in skeletal muscle. However, this UCP1 expression was later proved to originate in the brown adipocytes interspersed between muscle bundles, but not in the myocytes (Almind et al., 2007). Brown fat and skeletal muscle share a similar developmental origin (i.e. arise from precursor pools residing in the dermomyotome) [reviewed in (Sanchez-Gurmaches and Guertin, 2014a)]. But why is *Ucp1* exclusively expressed in brown adipocytes? During brown fat development, several fate-determination factors drive activation of brown adipocyte commitment genes but induce stable silencing of the myogenic gene program. It is now becoming clear that the fate determination process is tightly associated with epigenetic changes such as DNA methylation, histone modifications, and chromatin remodeling, thus allowing lineage-specific gene expression. One of these fate-determining factors in BAT development is a histone methyltransferase, EHMT1, which is a crucial enzymatic part of the PRDM16 complex. Disruption of Ehmt1 gene blocks brown adipocyte differentiation and induce expression of muscle-specific genes, including myogenin (Inagaki et al., 2016). This may explain why the signaling molecules discussed in this dissertation, such as PGC1α, FoxO1, and p38-MAPK, are ubiquitously

expressed in a wide range of cell types but rather engage in *Ucp1* expression specifically in brown adipocytes or brown-like adipocytes.

The physiological significance of diet-induced thermogenesis

Compared to cold-induced thermogenesis (CIT), dietary effects on activating thermogenesis has been a matter of debate. The contribution of BAT in "diet-induced thermogenesis (DIT)" was first introduced by a fundamental study (Rothwell and Stock, 1979). The initial observations were that the responses of BAT to dietary stimuli declining with ages and becoming undetectable when BAT is maximally stimulated by the cold. More recently, Kozak dismissed this phenomenon as a myth (Kozak, 2010); however, it was further proved by an elegant experimental design with Ucp1-ablated mice (Feldmann et al., 2009). The transgenic mice that lack UCP1-mediated thermogenesis exhibited higher weight gain in response to HFD feeding at thermoneutrality. Such phenotype was otherwise masked at room temperature due to elevated basal metabolism stimulated by cold stress. Consistent with this notion, our *Ucp1-Cre* driven *Rictor* knockout mice demonstrate elevated expression of thermogenic program genes, and they are less vulnerable to HFD-induced obesity at 30°C. Nonetheless, the molecular mechanisms behind DIT and which dietary components can induce this effect are still unknown. These are intriguing questions to be followed in the future, especially regarding how dietary components might directly modulate mTORC2 signaling.

Although current evidence supports the presence of diet-induced thermogenesis, the evolutionary significance of this regulatory mechanism remains mysterious. At first glance, the existence of such mechanism seems to be irrational; why would the animals develop an energy-wasting measure following food intake? One possible explanation is that DIT is evolved mainly to deal with nutrient-deficient or unbalanced diets (Stock, 1999). Some early rodent studies suggested low protein content in foods may be a key factor to trigger thermogenesis, which implies the role of DIT in the regulation of energy balance could be secondary to its original role in the quality control of nutrient supply. However, up to date, meticulously designed experiments to test this hypothesis have not yet been conducted.

An alternative view of mTORC2-deficient phenotypes

The deficiency in mTORC2 signaling appears to have great impacts on BAT metabolism. In particular, the paucity of lipid storage is evident and consistent with my previous results from the *Myf5-Cre* model. It is now becoming clear that altered glucose metabolism is one of the key features upon mTORC2 loss. A handful of studies (Albert et al., 2016; Olsen et al., 2014) pointed towards that mTORC2 activity is directly involved in glucose uptake in adipocytes. However, the fact that the expression of the DNL genes is substantially reduced (Figure 3.2A) while basal glucose uptake is not affected by mTORC2 inhibition (Figure 3.2C), which indicates mTORC2 may have a primary role in regulating glucose catabolic pathways (e.g. glycolysis and glucose

oxidation) rather than directly regulating the glucose uptake process. For example, Hall and colleagues found mTORC2 regulates glucose metabolism via phosphorylating mitochondrial HK-II (Betz et al., 2013). On the other hand, a recent study (Chen et al., 2016) argued that a direct link between mTORC2 and ACLY (ATP-citrate lyase) in acetyl-CoA production. In this study, they characterized ACLY S455 site as an mTORC2 substrate in HER2/PIK3CA breast cancer cells and acetyl-CoA production is reduced when mTORC2 is absent. This phosphorylation site has been proved to be critical for ACLY activity (Lee et al., 2014). Consistent with this finding, I also observed that ACLY S455 phosphorylation is diminished when mTORC2 is lost in brown adipocytes [unpublished data]. Thus, it is possible that the activation of mTORC2 signaling is required for adequate acetyl-CoA biosynthesis in brown adipose tissue. Acetyl-CoA is a central metabolite of intermediary metabolism. It is not only the breakdown product of glucose and fatty acids but also serves as precursors for many biochemical reactions. Besides its metabolic functions, accumulating literature has focused on the role of acetyl-CoA metabolism and cellular signaling [reviewed in (Choudhary et al., 2014; Gut and Verdin, 2013)]. Specifically, it has been shown that ACLY activity positively correlates with global histone acetylation state (Wellen et al., 2009). In addition, acetylation levels of non-histone proteins (including transcription factors and metabolic enzymes) have also been shown to be regulated by compartmentalization of acetyl-CoA production. Therefore, mTORC2 could function as a critical signaling hub that coordinates cellular metabolism and gene expression through regulating acetylation states of histone and non-histone proteins (Figure 5.3). In this

model, mTORC2 regulates multiple metabolic processes to optimize cellular lipid biosynthesis: (1) suppressing fatty acid oxidation and thermogenesis via inhibiting FoxO1; (2) promoting glucose uptake and acetyl-CoA production, which is not only a precursor metabolite for *de novo* lipid synthesis but also an acetyl group donor for protein acetylation.

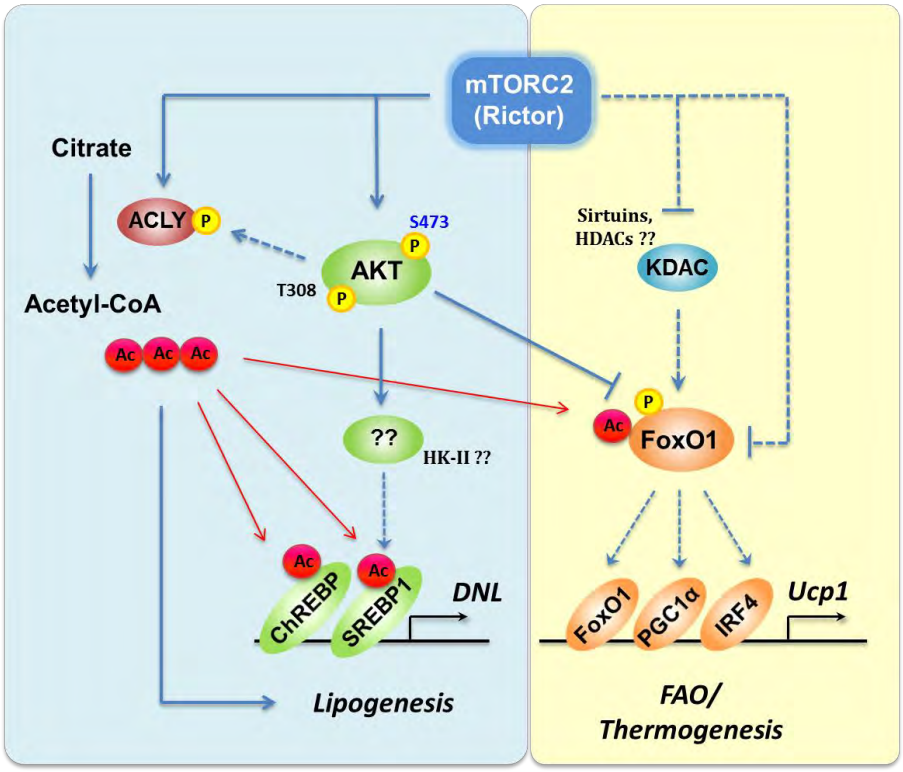

Figure 5.3 Model summarizing the role of mTORC2 in brown adipose tissue
When activated, mTORC2 promotes de novo lipogenesis by facilitating glucose uptake and glycolysis (via AKT activity), leading to activation of ChREBP and SREBP1c. Conversely, mTORC2 signaling suppresses FoxO1 activity through phosphorylation and acetylation to inhibit transcription of lipid oxidation genes and thermogenic genes. Importantly, mTORC2 could regulate acetylation of FoxO1 through negatively regulating deacetylases (i.e., Sirtuins or HDACs) and/or through regulating acetyl-CoA production. Of note, ChREBP (Bricambert et al., 2010) and SREBP1 (Walker et al., 2010) are also known to be regulated by acetylation.

Conclusion and future directions

In this dissertation, I have unraveled the complex role of mTORC2 in controlling metabolism in brown adipose tissue. mTORC2 inhibition causes remarkable alternations in BAT metabolism which is shifted from glycolytic pathways towards oxidative metabolism and thermogenesis. Importantly, the mice with mTORC2-ablated BAT are protection from obesity and its associated adverse effects. However, as mentioned above, targeting mTORC2 might not be the best strategy in developing treatments for obesity because it also seems to lock BAT metabolism into a state with less metabolic flexibility. Given these caveats, understanding the wiring and the interplay between signaling circuits and metabolic networks is crucial and could also be valuable even beyond the topic discussed in this dissertation. It has been long understood that obesity is intimately associated with the development of type II diabetes and cardiovascular disease. There is also growing evidence connecting obesity and the incidence of particular cancers. Moreover, many cancer cells also utilize and adapt aberrant metabolic pathways, which gives them growth and survival advantages. For example, elevated *de novo* lipogenesis and upregulated lipogenic enzymes (e.g. ACC and FASN) are frequently observed in several cancer types including breast, prostate and liver cancers. Given there is a critical role of mTORC2 in regulating glucose metabolism and lipogenesis in adipocytes, it is highly anticipated that mTORC2 might have a similar role in some of those cancer cells. Therefore, developing therapeutic strategies that specifically obstruct mTORC2 signaling or its downstream effectors might be a potential direction to attack the Achilles' heel of these diseases.

Materials and Methods

Antibodies and reagents

Rictor (Cat# 2140), mTOR (2983), pan-AKT (9272), GSK3β (9315), ACC (3676), ACLY (4332), NDRG1 (9408) and β-actin (4970), Insulin receptor β (3025) and anti-HA-tag (2367) HDAC4 (7628), HDAC5 (20458), p38MAPK (8690), Erk1/2 (4695), HSL (4107), Sirt1 (9475), Sirt3 (5490), and α-tubulin antibodies were purchased from Cell Signaling Technologies. SREBP1 (sc-366), p70 S6K (sc-9027), UCP1 antibody (sc-6528), and HRP-conjugated secondary antibodies were from Santa Cruz biotechnology. UCP1 antibody (sc-6528) is from Abcam. All phosphorylation-specific antibodies: S473-AKT (4058), T308-AKT (4056), T24-FoxO1 (9464), S9-GSK3β (9323), T1462-TSC2 (3617), T389-S6K (9234), p-HDAC4/5/7 (3443&3424) , p-p38MAPK (4511) , p-Erk1/2 (4376), p-S660-HSL (4126) and p-S565-HSL (4137) were from Cell Signaling Technologies. 4-hydroxy-tamoxifen (4-OHT) was from Toronto Research Chemicals. Indomethacin, dexamethasone, 3-isobutyl-1-methylxanthine (IBMX) and all other reagents were from Sigma-Aldrich. AS1842856 is from Calbiochem. HDAC and Sirtuin inhibitors are Selleckchem.

Plasmids

Full length AKT1 cDNA obtained by PCR amplification from pcDNA3-myr-HA-AKT1 (addgene #9008) was subcloned into the pCMV-HA vector. Full length AKT2 cDNA obtained by PCR amplification from pBabe-myr-HA-AKT2 (addgene #9018) was

subcloned into the pCMV-HA vector. SGK1 cDNA (Thermo Scientific #MHS6278-202755905) was PCR amplified to obtain a truncated SGK sequence (SGK-delta-60N, N-terminal 1-60 amino acids deletion). Phosphomimetic constructs with indicated mutation were done by QuikChange Site-Directed Mutagenesis kit (Stratagene) with appropriate primers. All cDNA constructs were also transferred into pBabe-puro retroviral vector for stable expression.

Mice

Rictor floxed (Rictorfl/fl) mice (Shiota et al., 2006) or Raptorfl/fl mice (Peterson et al., 2011) were crossed with Myf5-Cre (JAX #007893)(Tallquist et al., 2000), Ubc-CreERT2 (JAX #007001)(Ruzankina et al., 2007) and Pax7-CreERT2 (JAX #012476)(Lepper et al., 2009), to make conditional or inducible knockout mice. Akt1 and Akt2 floxed mice (provided by Morris Birnbaum) were also crossed with Myf5-Cre. Rosa26-mTmG (JAX #007676) and Rosa26–LSL-LacZ (JAX #003474) were also obtained from Jackson laboratory. In chapter III, Rictor floxed (Rictorfl/fl) mice (Shiota et al., 2006) were crossed with different Cre-driver mice including Ucp1-Cre mice (The Jackson Laboratory), Ucp1-CreER^{T2} (a gift from Dr. Wolfrum. Rosenwald et al., 2013) and Adiponectin-Cre (The Jackson Laboratory) to make conditional or inducible knockout mice. For reporter mice, Rosa26-mT-LSL-mG was obtained from Jackson laboratory. FoxO1 floxed mice are from The Jackson Laboratory. Male 129/C57B6 mice were used for all studies. Mice were kept on a daily 12 h light/dark cycle and fed a normal chow diet (Prolab® Isopro® RMH 3000) from LabDiet ad libitum at 22°C (except

thermoneutrality studies). All animal experiments were approved by the University of Massachusetts Medical school animal care and use committee.

Embryo analysis

Timed matings were performed and embryos were dissected at the indicated days. Embryos were fixed overnight in paraformaldehyde, paraffin embedded, and processed for histological analysis according to conventional methods.

Satellite cells isolation and in vitro differentiation

Adult muscle satellite cells were isolated according to (Sherwood et al., 2004). Limb muscle including triceps surae (TS), tibialis anterior (TA), quadriceps and triceps were dissected and minced from 6 to 8-wks mice. Isolated interstitial and myofiber-associated cells were passed through 70μm nylon mesh and centrifuged at 1200 rpm. Red blood cells were removed from preparations by incubation with RBC lysis buffer (0.15 M ammonium chloride, 0.01 M potassium bicarbonate) on ice for 3 minutes. Antibody staining was performed for 20 min on ice in Hank's balanced salt solution supplemented with 2% FCS and 2 mM EDTA. After staining cells were filtered through a 35-μm cell-strainer capped tube to ensure single cell suspension. Sorting was performed immediately after filtration using a FACS Aria II cell sorter equipped with FASCDiva software. Cells were initially selected by size and shape and only live (PI-, calcein blue+) singlets were gated for further analysis of surface markers. Finally an enriched pool of cells (Sca-1-, Mac1-, Ter119-, CD45-, CXCR4+ and β1 intergrin+) were purified and re-

sorted with the same scheme described above to ensure the purity. Double sorted satellite cells were plated at 4x103 cells/well in collagen/laminin coated 96-well plates. Cells were maintained in growth media (20% horse serum in F10 media, Invitrogen) and feed with 5ng bovine FGF daily for 5 days. For inducing muscle fiber formation, cells were first transferred into matrigel (BD Biosence)-coated chamber slides and grown in growth media with bFGF. 2~3 days later, cells were exposed to differentiation media (2% horse serum in F10 without bFGF). After 2 to 4 days myofiber can be observed and fixed with 4% paraformaldehyde. Myosin heavy chains and DAPI staining were performed as described in immunofluorescence section.

Muscle regeneration after cardiotoxin injury

To induce Rictor deletion in vivo, Pax7-CreERT2 mice were i.p. injected with 200μg/g of tamoxifen (dissolved in ethanol first then diluted in corn oil to 10mg/mL) for consecutive 4 days. One day later the mice were anesthetized with 12mg/kg xylazine and 60mg/kg ketamine and 30μL cardiotoxin (10μmol/L from Naja nigricollis, Calbiochem) was directly injected into tibialis anterior muscle. 30μL PBS was given in contralateral TA muscle as control. 1 day and 10 days post injury, TA muscle was removed and muscle regeneration was examined by H&E staining and LacZ staining.

LacZ staining

Adipose tissue depots were fixed in 2% paraformaldehyde, 0.2% glutaraldehyde in PBS for 30 min at room temperature. The tissues were then washed 3 times for 15 min in wash

buffer (PBS carrying 2 mM MgCl2 and 0.02% Igepal® CA-630). Staining was perform in wash buffer containing X-gal (1mg/mL), potassium ferricyanide (5 mM) and potassium ferrocyanide (5 mM) at room temperature for at least 16 h. Next, tissues were further fixed in fixing solution for at least 12 h at room temperature, transferred to ethanol for dehydratation, then sectioned at 5 µm thicknesses. Sections were counter-stained with nuclear fast red dehydrated and mounted using CitosealTM 60 (Thermo Scientific). Lean tissues were snap frozen in isopentane-liquid nitrogen in OCT. Sections (10 µm) were stained overnight (X-gal (1mg/mL), potassium ferricyanide (5 mM) and potassium ferrocyanide (5 mM), MgCl2 (2 mM) in PBS at 37°C and counter-stained with nuclear fast red, dehydrated and mounted.

Tissue harvest and histology

Adipose tissue depots notations are described in (Walden et al., 2011). Each tissue was carefully dissected to avoid contamination from surrounding tissue. Samples for RNA were first immersed in RNAlater (Invitrogen) and stored at -80°C; otherwise, they were frozen down immediately in liquid nitrogen. For histology, tissue pieces were fixed by 10% formalin. Embedding, sectioning and Hematoxylin & Eosin (HE) staining was done by the UMass Morphology Core.

Immunohistochemistry

Adipose tissue sections were subjected to UCP1 IHC according to (Cohen et al., 2014). Briefly, fat sections were hydrated and antigen retrieval was done by incubating the

sections in citrate buffer at 90-95°C water for 20 min. After blocking, primary antibody (anti-Ucp1 antibody, Abcam #ab10983) was applied overnight at 4°C. Next day, SuperPicture 3rd Gen IHC Detection Kit (Novex) was used for detection.

Whole-mount confocal microscopy

Indicated brown and white adipose tissues were dissected from 6 week-old mice and were mounted with Fluoromount-G (Southern Biotech) as described in (Berry and Rodeheffer, 2013). Mounted samples were imaged on a LSM 5 Pascal (Zeiss) point scanner confocal system. 40x objective was used with oil immersion. Background fluorescence was offset by using wild-type tissues (no mT/mG allele). GFP was excited at 488 nm and detected from 515 to 565 nm and iBAT form Myf5-cre;Rosa26mT/mG mice was used as positive control for GFP signal. TdTomato was excited at 543 nm and detected from 575 to 640 nm and pgWAT from mT/mG mice (without Cre-driver) was used as positive control for TdTomato.

Nuclei number and cell size quantification

ImageJ was used to quantify nuclei number in iBAT and cell size (diameter) in rWAT and asWAT. For each individual sample, 4 to 6 images were taken and analyzed. Nuclei density was presented as nuclei number per mm^2.

Genomic DNA quantification

Total genomic DNA was extracted and purified by using DNeasy Blood & Tissue kit (Qiagen) according to manufacturer's instruction. Isolated genomic DNA was quantified by NanoDrop 2000 (Thermo Scientific) spectrophotometer.

Immunofluorescence

Frozen section of interscapular brown adipose tissues were thawed and then fixed with methanol for 15 min at room temperature. The fixed sections were washed with 1mL PBS twice and then were permeabilized and blocked with PBSAT buffer (PBS with 1% BSA and 0.5% Triton X-100) for 15 min twice. Primary antibody against mitochondria Cox IV (1:100 dilution, CST #4850) was added to sections for overnight incubation. Slides were washed three times with 1mL PBSAT and incubated with secondary antibody conjugated with Alexa-568 or Alexa-647 (1:1000 dilution, Invitrogen) for 4 hours. Intensive wash was applied to remove unstained antibodies. DAPI was used to stain nuclei for 5 min and washed away by PBS immediately. The slides were embedded with 5μL mounting media (Prolong Gold, Invitrogen).

Glucose uptake by ^{18}F-FDG PET-CT

6-week old mice (n=5 per each genotype) were i.p. injected with 18F-FDG, 364-483 uCi in100 ul saline, and 30 min later the PET imaging was performed in anesthetized animals (1.2-2% isoflurane carried in oxygen) immobilized on a Minerve bed (Bioscan).

Immediately after PET acquisition, each mouse was transferred to the NanoSPECT/CT (Bioscan), for the CT acquisition. The PET images were reconstructed without photon attenuation correction using the PETView program (Philips) with the fully 3D iterative reconstruction algorithm, giving a pixel size of 1 mm. The CT acquisition was performed at standard frame resolution, 45 kVp tube voltage and 500 ms of exposure time. The CT reconstruction was accomplished using In-VivoScope 1.37 software (Bioscan). The PET image DICOM files were transferred to the NanoSPECT/CT reconstruction workstation to provide the PET/CT fusion images. Volume-of-Interest (VOI) analysis of the PET acquisitions was accomplished with the InVivo- Scope 1.37 software.

Transmission electron microscopy

iBATs (n=3 for each group) were dissected from 5 week-old mice and subjected to electron microscopy study done by Core Electron Microscopy Facility, UMass medical school.

Metabolite profiling

See in the published paper (Hung et al., 2014).

Cold challenge

Randomly-fed Mice were transferred into a 4°C cold room with or without food (as indicated in the text) in the cage. Rectal temperature was measured by rectal probe

(RET-3, ThermoWorks) hourly for 6 or 7 hours. Mice were sacrificed and tissues were collected at the end of experiment. For chronic cold acclimation, mice were moved into an environment-controlled chamber with temperature set at 6°C for 2 weeks. Food and water were freely accessible.

Cell culture and retrovirus production

All cells were cultured in DMEM (Invitrogen) supplemented with 10% FBS and penicillin/streptomycin at a 37°C. Primary brown preadipocytes (bBPAs) were isolated from P1 neonates of *Ubc-creER^{T2};Rictor$^{fl/fl}$* mice, *Myf5-cre;Rictor$^{fl/fl}$*, *Myf5-cre;Akt1$^{fl/fl}$*, *Myf5-cre;Akt2$^{fl/fl}$* mice, *Ubc-CreER^{T2}; Akt1$^{fl/fl}$; Akt2$^{fl/fl}$* mice, *Ubc-CreER^{T2}; Raptor$^{fl/fl}$* mice and control littermates according to (Fasshauer et al., 2001) and were immortalized with pBabe-SV40 Large T antigen and selected by puromycin or zeocin resistance. For recombinant AKT and SGK construct expression, retroviruses were made by cotransfecting pBabe-puro plasmid harboring different Akt or Sgk cDNAs with pCL-Ampho in HEK-293T cells. 24h and 48h after transfection the viral supernatant was harvested and applied to MEFs for 12h. Cells stably expressing each construct were obtained after puromycin selection.

For Ucp1 induction experiment, cells were differentiated as described previously (Hung et al., 2014) and were treated with Ethanol or 4-OHT to induce gene deletion at Day 6. At Day 11, cells were incubated with fresh medium with CL-316,243 or forskolin for 8hrs. FoxO1 inhibitor (AS1842856) was given 30mins prior to CL-316,243 or forskolin

stimulation.

Differentiation

To generate RictoriKO cells ubc-creERT2;Rictorfl/fl bAPCs were treated with two doses of 1μM 4-OHT for 3 days. For brown preadipocyte differentiation, BPAs were seeded at 4x104 cells/ml and allowed to proliferate to confluence over 3 days in differentiation media (20nM insulin, 1nM T3). On the 4th day, cells were induced to differentiate by adding induction media (20nM insulin, 1nM T3, 0.125mM indomethacin, 2μg/mL dexamethasone and 0.5mM 3-isobutyl-1-methylxanthine (IBMX)) for 2 days; the medium was then changed every two days with fresh differentiation media until day 10. Differentiated bAPCs were fixed with PBS-buffered formalin and stained with Oil-Red-O dye.

CRISPR-mediated knockout

For CRISPR knockdown, guide RNAs for FoxO1 knockout were designed by CHOPCHOP (https://chopchop.rc.fas.harvard.edu/). PAM motif and enzyme site sequences were added according to the protocol (Sanjana et al., 2014; Shalem et al., 2014). DNA oligos for each sgRNA were cloned into lentiCRISPRv2 vector.
The sgRNA sequences are:
sgFoxO1#1: 5'-GGCCGAAGCGCCCCAGGTGG-3';
sgFoxO1#2: 5'-GAGCAACCTGAGCCTGCTGG-3';
sgFoxO1#3: 5'- TGCGACAGCGGCCCGGTCGG-3';

sgFoxO1#4: 5'-GGCCGAAGCGCCCCAGGTGG-3'.

Western blots

Cells were lysed in a buffer containing 50mM Hepes, pH 7.4, 40mM NaCl, 2mM EDTA, 1.5mM NaVO4, 50mM NaF, 10mM sodium pyrophosphate, 10mM sodium β-glycerophosphate and 1% Triton X-100 typically 1 hour after the cells were replenished with fresh culture medium. Tissues were homogenized using a TissueLyser (Qiagen) in the same lysis buffer but additionally supplemented with 0.1% SDS, 1% sodium deoxycholate. An equal amount of total protein was loaded into acrylamide/bis-acrylamide gels and transferred to PVDF membranes for detection with the indicated antibodies. Briefly, membranes were incubated with primary antibodies in 5% milk/PBST or 5% BSA/PBST overnight. HRP-conjugated secondary antibodies were given for 1h. Western blots were developed by enhanced chemiluminescence (PerkinElmer) and detected by X-ray films.

Immunoprecipitation

AKT1-specific antibody (CST# 2967) and AKT2-specific antibody-conjugated beads (CST#4090) were used to purify each isoform. 500ug Cell lysates or tissue lysates were incubated with 1ul of antibodies at 4°C overnight. For AKT1 purification, protein-antibody complex was precipitated by 2 hrs incubation with protein G sepharose beads (Invitrogen). Samples were then boiled in 2x SDS sample buffer.

Ex vivo oxygen consumption

Freshly isolated brown adipose tissues were rinsed with KHB buffer (111nM NaCl, 4.7mM KCl, 2mM MgSO4, 1.2mM Na2HPO4, 0.5mM carnitine and 2.5mM glucose) and then cut into small pieces (5~10mg). After 5 times of washing with KHB buffer, each piece was placed into the center of one single well in a XF24 islet capture microplate (Seahorse Bioscience #101122-100) and covered by a provided screen. 450ul KHB buffer was loaded in each well and tissue metabolic rates were measured following program: 3 cycles for basal oxygen consumption rate (OCR) (2 min mix, 2 min wait, and 3 min measure), then injection of 50ul 100mM pyruvate, then followed by 3 cycles for pyruvate-stimulated OCR (3 min mix, 3 min wait, and 2 min measure). Each OCR value was obtained from five different pieces of a tissue and from 3 repeated measurements. The final OCR values were the average of five independent experiments and normalized to genomic DNA content.

Gene expression analysis

Total RNA was isolated from cells or tissues using Qiazol (Invitrogen) and an RNeasy kit (Invitrogen). Equal amounts of RNA were retro-transcribed to cDNA using a High capacity cDNA reverse transcription kit (#4368813, Applied Biosystems). Quantitative RT-PCR was performed in 10μL reactions using a StepOnePlus real-time PCR machine from Applied Biosystems using SYBR Green PCR master mix (#4309156, Applied Biosystems) according to manufacturer instructions. Standard and melting curves were run in every plate for every gene to ensure efficiency and specificity of the reaction. Tbp expression was used as a normalization gene in all conventional RT-PCR experiments.

Primer information is listed in the table below. Quantitative RT-PCR arrays for mitochondria (PAMM-087) and mitochondria energy metabolism (PAMM-008) were purchased from Qiagen. Interscapular brown fat pads were removed from 6-wks mice ad libitum and Rictor protein deletion in Myf5-re;Rictorfl/fl samples was confirmed by western blots before analyzing expression. Data analysis was performed on web-based software provided by the manufacturer.

In vivo glucose and free fatty acid uptake

14C-bromopalmitate ([1-14C]-2-bromopalmitic acid) and 3H-deoxyglucose ([1,2-3H(N)]-Deoxy-D-glucose) were used to respectively evaluate NEFA and glucose uptake in BAT, eWAT and iWAT, as previously described (Ferre, 1985; Menard, 2009; Menard, 2010). Both radioactive tracers (Moravek Biochemicals, Inc. Brea, CA, USA) were dissolved in normal saline supplemented with 4% bovine serum albumin (BSA). Following a 6hr fasting, mice received an intraperitoneal bolus of 10 µCi of each tracer in a total volume of 150 µl. Two hours following the injection, mice were euthanized with an overdose of anesthetic and tissues were collected, weighed and homogenized. Specific fractional uptakes of 14C-bromopalmitate and 3H-deoxyglucose were determined using a scintillation counter (liquid scintillation analyzer Tri-Carb 2900TR, PerkinElmer, Montreal, QC, Canada), as previously described (Ci, 2006; Monge-Roffarello, 2014). Uptake data were expressed as the percentage of injected dose of [14C] and [3H] per milligram of tissues.

Infrared thermography

An Infrared camera (T1020, FLiR system) was mounted on a tripod to keep the same height. Mice were anesthetized with a short isoflurane intake and place on top of a laboratory paper sheet with the doral side facing up. Duplicate thermoimages were taken for each mouse and were analyzed in the provided software (FLIR tool). Region-of-interest (ROI) circle (35 unit in diameter) was overlaid mouse interscapular region to obtain maximal, mininal, average temperature. In addition, tail temperature was also analyzed.

Thermoneutrality and high-fat diet feeding

6-week-old *Ucp1-Cre;Rictor*$^{fl/fl}$ male mice were transferred to 30C. At 10 weeks of age, mice were fed a chow diet (Prolab Isopro RMH3000, LabDiet) or a high-fat diet (45% calories from fat; ResearchDiet # D12451). Body weight and food intake were accessed weekly for 16 weeks. Glucose tolerance tests were performed at the 15th week. Overnight fasted animals were subjected to GTT by intraperitoneally injecting glucose at 2 g/kg of body weight, and blood glucose levels were measured with a commercially available glucose meter. For *Ucp1-Cre*^{ER}*;Rictor*$^{fl/fl}$ mice, 20 week-old mice were first with Tamoxifen (TAM) (100mg/kg per day) for 6 days. After TAM treatment, mice were transferred into a thermoneutral room for one-week adapation. 45% HFD feeding started when mice were at 22 week-old, and the body weight gain and the food intake of mice

were monitored weekly for a 9-week experiment. ITT & GTT were accessed before scarifying the mice.

Statistics

Unless otherwise stated, the results are described as mean ± SEM. Two-way ANOVA was performed where indicated. For most experiments, the Student's t test was used to determine statistical significance ($*p < 0.05$; $**p < 0.01$; $***p < 0.001$).

Table 6.1 Primer sequences for quantitative RT-PCR analysis

Gene	Forward primer (5'-3')	Reverse primer (5'-3')
Tbp	GAAGCTGCGGTACAATTCCAG	CCCCTTGTACCCTTCACCAAT
Prdm16	GACATTCCAATCCCACCAGA	CACCTCTGTATCCGTCAGCA
Ppargc1α	CCCTGCCATTGTTAAGACC	TGCTGCTGTTCCTGTTTTC
Pparγ	TCAGCTCTGTGGACCTCTCC	ACCCTTGCATCCTTCACAAG
C/ebpα	CAAGCCCAGCAACGAGTACCG	GTCACTGGTCAACTCCAGCAC
C/ebpβ	TCGGGACTTGATGCAATCC	AAACATCAACAACCCCGC
C/ebpδ	GCTTTGTGGTTGCTGTTGAA	ATCGACTTCAGCGCCTACA
Ucp1	CTGCCAGGACAGTACCCAAG	TCAGCTGTTCAAAGCACACA
DiO2	TGCGCTGTGTCTGGAACAG	CTGGAATTGGGAGCATCTTCA
Lpl	GGCCAGATTCATCAACTGGAT	GCTCCAAGGCTGTACCCTAAG
aP2	GATGCCTTTGTGGGAACCT	CTGTCGTCTGCGGTGATTT
Cidea	ATCACAACTGGCCTGGTTACG	TACTACCCGGTGTCCATTTCT
Dpt	CTGCCGCTATAGCAAGAGGT	TGGCTTGGGTACTCTGTTGTC
Srebf1a	TAGTCCGAAGCCGGGTGGGCGCCGG	GATGTCGTTCAAAACCGCTGTGTGTC
Srebf1c	AAGCAAATCACTGAAGGACCTGG	AAAGACAAGCTACTCTGGGAG
Srebf2	GGATCCTCCCAAAGAAGGAG	TTCCTCAGAACGCCAGACTT
Chrebp	CACTCAGGGAATACACGCCTAC	ATCTTGGTCTTAGGGTCTTCAGG
Chrebpα	CGACACTCACCCACCTCTTC	TTGTTCAGCCGGATCTTGTC
Chrebpβ	TCTGCAGATCGCGTGGAG	CTTGTCCCGGCATAGCAAC
Acly	CTCACACGGAAGCTCCATAA	ACGCCCTCATAGACACCATC
Acc	GGAGATGTACGCTGACCGAGAA	ACCCGACGCATGGTTTTCA

Fasn	GCTGCGGAAACTTCAGGAAAT	AGAGACGTGTCACTCCTGGACTT
Elvol6	TCAGCAAAGCACCCGAAC	AGCGACCATGTCTTTGTAGGAG
Scd1	CCCTGCGGATCTTCCTTATC	TGTGTTTCTGAGAACTTGTGGTG
Insig1	TGTGGTTCTCCCAGGTGACT	TAGCCACCATCTTCTCCTCC
Insig2	TGAAGCAGACCAATGTTTCAA	GGTGAACTGGGGGTCTCC
Tfam	GTCCATAGGCACCGTATTGC	CCCATGCTGGAAAAACACTT
Cpt1b	GGGCACCTCTGGGAGTTTGT	TTGGCTCACCCACACAGTGT
Necdin	CACTTCCTCTGCTGGTCTCC	ATCGCTGTCCTGCATCTCAC
Pref1	AGTACGAATGCTCCTGCACAC	CTGGCCCTCATCATCCAC
Wnt10a	CACCCGGCCATACTTCCT	CACTTACGCCGCATGTTCT

Reference

Ahmadian, M., Abbott, M.J., Tang, T., Hudak, C.S., Kim, Y., Bruss, M., Hellerstein, M.K., Lee, H.Y., Samuel, V.T., Shulman, G.I.*, et al.* (2011). Desnutrin/ATGL is regulated by AMPK and is required for a brown adipose phenotype. Cell Metab *13*, 739-748.

Albert, V., Svensson, K., Shimobayashi, M., Colombi, M., Munoz, S., Jimenez, V., Handschin, C., Bosch, F., and Hall, M.N. (2016). mTORC2 sustains thermogenesis via Akt-induced glucose uptake and glycolysis in brown adipose tissue. EMBO Mol Med *8*, 232-246.

Almind, K., Manieri, M., Sivitz, W.I., Cinti, S., and Kahn, C.R. (2007). Ectopic brown adipose tissue in muscle provides a mechanism for differences in risk of metabolic syndrome in mice. Proc Natl Acad Sci U S A *104*, 2366-2371.

Asada, S., Daitoku, H., Matsuzaki, H., Saito, T., Sudo, T., Mukai, H., Iwashita, S., Kako, K., Kishi, T., Kasuya, Y.*, et al.* (2007). Mitogen-activated protein kinases, Erk and p38, phosphorylate and regulate Foxo1. Cell Signal *19*, 519-527.

Balcke, G.U., Kolle, S.N., Kamp, H., Bethan, B., Looser, R., Wagner, S., Landsiedel, R., and van Ravenzwaay, B. (2011a). Linking energy metabolism to dysfunctions in mitochondrial respiration--a metabolomics in vitro approach. Toxicology letters *203*, 200-209.

Balcke, G.U., Kolle, S.N., Kamp, H., Bethan, B., Looser, R., Wagner, S., Landsiedel, R., and van Ravenzwaay, B. (2011b). Linking energy metabolism to dysfunctions in mitochondrial respiration - A metabolomics in vitro approach. Toxicology Letters *203*, 200-209.

Banks, A.S., Kim-Muller, J.Y., Mastracci, T.L., Kofler, N.M., Qiang, L., Haeusler, R.A., Jurczak, M.J., Laznik, D., Heinrich, G., Samuel, V.T.*, et al.* (2011). Dissociation of the glucose and lipid regulatory functions of FoxO1 by targeted knockin of acetylation-defective alleles in mice. Cell Metab *14*, 587-597.

Bartelt, A., Bruns, O.T., Reimer, R., Hohenberg, H., Ittrich, H., Peldschus, K., Kaul, M.G., Tromsdorf, U.I., Weller, H., Waurisch, C.*, et al.* (2011). Brown adipose tissue activity controls triglyceride clearance. Nature Medicine *17*, 200-U293.

Bartelt, A., and Heeren, J. (2014). Adipose tissue browning and metabolic health. Nat Rev Endocrinol *10*, 24-36.

Benavides-Serrato, A., Anderson, L., Holmes, B., Cloninger, C., Artinian, N., Bashir, T., and Gera, J. (2014). mTORC2 modulates feedback regulation of p38 MAPK activity via DUSP10/MKP5 to confer differential responses to PP242 in glioblastoma. Genes Cancer *5*, 393-406.

Bentzinger, C.F., Romanino, K., Cloetta, D., Lin, S., Mascarenhas, J.B., Oliveri, F., Xia, J., Casanova, E., Costa, C.F., Brink, M.*, et al.* (2008). Skeletal muscle-specific ablation of raptor, but not of rictor, causes metabolic changes and results in muscle dystrophy. Cell Metab *8*, 411-424.

Betz, C., Stracka, D., Prescianotto-Baschong, C., Frieden, M., Demaurex, N., and Hall, M.N. (2013). Feature Article: mTOR complex 2-Akt signaling at mitochondria-associated endoplasmic reticulum membranes (MAM) regulates mitochondrial physiology. Proc Natl Acad Sci U S A *110*, 12526-12534.

Bornfeldt, K.E., and Tabas, I. (2011). Insulin resistance, hyperglycemia, and atherosclerosis. Cell Metab *14*, 575-585.

Boutant, M., Joffraud, M., Kulkarni, S.S., Garcia-Casarrubios, E., Garcia-Roves, P.M., Ratajczak, J., Fernandez-Marcos, P.J., Valverde, A.M., Serrano, M., and Canto, C. (2015). SIRT1 enhances glucose tolerance by potentiating brown adipose tissue function. Mol Metab *4*, 118-131.

Bricambert, J., Miranda, J., Benhamed, F., Girard, J., Postic, C., and Dentin, R. (2010). Salt-inducible kinase 2 links transcriptional coactivator p300 phosphorylation to the prevention of ChREBP-dependent hepatic steatosis in mice. J Clin Invest *120*, 4316-4331.

Brunet, A., Sweeney, L.B., Sturgill, J.F., Chua, K.F., Greer, P.L., Lin, Y., Tran, H., Ross, S.E., Mostoslavsky, R., Cohen, H.Y.*, et al.* (2004). Stress-dependent regulation of FOXO transcription factors by the SIRT1 deacetylase. Science *303*, 2011-2015.

Cannon, B., and Nedergaard, J. (2004). Brown adipose tissue: Function and physiological significance. Physiological Reviews *84*, 277-359.

Cannon, B., and Nedergaard, J. (2010). Metabolic consequences of the presence or absence of the thermogenic capacity of brown adipose tissue in mice (and probably in humans). Int J Obes (Lond) *34 Suppl 1*, S7-16.

Cannon, B., and Nedergaard, J. (2011). Nonshivering thermogenesis and its adequate measurement in metabolic studies. J Exp Biol *214*, 242-253.

Canto, C., Houtkooper, R.H., Pirinen, E., Youn, D.Y., Oosterveer, M.H., Cen, Y., Fernandez-Marcos, P.J., Yamamoto, H., Andreux, P.A., Cettour-Rose, P.*, et al.* (2012). The NAD(+) precursor nicotinamide riboside enhances oxidative metabolism and protects against high-fat diet-induced obesity. Cell Metab *15*, 838-847.

Cao, H., Gerhold, K., Mayers, J.R., Wiest, M.M., Watkins, S.M., and Hotamisligil, G.S. (2008). Identification of a lipokine, a lipid hormone linking adipose tissue to systemic metabolism. Cell *134*, 933-944.

Castro, A.F., Rebhun, J.F., Clark, G.J., and Quilliam, L.A. (2003). Rheb binds tuberous sclerosis complex 2 (TSC2) and promotes S6 kinase activation in a rapamycin- and farnesylation-dependent manner. J Biol Chem *278*, 32493-32496.

Cederberg, A., Gronning, L.M., Ahren, B., Tasken, K., Carlsson, P., and Enerback, S. (2001). FOXC2 is a winged helix gene that counteracts obesity, hypertriglyceridemia, and diet-induced insulin resistance. Cell *106*, 563-573.

Chakrabarti, P., English, T., Karki, S., Qiang, L., Tao, R., Kim, J., Luo, Z., Farmer, S.R., and Kandror, K.V. (2011). SIRT1 controls lipolysis in adipocytes via FOXO1-mediated expression of ATGL. J Lipid Res *52*, 1693-1701.

Chakrabarti, P., and Kandror, K.V. (2009). FoxO1 controls insulin-dependent adipose triglyceride lipase (ATGL) expression and lipolysis in adipocytes. J Biol Chem *284*, 13296-13300.

Chen, Y., Qian, J., He, Q., Zhao, H., Toral-Barza, L., Shi, C., Zhang, X., Wu, J., and Yu, K. (2016). mTOR complex-2 stimulates acetyl-CoA and de novo lipogenesis through ATP citrate lyase in HER2/PIK3CA-hyperactive breast cancer. Oncotarget *7*, 25224-25240.

Cho, H., Mu, J., Kim, J.K., Thorvaldsen, J.L., Chu, Q.W., Crenshaw, E.B., Kaestner, K.H., Bartolomei, M.S., Shulman, G.I., and Birnbaum, M.J. (2001). Insulin resistance and a diabetes mellitus-like syndrome in mice lacking the protein kinase Akt2 (PKB beta). Science *292*, 1728-1731.

Choudhary, C., Weinert, B.T., Nishida, Y., Verdin, E., and Mann, M. (2014). The growing landscape of lysine acetylation links metabolism and cell signalling. Nat Rev Mol Cell Biol *15*, 536-550.

Collins, S., Yehuda-Shnaidman, E., and Wang, H. (2010). Positive and negative control of Ucp1 gene transcription and the role of beta-adrenergic signaling networks. Int J Obes (Lond) *34 Suppl 1*, S28-33.

Cousin, B., Cinti, S., Morroni, M., Raimbault, S., Ricquier, D., Penicaud, L., and Casteilla, L. (1992). Occurrence of brown adipocytes in rat white adipose tissue: molecular and morphological characterization. J Cell Sci *103 (Pt 4)*, 931-942.

Cybulski, N., Polak, P., Auwerx, J., Ruegg, M.A., and Hall, M.N. (2009). mTOR complex 2 in adipose tissue negatively controls whole-body growth. Proc Natl Acad Sci U S A *106*, 9902-9907.

Cypess, A.M., Lehman, S., Williams, G., Tal, I., Rodman, D., Goldfine, A.B., Kuo, F.C., Palmer, E.L., Tseng, Y.-H., Doria, A.*, et al.* (2009). Identification and Importance of Brown Adipose Tissue in Adult Humans. New England Journal of Medicine *360*, 1509-1517.

Cypess, A.M., Weiner, L.S., Roberts-Toler, C., Elia, E.F., Kessler, S.H., Kahn, P.A., English, J., Chatman, K., Trauger, S.A., Doria, A.*, et al.* (2015). Activation of Human Brown Adipose Tissue by a beta 3-Adrenergic Receptor Agonist. Cell Metabolism *21*, 33-38.

Cypess, A.M., White, A.P., Vemochet, C., Schulz, T.J., Xue, R., Sass, C.A., Huang, T.L., Roberts-Toler, C., Weiner, L.S., Sze, C.*, et al.* (2013). Anatomical localization, gene expression profiling and functional characterization of adult human neck brown fat. Nature Medicine *19*, 635-639.

Czech, M.P., Tencerova, M., Pedersen, D.J., and Aouadi, M. (2013). Insulin signalling mechanisms for triacylglycerol storage. Diabetologia *56*, 949-964.

Daitoku, H., Hatta, M., Matsuzaki, H., Aratani, S., Ohshima, T., Miyagishi, M., Nakajima, T., and Fukamizu, A. (2004). Silent information regulator 2 potentiates Foxo1-mediated transcription through its deacetylase activity. Proc Natl Acad Sci U S A *101*, 10042-10047.

Daitoku, H., Sakamaki, J., and Fukamizu, A. (2011). Regulation of FoxO transcription factors by acetylation and protein-protein interactions. Biochim Biophys Acta *1813*, 1954-1960.

Daitoku, H., Yamagata, K., Matsuzaki, H., Hatta, M., and Fukamizu, A. (2003). Regulation of PGC-1 promoter activity by protein kinase B and the forkhead transcription factor FKHR. Diabetes *52*, 642-649.

Efeyan, A., Comb, W.C., and Sabatini, D.M. (2015). Nutrient-sensing mechanisms and pathways. Nature *517*, 302-310.

Eguchi, J., Wang, X., Yu, S., Kershaw, E.E., Chiu, P.C., Dushay, J., Estall, J.L., Klein, U., Maratos-Flier, E., and Rosen, E.D. (2011). Transcriptional control of adipose lipid handling by IRF4. Cell Metab *13*, 249-259.

Eijkelenboom, A., and Burgering, B.M. (2013). FOXOs: signalling integrators for homeostasis maintenance. Nat Rev Mol Cell Biol *14*, 83-97.

Eissing, L., Scherer, T., Todter, K., Knippschild, U., Greve, J.W., Buurman, W.A., Pinnschmidt, H.O., Rensen, S.S., Wolf, A.M., Bartelt, A.*, et al.* (2013). De novo lipogenesis in human fat and liver is linked to ChREBP-beta and metabolic health. Nat Commun *4*, 1528.

Fasshauer, M., Klein, J., Kriauciunas, K.M., Ueki, K., Benito, M., and Kahn, C.R. (2001). Essential role of insulin receptor substrate 1 in differentiation of brown adipocytes. Mol Cell Biol *21*, 319-329.

Fedorenko, A., Lishko, P.V., and Kirichok, Y. (2012). Mechanism of fatty-acid-dependent UCP1 uncoupling in brown fat mitochondria. Cell *151*, 400-413.

Feige, J.N., Lagouge, M., Canto, C., Strehle, A., Houten, S.M., Milne, J.C., Lambert, P.D., Mataki, C., Elliott, P.J., and Auwerx, J. (2008). Specific SIRT1 activation mimics low energy levels and protects against diet-induced metabolic disorders by enhancing fat oxidation. Cell Metab *8*, 347-358.

Feldmann, H.M., Golozoubova, V., Cannon, B., and Nedergaard, J. (2009). UCP1 ablation induces obesity and abolishes diet-induced thermogenesis in mice exempt from thermal stress by living at thermoneutrality. Cell Metab *9*, 203-209.

Filhoulaud, G., Guilmeau, S., Dentin, R., Girard, J., and Postic, C. (2013). Novel insights into ChREBP regulation and function. Trends Endocrinol Metab *24*, 257-268.

Foster, D.O., and Frydman, M.L. (1978). Brown adipose tissue: the dominant site of nonshivering thermogenesis in the rat. Experientia Suppl *32*, 147-151.

Ganley, I.G., Lam, D.H., Wang, J., Ding, X., Chen, S., and Jiang, X. (2009). ULK1 center dot ATG13 center dot FIP200 Complex Mediates mTOR Signaling and Is Essential for Autophagy. Journal of Biological Chemistry *284*, 12297-12305.

Garcia-Cao, I., Song, M.S., Hobbs, R.M., Laurent, G., Giorgi, C., de Boer, V.C., Anastasiou, D., Ito, K., Sasaki, A.T., Rameh, L.*, et al.* (2012). Systemic elevation of PTEN induces a tumor-suppressive metabolic state. Cell *149*, 49-62.

Garcia-Martinez, J.M., and Alessi, D.R. (2008). mTOR complex 2 (mTORC2) controls hydrophobic motif phosphorylation and activation of serum- and glucocorticoid-induced protein kinase 1 (SGK1). Biochem J *416*, 375-385.

Garofalo, R.S., Orena, S.J., Rafidi, K., Torchia, A.J., Stock, J.L., Hildebrandt, A.L., Coskran, T., Black, S.C., Brees, D.J., Wicks, J.R.*, et al.* (2003). Severe diabetes, age-dependent loss of adipose tissue, and mild growth deficiency in mice lacking Akt2/PKBβ. Journal of Clinical Investigation *112*, 197-208.

Gerhart-Hines, Z., Dominy, J.E., Jr., Blattler, S.M., Jedrychowski, M.P., Banks, A.S., Lim, J.H., Chim, H., Gygi, S.P., and Puigserver, P. (2011). The cAMP/PKA pathway rapidly activates SIRT1 to promote fatty acid oxidation independently of changes in NAD(+). Mol Cell *44*, 851-863.

Gerin, I., Bommer, G.T., Lidell, M.E., Cederberg, A., Enerback, S., and Macdougald, O.A. (2009). On the role of FOX transcription factors in adipocyte differentiation and insulin-stimulated glucose uptake. J Biol Chem *284*, 10755-10763.

Gesta, S., Tseng, Y.H., and Kahn, C.R. (2007). Developmental origin of fat: tracking obesity to its source. Cell *131*, 242-256.

Guertin, D.A., Stevens, D.M., Saitoh, M., Kinkel, S., Crosby, K., Sheen, J.H., Mullholland, D.J., Magnuson, M.A., Wu, H., and Sabatini, D.M. (2009). mTOR complex 2 is required for the development of prostate cancer induced by Pten loss in mice. Cancer Cell *15*, 148-159.

Guertin, D.A., Stevens, D.M., Thoreen, C.C., Burds, A.A., Kalaany, N.Y., Moffat, J., Brown, M., Fitzgerald, K.J., and Sabatini, D.M. (2006). Ablation in mice of the mTORC components raptor, rictor, or mLST8 reveals that mTORC2 is required for signaling to Akt-FOXO and PKCalpha, but not S6K1. Dev Cell *11*, 859-871.

Gut, P., and Verdin, E. (2013). The nexus of chromatin regulation and intermediary metabolism. Nature *502*, 489-498.

Hagiwara, A., Cornu, M., Cybulski, N., Polak, P., Betz, C., Trapani, F., Terracciano, L., Heim, M.H., Rueegg, M.A., and Hall, M.N. (2012). Hepatic mTORC2 Activates Glycolysis and Lipogenesis through Akt, Glucokinase, and SREBP1c. Cell Metabolism *15*, 725-738.

Hany, T.F., Gharehpapagh, E., Kamel, E.M., Buck, A., Himms-Hagen, J., and von Schulthess, G.K. (2002). Brown adipose tissue: a factor to consider in symmetrical tracer uptake in the neck and upper chest region. Eur J Nucl Med Mol Imaging *29*, 1393-1398.

Hao, Q., Yadav, R., Basse, A.L., Petersen, S., Sonne, S.B., Rasmussen, S., Zhu, Q., Lu, Z., Wang, J., Audouze, K*., et al.* (2015). Transcriptome profiling of brown adipose tissue during cold exposure reveals extensive regulation of glucose metabolism. Am J Physiol Endocrinol Metab *308*, E380-392.

Harms, M.J., Ishibashi, J., Wang, W., Lim, H.W., Goyama, S., Sato, T., Kurokawa, M., Won, K.J., and Seale, P. (2014). Prdm16 is required for the maintenance of brown adipocyte identity and function in adult mice. Cell Metab *19*, 593-604.

Herman, M.A., Peroni, O.D., Villoria, J., Schon, M.R., Abumrad, N.A., Bluher, M., Klein, S., and Kahn, B.B. (2012). A novel ChREBP isoform in adipose tissue regulates systemic glucose metabolism. Nature *484*, 333-338.

Hosokawa, N., Hara, T., Kaizuka, T., Kishi, C., Takamura, A., Miura, Y., Iemura, S.-i., Natsume, T., Takehana, K., Yamada, N*., et al.* (2009). Nutrient-dependent mTORC1 Association with the ULK1-Atg13-FIP200 Complex Required for Autophagy. Molecular Biology of the Cell *20*, 1981-1991.

Hsu, P.P., Kang, S.A., Rameseder, J., Zhang, Y., Ottina, K.A., Lim, D., Peterson, T.R., Choi, Y., Gray, N.S., Yaffe, M.B*., et al.* (2011). The mTOR-regulated phosphoproteome reveals a mechanism of mTORC1-mediated inhibition of growth factor signaling. Science *332*, 1317-1322.

Huang, H., and Tindall, D.J. (2011). Regulation of FOXO protein stability via ubiquitination and proteasome degradation. Biochim Biophys Acta *1813*, 1961-1964.

Hung, C.-M., Calejman, C.M., Sanchez-Gurmaches, J., Li, H., Clish, C.B., Hettmer, S., Wagers, A.J., and Guertin, D.A. (2014). Rictor/mTORC2 Loss in the Myf5 Lineage Reprograms Brown Fat Metabolism and Protects Mice against Obesity and Metabolic Disease. Cell Reports *8*, 256-271.

Inagaki, T., Sakai, J., and Kajimura, S. (2016). Transcriptional and epigenetic control of brown and beige adipose cell fate and function. Nat Rev Mol Cell Biol *17*, 480-495.

Infantino, V., Iacobazzi, V., De Santis, F., Mastrapasqua, M., and Palmieri, F. (2007). Transcription of the mitochondrial citrate carrier gene: Role of SREBP-1, upregulation by insulin and downregulation by PUFA. Biochemical and Biophysical Research Communications *356*, 249-254.

Inoki, K., Li, Y., Xu, T., and Guan, K.L. (2003a). Rheb GTPase is a direct target of TSC2 GAP activity and regulates mTOR signaling. Genes Dev *17*, 1829-1834.

Inoki, K., Zhu, T.Q., and Guan, K.L. (2003b). TSC2 mediates cellular energy response to control cell growth and survival. Cell *115*, 577-590.

Jacinto, E., Facchinetti, V., Liu, D., Soto, N., Wei, S., Jung, S.Y., Huang, Q., Qin, J., and Su, B. (2006). SIN1/MIP1 maintains rictor-mTOR complex integrity and regulates Akt phosphorylation and substrate specificity. Cell *127*, 125-137.

Jespersen, N.Z., Larsen, T.J., Peijs, L., Daugaard, S., Homoe, P., Loft, A., de Jong, J., Mathur, N., Cannon, B., Nedergaard, J.*, et al.* (2013). A classical brown adipose tissue mRNA signature partly overlaps with brite in the supraclavicular region of adult humans. Cell Metab *17*, 798-805.

Jing, E., Gesta, S., and Kahn, C.R. (2007). SIRT2 regulates adipocyte differentiation through FoxO1 acetylation/deacetylation. Cell Metab *6*, 105-114.

Jung, C.H., Jun, C.B., Ro, S.-H., Kim, Y.-M., Otto, N.M., Cao, J., Kundu, M., and Kim, D.-H. (2009). ULK-Atg13-FIP200 Complexes Mediate mTOR Signaling to the Autophagy Machinery. Molecular Biology of the Cell *20*, 1992-2003.

Kajimura, S., Seale, P., and Spiegelman, B.M. (2010). Transcriptional control of brown fat development. Cell Metab *11*, 257-262.

Kitamura, Y.I., Kitamura, T., Kruse, J.P., Raum, J.C., Stein, R., Gu, W., and Accili, D. (2005). FoxO1 protects against pancreatic beta cell failure through NeuroD and MafA induction. Cell Metab *2*, 153-163.

Klotz, L.O., Sanchez-Ramos, C., Prieto-Arroyo, I., Urbanek, P., Steinbrenner, H., and Monsalve, M. (2015). Redox regulation of FoxO transcription factors. Redox Biol *6*, 51-72.

Kong, X., Banks, A., Liu, T., Kazak, L., Rao, R.R., Cohen, P., Wang, X., Yu, S., Lo, J.C., Tseng, Y.H.*, et al.* (2014). IRF4 is a key thermogenic transcriptional partner of PGC-1alpha. Cell *158*, 69-83.

Kops, G.J., Dansen, T.B., Polderman, P.E., Saarloos, I., Wirtz, K.W., Coffer, P.J., Huang, T.T., Bos, J.L., Medema, R.H., and Burgering, B.M. (2002). Forkhead transcription factor FOXO3a protects quiescent cells from oxidative stress. Nature *419*, 316-321.

Kozak, L.P. (2010). Brown fat and the myth of diet-induced thermogenesis. Cell Metab *11*, 263-267.

Kumar, A., Harris, T.E., Keller, S.R., Choi, K.M., Magnuson, M.A., and Lawrence, J.C., Jr. (2008). Muscle-specific deletion of rictor impairs insulin-stimulated glucose transport and enhances Basal glycogen synthase activity. Mol Cell Biol *28*, 61-70.

Kumar, A., Lawrence, J.C., Jr., Jung, D.Y., Ko, H.J., Keller, S.R., Kim, J.K., Magnuson, M.A., and Harris, T.E. (2010). Fat cell-specific ablation of rictor in mice impairs insulin-regulated fat cell and whole-body glucose and lipid metabolism. Diabetes *59*, 1397-1406.

Kursawe, R., Caprio, S., Giannini, C., Narayan, D., Lin, A., D'Adamo, E., Shaw, M., Pierpont, B., Cushman, S.W., and Shulman, G.I. (2013). Decreased transcription of ChREBP-alpha/beta isoforms in abdominal subcutaneous adipose tissue of obese adolescents with prediabetes or early type 2 diabetes: associations with insulin resistance and hyperglycemia. Diabetes *62*, 837-844.

Labbe, S.M., Caron, A., Bakan, I., Laplante, M., Carpentier, A.C., Lecomte, R., and Richard, D. (2015). In vivo measurement of energy substrate contribution to cold-induced brown adipose tissue thermogenesis. FASEB J *29*, 2046-2058.

Lamming, D.W., Ye, L., Katajisto, P., Goncalves, M.D., Saitoh, M., Stevens, D.M., Davis, J.G., Salmon, A.B., Richardson, A., Ahima, R.S*., et al.* (2012). Rapamycin-induced insulin resistance is mediated by mTORC2 loss and uncoupled from longevity. Science *335*, 1638-1643.

Laplante, M., and Sabatini, D.M. (2012). mTOR signaling in growth control and disease. Cell *149*, 274-293.

Lee, J., Choi, J., Aja, S., Scafidi, S., and Wolfgang, M.J. (2016). Loss of Adipose Fatty Acid Oxidation Does Not Potentiate Obesity at Thermoneutrality. Cell Rep *14*, 1308-1316.

Lee, J., Ellis, J.M., and Wolfgang, M.J. (2015). Adipose fatty acid oxidation is required for thermogenesis and potentiates oxidative stress-induced inflammation. Cell Rep *10*, 266-279.

Lee, J.V., Carrer, A., Shah, S., Snyder, N.W., Wei, S., Venneti, S., Worth, A.J., Yuan, Z.F., Lim, H.W., Liu, S*., et al.* (2014). Akt-dependent metabolic reprogramming regulates tumor cell histone acetylation. Cell Metab *20*, 306-319.

Lee, K.Y., Russell, S.J., Ussar, S., Boucher, J., Vernochet, C., Mori, M.A., Smyth, G., Rourk, M., Cederquist, C., Rosen, E.D.*, et al.* (2013). Lessons on Conditional Gene Targeting in Mouse Adipose Tissue. Diabetes *62*, 864-874.

Lettieri Barbato, D., Tatulli, G., Aquilano, K., and Ciriolo, M.R. (2013). FoxO1 controls lysosomal acid lipase in adipocytes: implication of lipophagy during nutrient restriction and metformin treatment. Cell Death Dis *4*, e861.

Lichtenbelt, W.D.v.M., Vanhommerig, J.W., Smulders, N.M., Drossaerts, J.M.A.F.L., Kemerink, G.J., Bouvy, N.D., Schrauwen, P., and Teule, G.J.J. (2009). Cold-Activated Brown Adipose Tissue in Healthy Men. New England Journal of Medicine *360*, 1500-1508.

Lidell, M.E., Betz, M.J., Dahlqvist Leinhard, O., Heglind, M., Elander, L., Slawik, M., Mussack, T., Nilsson, D., Romu, T., Nuutila, P.*, et al.* (2013). Evidence for two types of brown adipose tissue in humans. Nat Med *19*, 631-634.

Liu, D., Bordicchia, M., Zhang, C., Fang, H., Wei, W., Li, J.L., Guilherme, A., Guntur, K., Czech, M.P., and Collins, S. (2016). Activation of mTORC1 is essential for beta-adrenergic stimulation of adipose browning. J Clin Invest *126*, 1704-1716.

Mailloux, R.J., and Harper, M.E. (2011). Uncoupling proteins and the control of mitochondrial reactive oxygen species production. Free Radic Biol Med *51*, 1106-1115.

Mailloux, R.J., Seifert, E.L., Bouillaud, F., Aguer, C., Collins, S., and Harper, M.E. (2011). Glutathionylation acts as a control switch for uncoupling proteins UCP2 and UCP3. J Biol Chem *286*, 21865-21875.

Mammucari, C., Milan, G., Romanello, V., Masiero, E., Rudolf, R., Del Piccolo, P., Burden, S.J., Di Lisi, R., Sandri, C., Zhao, J.*, et al.* (2007). FoxO3 controls autophagy in skeletal muscle in vivo. Cell Metab *6*, 458-471.

Manning, B.D., Tee, A.R., Logsdon, M.N., Blenis, J., and Cantley, L.C. (2002). Identification of the tuberous sclerosis complex-2 tumor suppressor gene product tuberin as a target of the phosphoinositide 3-kinase/akt pathway. Mol Cell *10*, 151-162.

Masui, K., Tanaka, K., Akhavan, D., Babic, I., Gini, B., Matsutani, T., Iwanami, A., Liu, F., Villa, G.R., Gu, Y.*, et al.* (2013). mTOR Complex 2 Controls Glycolytic Metabolism in Glioblastoma through FoxO Acetylation and Upregulation of c-Myc. Cell Metabolism *18*, 726-739.

Matsuzaki, H., Daitoku, H., Hatta, M., Aoyama, H., Yoshimochi, K., and Fukamizu, A. (2005). Acetylation of Foxo1 alters its DNA-binding ability and sensitivity to phosphorylation. Proc Natl Acad Sci U S A *102*, 11278-11283.

Mizuarai, S., Miki, S., Araki, H., Takahashi, K., and Kotani, H. (2005). Identification of dicarboxylate carrier Slc25a10 as malate transporter in de novo fatty acid synthesis. Journal of Biological Chemistry *280*, 32434-32441.

Mullican, S.E., Tomaru, T., Gaddis, C.A., Peed, L.C., Sundaram, A., and Lazar, M.A. (2013). A Novel Adipose-Specific Gene Deletion Model Demonstrates Potential Pitfalls of Existing Methods. Molecular Endocrinology *27*, 127-134.

Muzumdar, M.D., Tasic, B., Miyamichi, K., Li, L., and Luo, L. (2007). A global double-fluorescent Cre reporter mouse. Genesis *45*, 593-605.

Nagashima, T., Shigematsu, N., Maruki, R., Urano, Y., Tanaka, H., Shimaya, A., Shimokawa, T., and Shibasaki, M. (2010). Discovery of novel forkhead box O1 inhibitors for treating type 2 diabetes: improvement of fasting glycemia in diabetic db/db mice. Mol Pharmacol *78*, 961-970.

Najafov, A., Shpiro, N., and Alessi, D.R. (2012). Akt is efficiently activated by PIF-pocket- and PtdIns(3,4,5)P3-dependent mechanisms leading to resistance to PDK1 inhibitors. Biochem J *448*, 285-295.

Nakae, J., Cao, Y., Hakuno, F., Takemori, H., Kawano, Y., Sekioka, R., Abe, T., Kiyonari, H., Tanaka, T., Sakai, J*., et al.* (2012). Novel repressor regulates insulin sensitivity through interaction with Foxo1. EMBO J *31*, 2275-2295.

Nakae, J., Oki, M., and Cao, Y. (2008). The FoxO transcription factors and metabolic regulation. FEBS Lett *582*, 54-67.

Nedergaard, J., and Cannon, B. (2010). The changed metabolic world with human brown adipose tissue: therapeutic visions. Cell Metab *11*, 268-272.

Nedergaard, J., and Cannon, B. (2013). How brown is brown fat? It depends where you look. Nature Medicine *19*, 540-541.

Nicholls, D.G. (2006). The physiological regulation of uncoupling proteins. Biochim Biophys Acta *1757*, 459-466.

Obsil, T., and Obsilova, V. (2008). Structure/function relationships underlying regulation of FOXO transcription factors. Oncogene *27*, 2263-2275.

Ohno, H., Shinoda, K., Ohyama, K., Sharp, L.Z., and Kajimura, S. (2013). EHMT1 controls brown adipose cell fate and thermogenesis through the PRDM16 complex. Nature *504*, 163-167.

Olsen, J.M., Sato, M., Dallner, O.S., Sandstrom, A.L., Pisani, D.F., Chambard, J.C., Amri, E.Z., Hutchinson, D.S., and Bengtsson, T. (2014). Glucose uptake in brown fat cells is dependent on mTOR complex 2-promoted GLUT1 translocation. J Cell Biol *207*, 365-374.

Ortega-Molina, A., Efeyan, A., Lopez-Guadamillas, E., Munoz-Martin, M., Gomez-Lopez, G., Canamero, M., Mulero, F., Pastor, J., Martinez, S., Romanos, E*., et al.* (2012). Pten positively regulates brown adipose function, energy expenditure, and longevity. Cell Metab *15*, 382-394.

Pearce, L.R., Komander, D., and Alessi, D.R. (2010). The nuts and bolts of AGC protein kinases. Nat Rev Mol Cell Biol *11*, 9-22.

Peterson, T.R., Sengupta, S.S., Harris, T.E., Carmack, A.E., Kang, S.A., Balderas, E., Guertin, D.A., Madden, K.L., Carpenter, A.E., Finck, B.N*., et al.* (2011). mTOR complex 1 regulates lipin 1 localization to control the SREBP pathway. Cell *146*, 408-420.

Petruzzelli, M., Schweiger, M., Schreiber, R., Campos-Olivas, R., Tsoli, M., Allen, J., Swarbrick, M., Rose-John, S., Rincon, M., Robertson, G*., et al.* (2014). A switch from white to brown fat increases energy expenditure in cancer-associated cachexia. Cell Metab *20*, 433-447.

Rothwell, N.J., and Stock, M.J. (1979). A role for brown adipose tissue in diet-induced thermogenesis. Nature *281*, 31-35.

Saito, M., Okamatsu-Ogura, Y., Matsushita, M., Watanabe, K., Yoneshiro, T., Nio-Kobayashi, J., Iwanaga, T., Miyagawa, M., Kameya, T., Nakada, K*., et al.* (2009). High incidence of metabolically active brown adipose tissue in healthy adult humans: effects of cold exposure and adiposity. Diabetes *58*, 1526-1531.

Sanchez-Gurmaches, J., and Guertin, D.A. (2014a). Adipocyte lineages: tracing back the origins of fat. Biochim Biophys Acta *1842*, 340-351.

Sanchez-Gurmaches, J., and Guertin, D.A. (2014b). Adipocytes arise from multiple lineages that are heterogeneously and dynamically distributed. Nature Communications *5*.

Sanchez-Gurmaches, J., Hung, C.-M., Sparks, C.A., Tang, Y., Li, H., and Guertin, D.A. (2012). PTEN Loss in the Myf5 Lineage Redistributes Body Fat and Reveals Subsets of White Adipocytes that Arise from Myf5 Precursors. Cell Metabolism *16*, 348-362.

Sanjana, N.E., Shalem, O., and Zhang, F. (2014). Improved vectors and genome-wide libraries for CRISPR screening. Nat Methods *11*, 783-784.

Sarbassov, D.D., Guertin, D.A., Ali, S.M., and Sabatini, D.M. (2005). Phosphorylation and regulation of Akt/PKB by the rictor-mTOR complex. Science *307*, 1098-1101.

Sato, M., Dehvari, N., Oberg, A.I., Dallner, O.S., Sandstrom, A.L., Olsen, J.M., Csikasz, R.I., Summers, R.J., Hutchinson, D.S., and Bengtsson, T. (2014). Improving type 2 diabetes through a distinct adrenergic signaling pathway involving mTORC2 that mediates glucose uptake in skeletal muscle. Diabetes *63*, 4115-4129.

Schulz, T.J., Huang, P., Huang, T.L., Xue, R., McDougall, L.E., Townsend, K.L., Cypess, A.M., Mishina, Y., Gussoni, E., and Tseng, Y.-H. (2013). Brown-fat paucity due to impaired BMP signalling induces compensatory browning of white fat. Nature *495*, 379-383.

Schulz, T.J., and Tseng, Y.H. (2013). Brown adipose tissue: development, metabolism and beyond. Biochem J *453*, 167-178.

Seale, P., Bjork, B., Yang, W., Kajimura, S., Chin, S., Kuang, S., Scime, A., Devarakonda, S., Conroe, H.M., Erdjument-Bromage, H*., et al.* (2008). PRDM16 controls a brown fat/skeletal muscle switch. Nature *454*, 961-967.

Shalem, O., Sanjana, N.E., Hartenian, E., Shi, X., Scott, D.A., Mikkelsen, T.S., Heckl, D., Ebert, B.L., Root, D.E., Doench, J.G*., et al.* (2014). Genome-scale CRISPR-Cas9 knockout screening in human cells. Science *343*, 84-87.

Sharp, L.Z., Shinoda, K., Ohno, H., Scheel, D.W., Tomoda, E., Ruiz, L., Hu, H., Wang, L., Pavlova, Z., Gilsanz, V*., et al.* (2012). Human BAT possesses molecular signatures that resemble beige/brite cells. PLoS One *7*, e49452.

Shaw, R.J., Bardeesy, N., Manning, B.D., Lopez, L., Kosmatka, M., DePinho, R.A., and Cantley, L.C. (2004). The LKB1 tumor suppressor negatively regulates mTOR signaling. Cancer Cell *6*, 91-99.

Shimizu, Y., Satoh, S., Yano, H., Minokoshi, Y., Cushman, S.W., and Shimazu, T. (1998). Effects of noradrenaline on the cell-surface glucose transporters in cultured brown adipocytes: novel

mechanism for selective activation of GLUT1 glucose transporters. Biochem J *330 (Pt 1)*, 397-403.

Shinoda, K., Luijten, I.H., Hasegawa, Y., Hong, H., Sonne, S.B., Kim, M., Xue, R., Chondronikola, M., Cypess, A.M., Tseng, Y.H.*, et al.* (2015). Genetic and functional characterization of clonally derived adult human brown adipocytes. Nat Med *21*, 389-394.

Shiota, C., Woo, J.T., Lindner, J., Shelton, K.D., and Magnuson, M.A. (2006). Multiallelic disruption of the rictor gene in mice reveals that mTOR complex 2 is essential for fetal growth and viability. Dev Cell *11*, 583-589.

Sidossis, L.S., Porter, C., Saraf, M.K., Borsheim, E., Radhakrishnan, R.S., Chao, T., Ali, A., Chondronikola, M., Mlcak, R., Finnerty, C.C.*, et al.* (2015). Browning of Subcutaneous White Adipose Tissue in Humans after Severe Adrenergic Stress. Cell Metab *22*, 219-227.

Stock, M.J. (1999). Gluttony and thermogenesis revisited. Int J Obes Relat Metab Disord *23*, 1105-1117.

Tallquist, M.D., Weismann, K.E., Hellstrom, M., and Soriano, P. (2000). Early myotome specification regulates PDGFA expression and axial skeleton development. Development *127*, 5059-5070.

Tang, Y., Wallace, M., Sanchez-Gurmaches, J., Hsiao, W.Y., Li, H., Lee, P.L., Vernia, S., Metallo, C.M., and Guertin, D.A. (2016). Adipose tissue mTORC2 regulates ChREBP-driven de novo lipogenesis and hepatic glucose metabolism. Nat Commun *7*, 11365.

Tee, A.R., Manning, B.D., Roux, P.P., Cantley, L.C., and Blenis, J. (2003). Tuberous Sclerosis Complex Gene Products, Tuberin and Hamartin, Control mTOR Signaling by Acting as a GTPase-Activating Protein Complex toward Rheb. Current Biology *13*, 1259-1268.

Townsend, K.L., and Tseng, Y.-H. (2014). Brown fat fuel utilization and thermogenesis. Trends in Endocrinology and Metabolism *25*, 168-177.

Tseng, Y.-H., Butte, A.J., Kokkotou, E., Yechoor, V.K., Taniguchi, C.M., Kriauciunas, K.M., Cypess, A.M., Niinobe, M., Yoshikawa, K., Patti, M.E.*, et al.* (2005). Prediction of preadipocyte differentiation by gene expression reveals role of insulin receptor substrates and necdin. Nature Cell Biology *7*, 601-611.

Tseng, Y.H., Cypess, A.M., and Kahn, C.R. (2010). Cellular bioenergetics as a target for obesity therapy. Nat Rev Drug Discov *9*, 465-482.

Tseng, Y.H., Kokkotou, E., Schulz, T.J., Huang, T.L., Winnay, J.N., Taniguchi, C.M., Tran, T.T., Suzuki, R., Espinoza, D.O., Yamamoto, Y.*, et al.* (2008). New role of bone morphogenetic protein 7 in brown adipogenesis and energy expenditure. Nature *454*, 1000-1004.

Tsoli, M., Moore, M., Burg, D., Painter, A., Taylor, R., Lockie, S.H., Turner, N., Warren, A., Cooney, G., Oldfield, B.*, et al.* (2012). Activation of thermogenesis in brown adipose tissue and dysregulated lipid metabolism associated with cancer cachexia in mice. Cancer Res *72*, 4372-4382.

Virtanen, K.A., Lidell, M.E., Orava, J., Heglind, M., Westergren, R., Niemi, T., Taittonen, M., Laine, J., Savisto, N.-J., Enerback, S.*, et al.* (2009). Brief Report: Functional Brown Adipose Tissue in Healthy Adults. New England Journal of Medicine *360*, 1518-1525.

Walker, A.K., Yang, F., Jiang, K., Ji, J.Y., Watts, J.L., Purushotham, A., Boss, O., Hirsch, M.L., Ribich, S., Smith, J.J.*, et al.* (2010). Conserved role of SIRT1 orthologs in fasting-dependent inhibition of the lipid/cholesterol regulator SREBP. Genes Dev *24*, 1403-1417.

Wang, F., Mullican, S.E., DiSpirito, J.R., Peed, L.C., and Lazar, M.A. (2013). Lipoatrophy and severe metabolic disturbance in mice with fat-specific deletion of PPAR gamma. Proceedings of the National Academy of Sciences of the United States of America *110*, 18656-18661.

Wang, F., and Tong, Q. (2009). SIRT2 suppresses adipocyte differentiation by deacetylating FOXO1 and enhancing FOXO1's repressive interaction with PPARgamma. Mol Biol Cell *20*, 801-808.

Wang, Y., Viscarra, J., Kim, S.J., and Sul, H.S. (2015). Transcriptional regulation of hepatic lipogenesis. Nat Rev Mol Cell Biol *16*, 678-689.

Wang, Y., Zhou, Y., and Graves, D.T. (2014). FOXO transcription factors: their clinical significance and regulation. Biomed Res Int *2014*, 925350.

Wellen, K.E., Hatzivassiliou, G., Sachdeva, U.M., Bui, T.V., Cross, J.R., and Thompson, C.B. (2009). ATP-citrate lyase links cellular metabolism to histone acetylation. Science *324*, 1076-1080.

Wu, J., Bostrom, P., Sparks, L.M., Ye, L., Choi, J.H., Giang, A.H., Khandekar, M., Virtanen, K.A., Nuutila, P., Schaart, G.*, et al.* (2012). Beige adipocytes are a distinct type of thermogenic fat cell in mouse and human. Cell *150*, 366-376.

Xu, F., Zheng, X., Lin, B., Liang, H., Cai, M., Cao, H., Ye, J., and Weng, J. (2016). Diet-induced obesity and insulin resistance are associated with brown fat degeneration in SIRT1-deficient mice. Obesity (Silver Spring) *24*, 634-642.

Xue, R., Lynes, M.D., Dreyfuss, J.M., Shamsi, F., Schulz, T.J., Zhang, H., Huang, T.L., Townsend, K.L., Li, Y., Takahashi, H.*, et al.* (2015). Clonal analyses and gene profiling identify genetic biomarkers of the thermogenic potential of human brown and white preadipocytes. Nature Medicine *21*, 760-+.

Yao, Y., Suraokar, M., Darnay, B.G., Hollier, B.G., Shaiken, T.E., Asano, T., Chen, C.H., Chang, B.H., Lu, Y., Mills, G.B.*, et al.* (2013). BSTA promotes mTORC2-mediated phosphorylation of Akt1 to suppress expression of FoxC2 and stimulate adipocyte differentiation. Sci Signal *6*, ra2.

Young, P., Arch, J.R., and Ashwell, M. (1984). Brown adipose tissue in the parametrial fat pad of the mouse. FEBS Lett *167*, 10-14.

Yu, X.X., Lewin, D.A., Forrest, W., and Adams, S.H. (2002). Cold elicits the simultaneous induction of fatty acid synthesis and beta-oxidation in murine brown adipose tissue: prediction from differential gene expression and confirmation in vivo. FASEB J *16*, 155-168.

Yu, Y., Yoon, S.-O., Poulogiannis, G., Yang, Q., Ma, X.M., Villen, J., Kubica, N., Hoffman, G.R., Cantley, L.C., Gygi, S.P.*, et al.* (2011). Phosphoproteomic Analysis Identifies Grb10 as an mTORC1 Substrate That Negatively Regulates Insulin Signaling. Science *332*, 1322-1326.

Yuan, M., Pino, E., Wu, L., Kacergis, M., and Soukas, A.A. (2012). Identification of Akt-independent regulation of hepatic lipogenesis by mammalian target of rapamycin (mTOR) complex 2. J Biol Chem *287*, 29579-29588.

Yun, H., Park, S., Kim, M.J., Yang, W.K., Im, D.U., Yang, K.R., Hong, J., Choe, W., Kang, I., Kim, S.S.*, et al.* (2014). AMP-activated protein kinase mediates the antioxidant effects of resveratrol through regulation of the transcription factor FoxO1. FEBS J *281*, 4421-4438.

Zhang, Y., Gao, X., Saucedo, L.J., Ru, B., Edgar, B.A., and Pan, D. (2003). Rheb is a direct target of the tuberous sclerosis tumour suppressor proteins. Nat Cell Biol *5*, 578-581.

Zhao, J., Brault, J.J., Schild, A., Cao, P., Sandri, M., Schiaffino, S., Lecker, S.H., and Goldberg, A.L. (2007). FoxO3 coordinately activates protein degradation by the autophagic/lysosomal and proteasomal pathways in atrophying muscle cells. Cell Metab *6*, 472-483.